

CONCEPTUAL DESIGN OF A HYBRID (TURBOFAN/SOLAR) POWERED HALE
UAV

A THESIS SUBMITTED TO
THE GRADUATE SCHOOL OF NATURAL AND APPLIED SCIENCES
OF
MIDDLE EAST TECHNICAL UNIVERSITY

BY

ERDİNÇ MERMER

IN PARTIAL FULFILMENT OF THE REQUIREMENTS
FOR
THE DEGREE OF MASTER OF SCIENCE
IN
AEROSPACE ENGINEERING

MARCH 2016

Approval of the thesis:

**CONCEPTUAL DESIGN OF A HYBRID (TURBOFAN/SOLAR) POWERED
HALE UAV**

submitted by **ERDİNÇ MERMER** in partial fulfilment of the requirements for the degree
of **Master of Science in Aerospace Engineering Department, Middle East Technical
University** by,

Prof. Dr. Gülbin Dural Ünver
Dean, Graduate School of **Natural and Applied Sciences**

Prof. Dr. Ozan Tekinalp
Head of Department, **Aerospace Engineering**

Prof. Dr. Serkan Özgen
Supervisor, **Aerospace Engineering Dept., METU**

Examining Committee Members

Prof. Dr. Nafiz Alemdaroğlu
Airframe and Powerplant Maintenance Dept., ATU

Prof. Dr. Serkan Özgen
Aerospace Engineering Dept., METU

Prof. Dr. İsmail Hakkı Tuncer
Aerospace Engineering Dept., METU

Assoc. Prof. Dr. Kürşad Melih Güleren
Aeronautical Engineering Dept., UTAA

Asst. Prof. Dr. Durmuş Sinan Körpe
Aeronautical Engineering Dept., UTAA

Date: 29/03/2016

I hereby declare that all information in this document has been obtained and presented in accordance with academic rules and ethical conduct. I also declare that, as required by these rules and conduct, I have fully cited and referenced all material and results that are not original to this work.

Name, Last name : Erdiñ Mermer

Signature :

ABSTRACT

CONCEPTUAL DESIGN OF A HYBRID (TURBOFAN/SOLAR) POWERED HALE UAV

Mermer, Erdinç

M.S., Department of Aerospace Engineering

Supervisor: Prof. Dr. Serkan Özgen

March 2016, 133 Pages

The aim of the thesis is to design a HALE UAV using both turbofan engine and solar energy in order to obtain 24 hours endurance with 550 lb payload capacity and 30000 ft service ceiling. During daytime, required power is obtained from solar panels. However, excess solar energy is used for charging the lithium-ion battery. It is assumed that turbofan engine is used only for climbing to the required altitude. During loiter, only solar energy and battery power are used.

The design methodology consists of two main parts. In the first part, typical conceptual design methodology is used. Weight analysis, wing loading and thrust loading, required power analysis, aircraft performance analysis are performed. While performing the conceptual design, aircraft is assumed as only turbofan-powered aircraft. Due to long wingspan and large wing area, typical structural weight determination techniques are not suitable for the HALE UAV. Therefore, a new structural weight prediction model is used.

In the second part of the thesis, solar energy and battery energy are examined in order to assess whether endurance and service ceiling requirements are satisfied. Solar radiation model is used for verification. Also a simulink model is constructed for examining the flight duration.

It is considered that propulsion system consists of one or two small turbofan engines and four electric powered engines with one propeller each. Solar panel efficiency is assumed as 30% and 40%, in order to show the effects of cell efficiencies on flight endurance.

Finally, endurance of the aircraft is predicted for four different times of the year.

Key words: Aircraft conceptual design methodology, hybrid powered UAV, solar powered aircraft, continuous flight, HALE UAV, simulink

ÖZ

HİBRİT (TURBOFAN/GÜNEŞ ENERJİLİ) İTKİ SİSTEMLİ YÜKSEK İRTİFA İNSANSIZ HAVA ARACI KAVRAMSAL TASARIMI

Mermer, Erdinç

Yüksek Lisans, Havacılık ve Uzay Mühendisliği

Tez Yöneticisi: Prof. Dr. Serkan Özgen

Mart 2016, 133 Sayfa

Bu tezin amacı hem turbofan hem de güneş enerjisi ile çalışan yüksek irtifada (30000 ft), 24 saatten daha uzun süre havada kalabilen ve 550 lb faydalı yük taşıyabilen bir İHA tasarlamaktır. Gündüz güç sadece güneş panellerinden elde edilecektir. Bununla birlikte fazla olan güç lityum iyon pilleri şarj etmek için kullanılacaktır. Gereken yüksekliğe ulaşmak için sadece turbofan motoru kullanılacaktır. Turlama sırasında sadece güneş enerjisi ve pillerden gelen enerji kullanılacaktır.

Tasarım metodu iki ana kısımdan oluşmaktadır. Birinci kısımda kavramsal tasarım metotları kullanılmıştır. Ağırlık analizi, kanat yükü, itki yükü, gerekli güç analizleri ve uçak performans analizleri tamamlanmıştır. Bu hesaplamalar sırasında uçağın yalnızca turbofan motoru kullanacağı varsayımı yapılmıştır. Klasik ağırlık hesaplama yöntemleri uzun kanat açıklığı ve büyük kanat alanı olan uçaklarda doğru sonuç vermemektedir, bu yüzden yeni bir yapısal ağırlık tahmin yöntemi kullanılmıştır. İkinci kısımda turlama

sırasında güneş enerjisinin ve pil enerjisinin yeterliliđi incelenmiştir. Güneş radyasyon modeli esas alınmıştır.

İtki sisteminin bir veya iki turbofan motoru ve her biri bir pervaneli dört elektrik motorundan oluşacağı öngörülmektedir. Güneş panellerinin verimliliđi 30% ve 40% olarak alınmıştır. Böylece güneş hücrelerinin olası gelişimlerinin uçuş zamanına olan etkileri gözlenebilmiştir.

Son olarak yılın 4 farklı zamanında uçağın turlama süresi hesaplanmıştır.

Anahtar Kelimeler: Uçak kavramsal tasarım yöntemi, hibrit itki sistemli uçak, güneş enerjili uçak, aralıksız uçuş, yüksek irtifa insansız hava aracı, simülasyon

To my family...

ACKNOWLEDGEMENTS

I would like to express my deepest gratitude to my advisor Prof. Dr. Serkan ÖZGEN for his help, guidance, criticism and continuous support throughout the course of this thesis.

I would like to thank TÜBİTAK UZAY which involved me as a researcher for YİHAS (Yüksek İrtifa İnsansız Hava Aracı) Unmanned Aircraft Design framework since some parts of this thesis are studied during YİHAS conceptual design phase.

I would like to thank my friends Mustafa Yasin ŞAKA, Emrecan SUIÇMEZ, Ali Onur ŞAHİNOĞLU my colleagues Abdulkadir KÖKER, Abdurrahman AYDEMİR, Zahide SEYHAN and İsa KAVAS for their help. I am also grateful to Erdem MERMER for his help and motivation.

I wish to thank to my family for their endless support during this work.

TABLE OF CONTENTS

ABSTRACT	V
ÖZ	VII
ACKNOWLEDGEMENTS	X
TABLE OF CONTENTS	XI
LIST OF TABLES	XVI
LIST OF FIGURES	XVIII
LIST OF SYMBOLS	XXII
CHAPTERS	
INTRODUCTION	1
1.1. Solar Powered Airplanes	4
1.2. Reconnaissance HALE Airplanes	10
1.3. Competitor Study	12
1.4. Design Process	14
CONCEPTUAL DESIGN	17
2.1. Competitor Study Outputs	17
2.2. Mission Profile	18
2.3. Estimation of the Design Takeoff Gross Weight, W_0	18
2.4. Estimation of the Fuel Weight Fraction	19
2.5. Trade-off Study	21
2.5.1. Payload Trade	22

2.5.2.	Range Trade	22
2.6.	Airfoil and Wing Planform Selection.....	22
2.7.	Aspect Ratio	28
2.8.	Thrust to Weight Ratio.....	28
2.8.1.	Thrust to Weight Ratio for a Level Constant-Velocity Turn	28
2.8.2.	Thrust to Weight Ratio for Desired Rate of Climb	29
2.8.3.	Thrust to Weight Ratio for a Desired Takeoff Distance	29
2.8.4.	Thrust to Weight Ratio for a Desired Service Ceiling	30
2.8.5.	Thrust to Weight Ratio for a Desired Cruise Speed.....	30
2.9.	Wing Loading.....	31
2.9.1.	Takeoff Distance Wing Loading	32
2.9.2.	Landing Distance Wing Loading	33
2.9.3.	Cruise Speed Wing Loading	34
2.9.4.	Stall speed Wing Loading	37
2.9.5.	Instantaneous Turn and Sustained Turn Wing loading.....	37
2.10.	Refined Weight Sizing Equations	40
2.11.	Geometry Sizing and Configuration	42
2.11.1.	Fuel Volume.....	42
2.11.2.	Fuselage Length and Diameter.....	42
2.11.3.	Wing Sizing and Planform Shape	44
2.11.4.	Tail Sizing	46
2.11.4.1.	Horizontal Tail Sizing	46
2.11.4.2.	Vertical Tail Sizing	47
2.11.5.	Control Surface Sizing	48
2.11.6.	Engine Dimensions and Weight.....	48
2.11.7.	Capture Area	49
2.12.	Preliminary Center of Gravity Estimation, Landing Gear Placement and Sizing	52

2.12.1.	Weights of Major Components	52
2.12.1.1.	Wing Weight	52
2.12.1.2.	Fuselage Weight.....	53
2.12.1.3.	Horizontal Tail Weight	54
2.12.1.4.	Vertical Tail Weight.....	54
2.12.1.5.	Landing Gear Weight.....	54
2.12.1.6.	All Else Weight.....	55
2.12.1.7.	Fuel Weight.....	55
2.12.1.8.	Solar Panels and Propulsion Weight.....	55
2.12.2.	Center of Gravity Estimation	56
PERFORMANCE ANALYSIS		59
3.1.	Estimation of $C_{L\alpha}$	59
3.2.	Estimation of C_{Lmax}	61
3.3.	Estimation of α_{CLmax}	62
3.4.	Estimation of the Parasite Drag Coefficient C_{D0}	63
3.4.1.	Wing Parasite Drag	64
3.4.2.	Fuselage Parasite Drag	65
3.4.3.	Horizontal Tail Drag	66
3.4.4.	Vertical Tail Drag	66
3.4.5.	Miscellaneous Drag, Landing Gear Drag Calculation and Total Zero Lift Drag Calculation	67
3.5.	Zero Lift Drag Coefficient of Aircraft at Different Altitudes.	68
3.6.	Required Power and Velocity Calculations	69
3.7.	Electric Engine Selection and Propeller Sizing	70
3.8.	Thrust and Velocity Calculations at Different Altitudes.....	71
3.9.	Rate of Climb, Service and Absolute Ceilings.....	75
3.10.	Time to Climb	77

3.11.	Maximum Range of Aircraft at 30000 ft.....	78
3.12.	Ground Roll for Takeoff	78
3.13.	Ground Roll and Total Distance for Landing.....	79
3.14.	Gliding (unpowered) Flight.....	79
3.15.	Maneuverability and V-n Diagrams	80
3.15.1.	V vs. n_{max} Chart	80
3.15.2.	Minimum Turn Radius	81
3.15.3.	Maximum Turn Rate	82
3.15.4.	V-n Diagram.....	82
3.16.	Longitudinal Stability Analysis.....	84
3.16.1.	Neutral Point	84
3.16.1.1.	Wing Term	84
3.16.1.2.	Fuselage Term.....	84
3.16.1.3.	Horizontal Tail Term.....	85
3.16.1.4.	Aspect Ratio Factor.....	86
3.16.1.5.	Taper Ratio Factor.....	86
3.16.1.6.	Horizontal Tail Location Factor	86
3.16.2.	Determination of Static Margin.....	87
3.17.	Landing Gear Placement and Sizing	87
3.17.1.	Landing Gear Configuration	87
3.17.2.	Landing Gear Placement	88
	ENERGY BALANCE FOR LOITERING.....	91
4.1.	Solar Irradiance	91
4.2.	Solar Energy Calculation	94
4.3.	Required Energy Calculation	95
4.4.	Battery Energy Calculation	95
4.5.	Real Time Simulation.....	96

4.6.	Methods for Reconstructing Solar Cycle	96
4.7.	Simulations of Various Cases	97
4.7.1.	Simulations for 30% Efficient Solar Cells	97
4.7.1.1.	20000 ft, June 21, 30% Efficient Solar Cells	97
4.7.1.2.	20000 ft, March 21, 30% Efficient Solar Cells	99
4.7.1.3.	20000 ft, September 23, 30% efficient solar cells	101
4.7.1.4.	20000 ft, December 21, 30% Efficient Solar Cells	101
4.7.2.	Simulations for 40% Efficient Solar Cells	102
4.7.2.1.	20000 ft, June 21, 40% Efficient Solar Cells	102
4.7.2.2.	20000 ft, March 21, 40% Efficient Solar Cells	104
4.7.2.3.	20000 ft, September 23, 40% Efficient Solar Cells	105
4.7.2.4.	20000 ft, December 21, 40% Efficient Solar Cells	106
4.7.2.5.	30000 ft, June 21, 40% Efficient Solar Cells	107
4.7.2.6.	30000 ft, March 21, 40% Efficient Solar Cells	108
4.7.3.	30000 ft, September 23, 40% Efficient Solar Cells	109
4.7.4.	30000 ft, December 21, 40% Efficient Solar Cells	110
4.7.5.	45000 ft, June 21, 40% Efficient Solar Cells	110
4.7.6.	45000 ft, March 21, 40% Efficient Solar Cells	112
4.7.7.	45000 ft, September 23, 40% Efficient Solar Cells	113
4.7.8.	45000 ft, 21 December, 40% Efficient Solar Cells	113
4.7.9.	45000 ft, June 21, 40% Efficient Solar Cells with Batteries Having 328 kWh Energy Density	114
COST ANALYSIS		115
CONCLUSION		121
6.1.	Comments on Hybrid Propulsion and Future Works	124
REFERENCES		127

LIST OF TABLES

TABLES

Table 1.1 Competitor Aircrafts	13
Table 1.2 Air Conditions Variations with Altitude	13
Table 2.1 Requirements.....	17
Table 2.2 Empty Weight Fraction vs W_0 [1].....	19
Table 2.3 Payload Trade.....	22
Table 2.4 Range Trade	22
Table 2.5 Airfoil Properties at Sea Level.....	24
Table 2.6 Airfoil Properties at 30000 ft Altitude	24
Table 2.7 Airfoil Properties at 65000 ft Altitude	25
Table 2.8 3D Properties at Sea Level.....	26
Table 2.9 3D Properties at 30000 ft Altitude	26
Table 2.10 3D Properties at 65000 ft Altitude	27
Table 2.11 Typical Aerodynamic Characteristics of Selected Classes of Aircraft [3]	29
Table 2.12 Specifications of FJ44-1A [36]	39
Table 2.13 Fuselage Length vs W_0 [1].....	43
Table 2.14 Fuselage Length Comparison.....	43
Table 2.15 Tail Volume Coefficients [2]	47
Table 2.16 Mass to Power Ratio and Propulsive Efficiency of Solar Powered Airplanes [4]	55
Table 2.17 Horizontal Center of Gravity Estimation	57
Table 2.18 Vertical Center of Gravity Estimation	58
Table 3.1 $C_{D,0}$ at Sea Level.....	68
Table 3.2 $C_{D,0}$ at 20000 ft Altitude	68

Table 3.3 $C_{D,0}$ at 45000 ft Altitude 68

Table 3.4 JM2 Engine Specifications [51] 70

Table 3.5 Rate of Climb for Different Altitudes 76

Table 3.6 Time to Climb for Certain Altitudes 78

Table 4.1 Representation of Solar Irradiance Constant 92

Table 4.2 Efficiency of Solar Instruments 95

Table 6.1 UAV Performance Results 124

LIST OF FIGURES

FIGURES

Figure 1.1 Solar Cell Efficiency Yearly Development [4].....	2
Figure 1.2 Lithium-ion Battery Energy Density Evaluations [8].....	3
Figure 1.3 Sunrise I [9]	4
Figure 1.4 Solar One [12].....	5
Figure 1.5 Gossamer Penguin [13].....	5
Figure 1.6 Solar Challenger [14].....	6
Figure 1.7 Sunseeker [15]	6
Figure 1.8 Icare 2 [56].....	7
Figure 1.9 NASA Helios [16]	7
Figure 1.10 Solong UAV (left) [17] and Sky Sailor (right) [18]	8
Figure 1.11 Zephyr (left) [19] and Solar Impulse 2 (right) [20]	9
Figure 1.12 Boeing Solar Eagle [21].....	10
Figure 1.13 U2-S (left) [49] and RB-57F Canberra (right) [22]	10
Figure 1.14 Boeing Condor (left) [29] and Proteus (right) [23].....	11
Figure 1.15 Global Hawk (left) [28] and Heron TP (right) [24]	12
Figure 1.16 Global Observer (left) [27] and Phantom Eye (right) [50]	12
Figure 1.17 TUYGUN.....	15
Figure 2.1 Mission Profile.....	18
Figure 2.2 Sample Wing Geometry.....	25
Figure 2.3 Fx_63_137sm Airfoil.....	27
Figure 2.4 Thrust Loading vs. Wing Loading.....	31
Figure 2.5 Takeoff Distance Estimation [1].....	32
Figure 2.6 Wing Loading vs. Takeoff Parameter.....	33

Figure 2.7 Wing Loading vs. Landing Distance	33
Figure 2.8 Oswald's Span Efficiency vs. Aspect Ratio [3].....	34
Figure 2.9 Skin Friction Coefficient vs Reynolds Number [30].....	35
Figure 2.10 Wetted Area Ratios [1]	36
Figure 2.11 Wing Loading vs. Cruise Speed	36
Figure 2.12 Wing Loading vs. Stall Speed	37
Figure 2.13 Wing Loading vs. Turning Equations.....	38
Figure 2.14 FJ44-1 Engine [48]	40
Figure 2.15 Fuselage Length with Weight Variations	44
Figure 2.16 Wing Geometry	45
Figure 2.17 Nasa/Langley Ls (1)-0013 Airfoil	46
Figure 2.18 Top View of TUYGUN	50
Figure 2.19 Side View of TUYGUN	51
Figure 2.20 Front View of TUYGUN.....	51
Figure 2.21 Isometric View of TUYGUN	52
Figure 2.22 Location of Parts and Instruments	57
Figure 3.1 C_{Lmax} vs M	62
Figure 3.2 Drag vs. Velocity	69
Figure 3.3 Power Required vs Velocity	70
Figure 3.4 JM2 Electric Motor [51]	71
Figure 3.5 Thrust Required and Thrust Available vs. Velocity at Sea Level	72
Figure 3.6 Thrust Required and Thrust Available vs Velocity at 20000 ft.....	72
Figure 3.7 Thrust Required and Thrust Available vs Velocity at 30000 ft.....	73
Figure 3.8 Thrust Required and Thrust Available vs Velocity at 45000 ft.....	73
Figure 3.9 Lift to Drag Ratios vs Velocity at 30000 ft	74
Figure 3.10 Rate of Climb for Different Altitudes.....	77
Figure 3.11 Maximum Load Factors vs Velocity at 30000 ft.....	81
Figure 3.12 V-n Diagram	83

Figure 3.13 Aerodynamic Properties of the Wing88

Figure 3.14 Properties of Landing Gear [1]89

Figure 4.1 Average Annual Solar Radiation Fluxes of Ankara93

Figure 4.2 Solar Radiation of Ankara on June 2194

Figure 4.3 Energy Balance Diagram with 30% efficient solar cells on June 2197

Figure 4.4 Required Time Calculation for Reconstructing Solar Cycle Diagram with 30% Efficient Solar Cells on June 2198

Figure 4.5 Energy Balance Diagram with 30% Efficient Solar Cells on March 21100

Figure 4.6 Required Time Calculation for Reconstructing Solar Cycle Diagram with 30% Efficient Solar Cells on March 21100

Figure 4.7 Energy Balance Diagram with 30% Efficient Solar Cells on September 23 101

Figure 4.8 Energy Balance Diagram with 30% Efficient Solar Cells at December 21 ..102

Figure 4.9 Energy Balance Diagram with 40% Efficient Solar Cells on June 21.....103

Figure 4.10 Required Time Calculation for Reconstructing Solar Cycle Diagram with 40% Efficient Solar Cells on June 21103

Figure 4.11 Energy Balance Diagram with 40% Efficient Solar Cells on March 21104

Figure 4.12 Required Time Calculation for Reconstructing Solar Cycle Diagram with 40% Efficient Solar Cells on March 21.....105

Figure 4.13 Energy Balance Diagram with 40% Efficient Solar Cells on September 23106

Figure 4.14 Energy Balance Diagram with 40% Efficient Solar Cells on December 21106

Figure 4.15 Energy Balance Diagram with 40% Efficient Solar Cells on June 21 at 30000 ft107

Figure 4.16 Required Time Calculation for Reconstructing Solar Cycle Diagram with 40% Efficient Solar Cells on June 21107

Figure 4.17 Energy Balance Diagram with 40% Efficient Solar Cells on March 21 at 30000 ft108

Figure 4.18 Required Time Calculation for Reconstructing Solar Cycle Diagram with 40% Efficient Solar Cells on March 21.....	109
Figure 4.19 Energy Balance Diagram with 40% Efficient Solar Cells on September 23 at 30000 ft	109
Figure 4.20 Energy Balance Diagram with 40% Efficient Solar Cells on December 21 at 30000 ft	110
Figure 4.21 Energy Balance Diagram with 40% Efficient Solar Cells on June 21 at 45000 ft	111
Figure 4.22 Required Time Calculation for Reconstructing Solar Cycle Diagram with 40% Efficient Solar Cells on June 21 at 45000 ft	111
Figure 4.23 Energy Balance Diagram 40% Efficient Solar Cells on March 21 at 45000 ft	112
Figure 4.24 Required Time Calculation for Reconstructing Solar Cycle Diagram with 40% Efficient Solar Cells on March 21 at 45000 ft	112
Figure 4.25 Energy Balance Diagram with 40% Efficient Solar Cells on September 23 at 45000 ft	113
Figure 4.26 Energy Balance Diagram with 40% Efficient Solar Cells on December 21 at 45000 ft	114
Figure 4.27 Energy Balance Diagram for Continuous Flight	114
Figure 5.1 Yearly PV System Costs and Prediction per kW [53].....	116
Figure 5.2 Production Quantity vs Total Cost per Aircraft with 30% and 40% Efficient Solar Cells	118
Figure 5.3 Annual Reduction in the Cost of TUYGUN Thanks to Decreasing in Solar Cell Prices.....	119

LIST OF SYMBOLS

A	Weight estimation constant
α_{CLmax}	Angle of attack where the maximum lift occurs
AR	Aspect ratio
b	Span
c	Chord
c_t	Thrust specific fuel consumption
C	Weight estimation constant
C_{fe}	Skin friction coefficient
C_{Lmax}	Maximum lift coefficient
$C_{L,TO}$	Takeoff lift coefficient
$C_{m\alpha}$	Moment coefficient
C_{D0}	Zero lift coefficient
c_{vt}	Vertical tail volume coefficient
c_{ht}	Horizontal tail volume coefficient
D	Drag
D_m	Fuselage maximum deep
e	Oswald span efficiency factor
HALE	High Altitude Long Endurance
ISR	Intelligence, Surveillance and Reconnaissance
j	Ground roll parameter
l	Length of fuselage
K_{vs}	Weight estimation factor
K_f	Position for quarter chord

L/D	Lift to drag ratio
L_f	Length of fuselage
n	Load factor
P	Power
q	Dynamic pressure
R	Range
R/C	Rate of climb
Re	Reynolds number
S	Area
S_w	Wing area
S_{ref}	Wing reference area
S_g	Ground roll distance
T	Thrust
T/W	Thrust loading
UAV	Unmanned aerial vehicle
V_v	Rate of climb
V	Velocity
W	Weight
W_m	Fuselage maximum width
W/S	Wing Loading
μ_r	Ground friction coefficient
λ	Taper ratio
η	Propeller efficiency
μ	Dynamic viscosity
ρ	Density

CHAPTER 1

INTRODUCTION

Solar powered aircraft systems have been studied approximately since 40 years. As shown in Figure 1.1, one could see the improvement in solar cell technology in terms of cell efficiency, which is promising for solar-based aircraft concept when compared to conventional long endurance aircraft. The most recent solar-based aircraft are the Solar Impulse and Qinetiq Zephyr aircraft systems which are using solar cells with efficiency of 22% and 28%, respectively. Moreover, GaAs-based solar cells with around 30% efficiency are commonly used in space industry and this technology has almost exceeded 40% of efficiency recently. Although the cost of this technology is high at the moment, the use of GaAs-based solar cells in airborne and spaceborne missions in the near future will be commonly used, decreasing the cost for affordable missions.

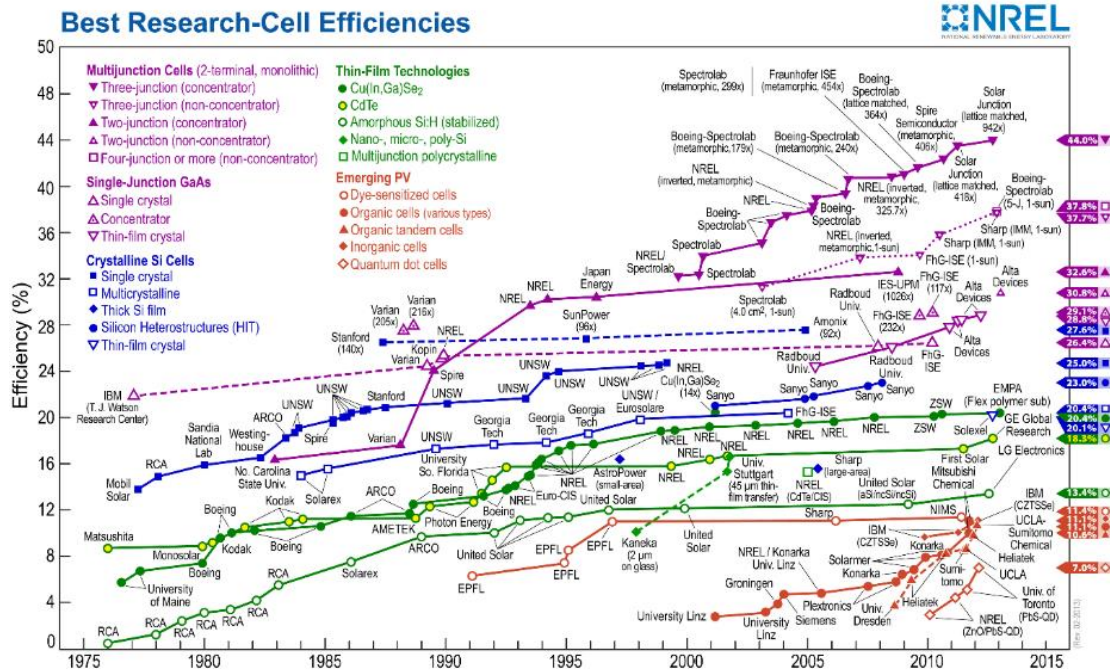


Figure 1.1 Solar Cell Efficiency Yearly Development [4]

Due to the fact that the solar radiation is available only during daytime, the battery is the only source of power during night flight. Solar Impulse is one of the most important competitor for this study because of its battery technology. Solar Impulse obtains its nighttime energy from 4 pieces of 164 kWh Li-Ion battery. The mass of batteries must be as light as possible for solar airplanes. Solar Impulse has four batteries which are approximately 361 lb each [5]. Figure 1.2 indicates improvement of energy density of the Li-Ion batteries.

Energy density of batteries has been increasing for years. [Figure 1.2, red line] However, cost of energy obtained from batteries has been decreasing. [Figure 1.2, blue line]. Energy density of batteries per lb has been increasing. [Figure 1.2, grey line]

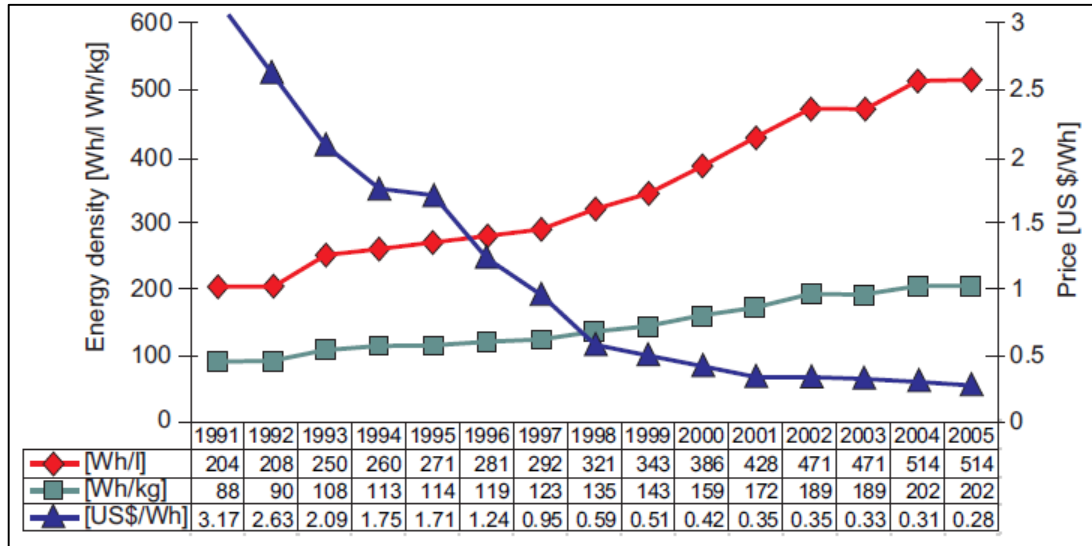


Figure 1.2 Lithium-ion Battery Energy Density Evaluations [8]

High altitude long endurance (HALE) aircraft systems have some typical specifications, such as high wing aspect ratio, very long wingspan, large wing area, low wing loading etc. Mentioned specifications are similar with solar based systems. However, solar aircraft systems have poor payload carrying capacity and climbing to high altitudes with heavy payload is almost impossible. Therefore a small turbofan engine is crucial to compensate for accommodating the heavy payload and attaining high altitudes.

This thesis is the combination of two difficult design studies. Also it is the first aircraft design study, which is including a turbofan engine and solar cell and battery together.

This thesis is composed of six chapters. The first chapter focuses mainly on solar cell and battery technology developments, history of solar powered systems and HALE systems. The second chapter includes conceptual design, namely sizing of the aircraft components such as wing, fuselage, horizontal and vertical tails, weight predictions and thrust and wing loadings. In the third chapter, the performance characteristics such as lift, drag and maximum velocity of the aircraft are calculated. In the fourth chapter, available solar battery energy calculations are performed. In the fifth chapter, cost analysis of the system

is performed. Last chapter includes the conclusion of the design processes. In this part simulation results are also discussed.

1.1. Solar Powered Airplanes

History of solar powered flight began in November 1974 with Sunrise I [9]. It had a 32 ft wingspan, and it was a 27.6 lb airplane. Solar cells produced 450 watt power, which allowed Sunrise I to fly 20 minutes. Later, in 1975 some improvements were performed on the airplane such as decreasing its weight and increasing its solar cell quantity. Solar cells had 14% efficiency and delivered 600 watts of energy.



Figure 1.3 Sunrise I [9]

After trying solar power on model airplanes, scientists began to study manned solar powered flight. If model airplanes are disregarded, the world's first solar powered airplane was designed by Britons David Williams in 1978. Solar One had a 68 ft wingspan and 258 ft² wing area, Figure 1.4. It weighed 229 lb and had approximately a 79 ft service ceiling. Designers used nickel-cadmium batteries.



Figure 1.4 Solar One [12]

Another crucial solar powered aircraft study is designed by Aerovironment and Paul MacCready. Gossamer Condor and Gossamer Albatros, which were human powered airplanes, were designed in 1977 and 1979 respectively by Paul MacCready. Success of Solar One gave an idea for converting Gossamer airplane series to a solar powered airplane called Gossamer Penguin, Figure 1.5. It had a 71 ft wingspan and a 297 ft² wing area, weighing approximately 67.8 lb.



Figure 1.5 Gossamer Penguin [13]

After designing Gossamer Series Aerovironment and Paul MacCready began their studies with a new airplane whose service ceiling was higher than Gossamer Penguin called Solar

Challenger which was able to fly up to 11000 ft, Figure 1.6. It had a 56.6 ft wingspan and 5 hour 23 min endurance. 16128 solar cells provided the airplane up to 2500 watt power at sea level.



Figure 1.6 Solar Challenger [14]

Sunseeker which was designed in 1990 is another important solar power airplane application, Figure 1.7. It had a 55.8 ft long wingspan. It flew about 5.5 hours.



Figure 1.7 Sunseeker [15]

Icare 2, which was designed in 1996 by Prof Rudolf Voit-Nitschmann from Stuttgart University was the fastest solar powered airplane in 1996. It had a 109.3 ft/s maximum speed, Figure 1.8.



Figure 1.8 Icare 2 [56]

After manned solar powered aircraft, in the late 1990s some design considerations were changed. Some scientists were interested in fuel cell technology in order to achieve perpetual endurance, but this technology was not developed enough. In 2001, solar powered aircraft designers' vision changed. The new challenge was to reach very high altitudes. NASA designed Helios aircraft which set a record by climbing to 96000 ft and flying approximately 40 minutes at that altitude, Figure 1.9. Although at higher altitudes wind speed is low, which is very advantageous for light airplanes, low air density does not provide enough cooling for solar cells. Low wind speed is very crucial for solar powered airplanes, since solar powered airplanes must have very light structural weight. Designed for attaining perpetual endurance, Helios faced a serious crash on June 26, 2003. Structural vibration led to failure of the wing.



Figure 1.9 NASA Helios [16]

The most important development in continuous flight occurred in 2005 with Solong which, flew approximately 48 hours, Figure 1.10. The main aim of the project was to perform continuous flight. Consequently, the size of the airplane was relatively small. It had a 15.6 ft wingspan, weighed 28.2 lb and it needed 95 Watts of energy to sustain level flight.

With Solong, the dream of continuous flight came true and new designs emerged. One such new design was Sky Sailor created by Andre Noth, Figure 1.10. Andre Noth, published his PhD Thesis about solar powered continuous flight. His study focused mainly on attaining continuous flight. His demonstrations about the solar energy cycle in the thesis aims to simulate loiter the time of the aircraft. Sky sailor is a relatively small airplane which has 5.7 lb structural weight and a 11.8 ft wingspan. Thanks to its lithium-ion battery, it achieved 28 hour flight at 650 to 1300 feet above the ground.



Figure 1.10 Solong UAV (left) [17] and Sky Sailor (right) [18]

In 2005, Qinetiq firm designed a solar powered HALE UAV system called Zephyr. [19] Zephyr is an innovative platform because of its 54 hour endurance. Zephyr climbed to 58000 ft km altitude in 2007. It is a relatively bigger airplane compared to Solong. It has a 59 ft wingspan and weighs 66 lb, Figure 1.11.

Solar Impulse [20], a Swiss project, is another important solar power airplane application. It performed its first flight in 2009. Solar Impulse 1 had 208 ft wingspan and weighed only 3528 lb, Figure 1.11. It had 4 electric motors and efficient lithium-ion batteries which weighed approximately 1446 lb and delivered 21 kWh power each. The first design could perform 36 hours of flight. Then, the firm decided to improve the first design and in 2014 Solar Impulse design was begun. It had a 236 ft wingspan and weighed about 5070 lb. The cruise speed of first design was 64 ft/s; on the other hand, the cruise speed of Solar Impulse 2 was 70.1 ft/s. It has not become an operational airplane yet since some problems aroused in the batteries.



Figure 1.11 Zephyr (left) [19] and Solar Impulse 2 (right) [20]

The last important application is the Boeing Solar Eagle [21]. It is an ongoing project. The aim of the project is to attain one month endurance. It uses fuel cell to provide power at night. It has 400 ft wingspan and has the capacity to carry 1103 lb payload.



Figure 1.12 Boeing Solar Eagle [21]

1.2. Reconnaissance HALE Airplanes

Throughout history HALE airplanes have been very striking. Probably the most important and practical HALE category aircraft in the history is Lockheed U-2 since it is still in service in the US Air Force. U-2 performed its first flight in 1955. Its service ceiling is 65000 ft.



Figure 1.13 U2-S (left) [49] and RB-57F Canberra (right) [22]

Then in 1963 Martin/General Dynamics RB-57F Canberra was developed, Figure 1.13. It had a 32000 lb power plant, a 123 ft wingspan, an 82000 ft service ceiling and 0.79 Mach maximum speed. It was retired in 1974.

Boeing Condor is another important high altitude aircraft application which was developed in 1988. It had a 194 ft wingspan and a 65000 ft service ceiling. During flight tests in 1989, it attained 80 hour endurance.

Scaled Composites Proteus which was developed in 1998 is another inspiring design for high altitude category airplanes, Figure 1.14. It attained 65000 ft service ceiling.



Figure 1.14 Boeing Condor (left) [29] and Proteus (right) [23]

In 1998 a successfully designed HALE UAV began to fly called Global Hawk. Global Hawk is a surveillance unmanned aircraft. It had a 131 ft wingspan and weighed 32250 lb. Global Hawk 4B can fly approximately 32 hours at 65000 ft altitude.

Heron TP, known as AIA Eitan, was developed in 2004, Figure 1.15. It is a twin boom pusher aircraft which has a 85.3 ft wingspan, a 4410 lb payload capacity, a 9000 kW power plant. During test flight Heron TP attained 70 hour endurance. Service ceiling of Heron TP is 15 km. Heron TP is still in service.

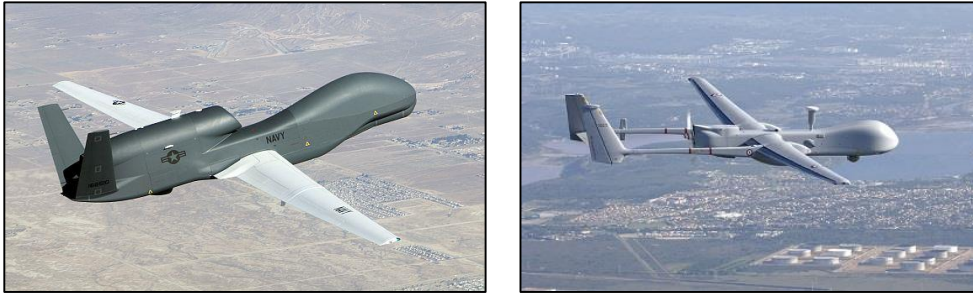


Figure 1.15 Global Hawk (left) [28] and Heron TP (right) [24]

In 2010 Global Observer was designed by Aerovironment. It uses hydrogen fuel cell and it had an electric powered engine. Global Observer has a 170 ft wingspan and its service ceiling is 50000 ft.

In 2012 another hydrogen powered HALE UAV called Phantom Eye began to fly. It was designed by Boeing. Unlike Global Observer, it had a turbine engine. Phantom Eye has a 151 ft wingspan and it can fly up to 4 days at 65000 ft altitude. Hydrogen propulsion UAV (Global Observer and Phantom Eye) designs have not finished yet.



Figure 1.16 Global Observer (left) [27] and Phantom Eye (right) [50]

1.3. Competitor Study

Since there is no hybrid aircraft designs in the literature, competitor aircrafts have been chosen among HALE UAVs and solar powered UAVs.

Table 1.1 Competitor Aircrafts

Aircraft	Phantom Eye 2010	Global Observer 2 2005	Global Hawk 1998	Lockheed U2S 2010	Condor 1989
Length	52.5 ft	82 ft	46 ft	63 ft	49.2 ft
Wingspan	213.2 ft	259 ft	115 ft	103 ft	193.4 ft
Empty Weight	8157 lb	6063 lb	8490 lb	31526 lb	7937 lb
Gross Weight	10055 lb	9189 lb	22900 lb	40785 lb	20062 lb
Propulsion	Hydrogen	Hydrogen	Turbofan	Turbofan	Turboprop
Engine	2x112 kW	Electric	31 kN	86 kN	130 kW
Range	42651 ft	56758 ft	82000 ft	33820 ft	--
Endurance	7 days	7 days	36 hours	12 hours	80 hours
Service Ceiling	65000 ft	65000 ft	65000 ft	70000 ft	65000 ft

There are very few aircraft which are designed to fly at 45000 ft between 65000 ft altitudes. Most important restriction for flying at high altitudes is the very low air density and low temperature. Subsystems need heater due to cold weather conditions. At 65000 ft altitude, density of air decreases by 14 times and pressure decreases by 18 times compared to sea level conditions. Also temperature decreases up to -80°C at 65000 ft, see Table 1.2.

Table 1.2 Air Conditions Variations with Altitude

Altitude (ft)	Temperature (°C)	Pressure (lb/ft²)	Density (10⁻³ slugs/ft³)	Dynamic Viscosity (10⁻⁷ lb.s/ft²)	Speed of sound (ft/s)
0	15.0	2116.2	2.38	3.74	1115.5
15000	-21.9	1194.8	1.50	3.43	1049.9
30000	-44.4	629.7	0.089	3.11	980.95
45000	-56.5	309.5	0.0462	2.97	968
65000	-56.5	118.9	0.0178	2.97	968
80000	-52.2	58.5	0.0086	3.02	968

1.4. Design Process

Conceptual design of a HALE hybrid UAV is very difficult, since many design books are about designing general aviation aircraft or known airplane types, which belong mainly to the MALE class aircraft. After examining HALE class UAVs, some typical properties are noted, such as they have high wing loadings, high aspect ratios, very efficient airfoils having high lift to drag ratio, etc. Therefore, many prediction methods do not work such as prediction of structural weight. Leland M. Nicolai [2] developed new weight prediction methods which are fitted to the HALE Hybrid UAV. Gliders are the most inspiring models for long endurance flight. When performance calculations are performed it is seen that one who wants to design a HALE UAV should examine the glider's airfoils before selecting an appropriate airfoil. Another important characteristic of the HALE UAVs is, they fly at high angle of attack. It is observed that some airplanes loiter at 8-10 degree angle of attack. Therefore airfoils, whose stall angles are high, are taken into account when choosing an appropriate one.

Second part of the design is about solar power calculations and battery survey of the aircraft. This part is also very difficult to establish since solar powered UAV studies give very little information about the design process. But as mentioned in the theory part, this type of airplane is very striking. Therefore solar systems have been studied extensively since 1970s. The first study was published by F.G. Irving in 1974[4]. The paper was mainly about the prediction of the weight of the solar powered airplanes. Author used glider's statistical data to construct the weight prediction model. It was a very successful model since this model is still being used by the designers. But this model does not work for large scale airplanes. The first solar powered airplanes, Sunrise and Solaris were designed in 1974 and 1975 respectively. But designers of the Sunrise and Solaris kept their methodology secret. Afterwards, Gossamer series aircrafts and Solar Challenger were designed, but there is no information about design methods. In 1984 a new method, guessing structural weight of a solar powered airplane, was constructed by David and Stan

Hall. [4] But this method works for relatively small size airplanes such as having 2200 to 6614 lb weight.

In 2005 Zephyr was designed. But designers did not give any information about solar cycle. Three years later in 2008, Andre Noth designed a solar powered UAV system called Sky Sailor. Thanks to this relatively open sourced study, structure of the solar cycle could be understandable. Using solar radiance equations and a Simulink model which was constructed by Andre Noth, a solar cycle model is constructed. In addition to this, in 2015 Servet Güçlü Özcan thesis was published which is an important project for small size solar powered aircraft designers. His study is mainly about designing a solar powered flying wing and testing solar avionics for small size solar powered flying wings.

HALE UAV name is TUYGUN. TUYGUN is a hunter bird which has a large and very light wing. Aspect ratio of their wings is high. They live in eastern and central Anatolia in Turkey.



Figure 1.17 TUYGUN

CHAPTER 2

CONCEPTUAL DESIGN

2.1. Competitor Study Outputs

Before starting the conceptual design methodologies, it is essential for designers to emphasize that most of the airplane designs are evolutionary not revolutionary. Therefore choosing suitable competitor aircraft and specifying applicable requirements is very important. The conceptual design begins with requirements. Hybrid UAV design requirements are stated in Table 2.1.

Table 2.1 Requirements

Payload	Endurance	Range	Cruise Speed	Service Ceiling	Stall Speed @ sea level	Rate of climb
(lb)	(hour)	(nm)	(ft/s)	(ft)	(ft/s)	(ft/s)
2205	24-48	1000	115	30000-65000	50	10

The competitor study is performed to predict the aircraft initial geometric and weight values, for instance, aspect ratio, and weight fractions. From the competitor study, average empty weight fraction is found as 0.6218, aspect ratio is found as 24.5. L/D_{max} is assumed as 40, average wingspan is calculated as 218 ft and average chord length is calculated as 8 ft.

2.2. Mission Profile

Simple cruise and loitering mission profile is sketched in Figure 2.1; Segment 0-1 indicates the engine start taxi and takeoff, segment 1-2 represents climb, phase 2-3 represents cruise, segment 3-4 represent loiter, segment 4-5 represents cruise back, segment 5-6 represents descent, and segment 6-7 represents landing and stop.

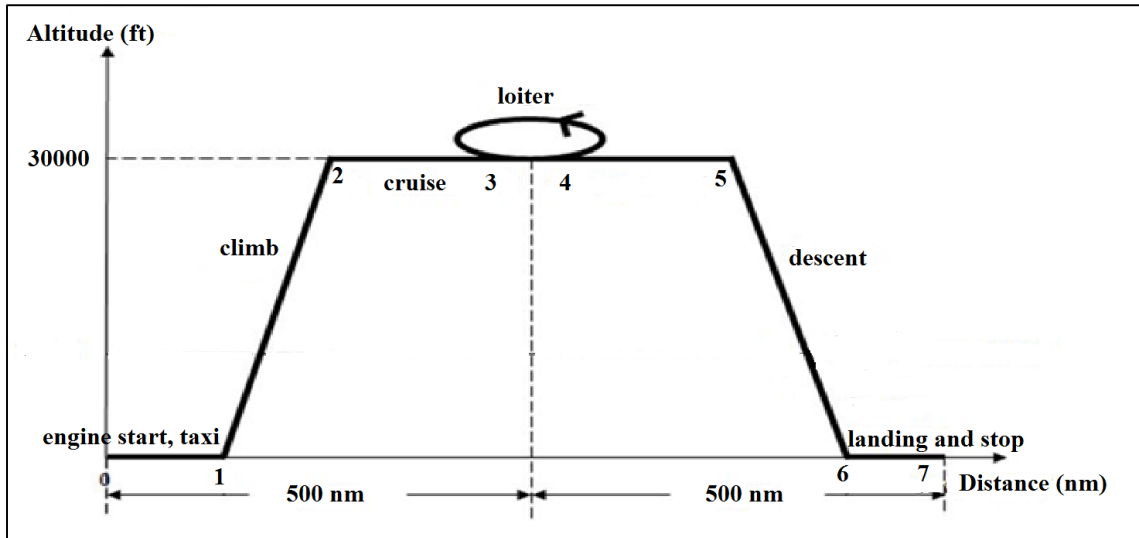


Figure 2.1 Mission Profile

2.3. Estimation of the Design Takeoff Gross Weight, W_0

Takeoff gross weight is the total aircraft weight including crew, payload, empty and fuel weights.

$$W_0 = W_{crew} + W_{payload} + W_{fuel} + W_{empty} \quad 2.1$$

While estimating takeoff gross weight Table 2.2 is used. Constants which are for high altitude UAV are used in equation 2.2 for calculations. $A = 2.75$, $c = -0.18$ and $K_{v_s} = 1$ For fixed sweep wing.

Table 2.2 Empty Weight Fraction vs W_0 [1]

$W_e/W_0=A(W_0)^cK_{vs}$	A	A-metric	C
Sailplane-unpowered	0.86	0.83	-0.05
Sailplane-powered	0.91	0.88	-0.05
Homebuilt-metal/wood	1.19	1.11	-0.09
Homebuilt-composite	1.15	1.07	-0.09
General aviation-single engine	2.36	2.05	-0.18
General aviation-twin engine	1.51	1.4	-0.10
Agricultural aircraft	0.74	0.72	-0.03
Twin turboprop	0.96	0.92	-0.05
Flying boat	1.09	1.05	-0.05
Jet trainer	1.59	1.47	-0.10
Jet fighter	2.34	2.11	-0.13
Military cargo/bomber	0.93	0.88	-0.07
Jet transport	1.02	0.97	-0.06
UAV-Tac Recce & UCAV	1.67	1.53	-0.16
UAV-High altitude	2.75	2.48	-0.18
UAV-small	0.97	0.86	-0.06

$$\frac{W_e}{W_0} = K_{vs}A(W_0)^c \quad 2.2$$

Equation 2.2 is used for calculating the empty weight fraction of the aircraft.

2.4. Estimation of the Fuel Weight Fraction

Fuel weight depends on the mission to be flown, the fuel consumption rate of the engine and aerodynamics of the aircraft. As indicated in Figure 2.1, mission profile is separated into 7 parts. Each phase of the mission is represented by a weight fraction. At the end of the mission, all weight fractions are multiplied and fuel weight fraction is calculated. For

a simple cruise mission Raymer [1] describes fuel weight and gross weight calculations (equation 2.2 to 2.12) as follows;

$$W_f = W_0 - W_7 \quad 2.3$$

Where W_f represents the fuel weight of the aircraft and W_0 symbolizes the takeoff weight of the aircraft. It is assumed that the fuel tanks are completely empty at the end of the flight. The weight fractions for each phase is calculated as follows.

(0-1) For the engine start, taxi and takeoff, historical trend is used: [1]

$$\frac{W_1}{W_0} = 0.97 \quad 2.4$$

W_0 is the takeoff weight of the aircraft.

(1-2) For climb, historical trend is used [1]

$$\frac{W_2}{W_1} = 0.985 \quad 2.5$$

Where W_2 is the weight of the aircraft at the beginning of cruise.

(2-3) For cruise, Breguet range equation is used: [1]

$$\begin{aligned} \frac{W_3}{W_2} &= \exp\left(\frac{-Rc_t}{V(L/D)}\right) \quad 2.6 \\ &= \exp\left(\frac{-6076100 \times 1.11 \times 10^{-4}}{2 \times 110 \times (34.64)}\right) = 0.9759, \end{aligned}$$

Where W_3 is the weight of the aircraft at end of the cruise.

Where $\left(\frac{L}{D}\right)_{cruise} = 0.866 \times \left(\frac{L}{D}\right)_{max}$ and specific fuel consumption is taken as 0.4.

(4-5) Cruise back:

$$\frac{W_5}{W_4} = \frac{W_3}{W_2} \quad 2.7$$

Where W_4 is the weight of the aircraft at end of the loiter and W_5 is the weight of the aircraft at end of the cruise back.

(5-6) For descent, historical trend is used: [1]

$$\frac{W_6}{W_5} = 0.992 \quad 2.8$$

W_6 is the landing weight of the aircraft.

(6-7) For landing and stop, historical trend is used: [1]

$$\frac{W_7}{W_6} = 0.993 \quad 2.9$$

As a result:

$$\begin{aligned} \frac{W_7}{W_0} &= \frac{W_7}{W_6} \frac{W_6}{W_5} \frac{W_5}{W_4} \frac{W_4}{W_3} \frac{W_3}{W_2} \frac{W_2}{W_1} \frac{W_1}{W_0} \\ &= 0.7896 \end{aligned} \quad 2.10$$

$$\begin{aligned} \frac{W_f}{W_0} &= 1.06 \left(1 - \frac{W_7}{W_0} \right) \\ &= 0.223 \end{aligned} \quad 2.11$$

assuming that 6% is the reserve or trapped fuel. Using the takeoff gross weight estimation equation.

$$W_0 = \frac{W_{payload}}{1 - 2.75(W_0)^{-0.18} - \frac{W_f}{W_0}} \quad 2.12$$

Takeoff gross weight and fuel weight is calculated as

$$W_0 = 9050 \text{ lb and } W_f = 2018.3 \text{ lb}$$

2.5. Trade-off Study

In this section effects of range and payload changes on aircraft gross weight is studied.

2.5.1. Payload Trade

In this section effects of payload variations on takeoff gross weight is studied using equation 2.12.

Table 2.3 Payload Trade

Payload (lb)	Takeoff Gross Weight (lb)
500	3485
1000	5285
1500	6913
2000	8445
2500	9914

2.5.2. Range Trade

In this section effects of range variations on takeoff gross weight is studied.

Table 2.4 Range Trade

Range (nautical mile)	Takeoff Gross Weight (lb)
150	6407
250	6660
500	7350
1000	9050
2000	14503

2.6. Airfoil and Wing Planform Selection

When design lift coefficient is selected for the cruise condition and loitering condition, almost all low speed high lift airfoils in other words low Reynolds number airfoils are examined. As indicated before both HALE and solar aircrafts must have high glide ratio airfoils. These type of airfoils is designed for providing long endurance flight. They have very high glide ratio which makes endurance longer. Also they let aircrafts cruise and

loiter at low velocities. Low speed high lift airfoils are analyzed using XFLR5 [33] and the most suitable one is chosen. This program uses vortex lattice method, 3D panel method and lifting line theory when predicting lift and drag values of the airfoils and wings. Panel method is used for analysis. At first, design lift coefficient is found from equation 2.13, for cruise;

$$W = L = 0,5 \times \rho \times V^2 \times S \times C_L \quad 2.13$$

There are two ways for guessing the wing area of the aircraft: Using competitor's average wing loading which is not suitable for hybrid platform is the first one, assuming a wing loading value using literature survey is the second one. During literature review it is seen that solar powered airplanes have very low wing loadings such as 2-3 lb/ft². Many solar powered design's wing loadings are very similar with gliders. On the other hand, high altitude platforms have higher wing loadings than solar powered aircraft. Competitor aircraft which use alternative fuel, Boeing Phantom Eye and Aerovironment Global Observer, have approximately. Wing loading of 5 lb/ft² which is nearly twice of the solar powered platform's wing loading. Boeing Condor has approximately 17 lb/ft² wing loading. Finally, it is estimated that competitor's average wing loading is approximately 5 lb/ft². 5 lb/ft² wing loading is used only for predicting the thrust to weight ratio term in the instantaneous and sustained turn wing loading calculations.

$$\frac{W}{S} = 0.5 \times \rho \times V^2 \times C_L ,$$

Density of air at 30000 ft is 0.000891 slugs/ft³. Lift coefficient can be calculated as follows:

$$5 = 0.5 \times 0.000891 \times 110^2 \times C_L$$

$$C_L = 0.93$$

Lift coefficient, found above, is a relatively high cruise lift coefficient for an aircraft. This condition can be satisfied only by using low speed high lift airfoils. During literature

review it is observed that HALE platform's cruise lift coefficients are between 0.9 and 1.75.

Airfoil selection is a very important issue for designers. Since it affects the entire aerodynamics of the aircraft. Airfoils designed for low speed and high lift are examined carefully at three different altitudes and listed in Table 2.5, Table 2.6, and Table 2.7.

Table 2.5 Airfoil Properties at Sea Level




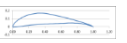


Properties (Re=7800000)	Fx63_137sm 	S1210 	S1223rtl 	Fx74cl5140 	Eppler422 	S1223 
Max thickness	13.70%	12%	12.10%	13.10%	14%	12.1%
Max C_l/C_d	209	201	182	260	251	197
$(C_l)_{max}$	2.15	2.07	2.46	2.09	2	2.4
α stall	14	-	15	11	14	-
$C_{di} @ (C_l)_{max}$	0.027	-	0.033	0.0345	0.0179	-
$C_m @ (C_l)_{max}$	-0.165	-	-0.198	-0.215	-0.085	-
$C_l @ (C_l/C_d)_{max}$	1.09	1.38	1.95	1.88	1.5	1.86
$\alpha @ (C_l/C_d)_{max}$	1	2	7	5	7	5

Table 2.6 Airfoil Properties at 30000 ft Altitude



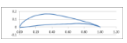
Properties (Re=1850000)	Fx63_137sm 	S1210 	S1223rtl 	Fx74cl5140 	Eppler422 	S1223 
Max thickness	13.70%	12%	12.10%	13.10%	14%	12.1%
Max C_l/C_d	176	167	127	186	181	145
$(C_l)_{max}$	2.05	2.07	2.52	2.23	1.935	2.35
α stall	17	13	16	9	13	14
$C_{di} @ (C_l)_{max}$	0.068	0.045	0.035	0.125	0.015	-
$C_m @ (C_l)_{max}$	-0.14	-0.18	-0.19	-0.22	-0.09	-
$C_l @ (C_l/C_d)_{max}$	1.17	1.57	1.69	2.15	1.58	1.91
$\alpha @ (C_l/C_d)_{max}$	1	2	7	5	7	5

Table 2.7 Airfoil Properties at 65000 ft Altitude

Properties ($Re=700000$)	Fx63_137sm	S1210	S1223rtl	Fx74cl5140	Eppler422	S1223
Max thickness	13.70%	12%	12.10%	13.10%	14%	12.1%
Max C_l/C_d	143.5	130.78	89.2	113	125	109
$(C_l)_{max}$	1.87	2.015	2.42	2.3	1.93	2.27
α stall	15	12	18	12	14	12
$C_{di} @ (C_l)_{max}$	0.066	0.037	0.063	0.024	0.022	0.028
$C_m @ (C_l)_{max}$	-0.13	-0.18	-0.16	-0.22	-0.08	-0.22
$C_l @ (C_l/C_d)_{max}$	1.26	1.73	1.71	2.157	1.54	1.74
$\alpha @ (C_l/C_d)_{max}$	3	6	6	9	8	5

After analyzing airfoils, a wing geometry is predetermined in order to see the airfoil performance on the wing. Under the same conditions with 2D analysis, airfoil 3D analysis are performed at three different altitudes. Like 2D analysis, 3D analysis are done by XFLR5 using panel method. [33]. Wing is analyzed for 3 and 0 degree angle of attack in order to calculate the lift curve slope. Analysis are performed with unit chord length and velocity

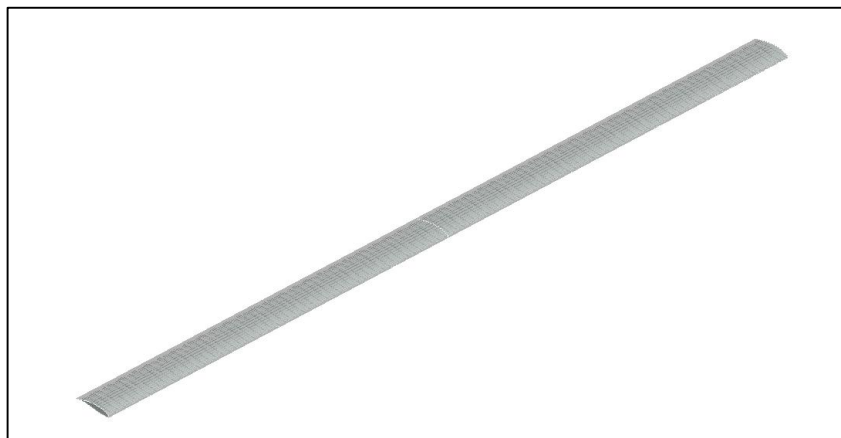


Figure 2.2 Sample Wing Geometry

Table 2.8 3D Properties at Sea Level







Properties (Re=780000)	Fx63_137sm 	S1210 	S1223rtl 	Fx74cl5140 	Eppler422 	S1223 
$C_L @3$	1.06	-	1.33	-	0.89	1.34
$C_{Di} @3$	0.03	-	0.04	-	0.02	0.04
$L/D@3$	37.88	-	30.33	-	41.12	30.24
$C_m @3$	-0.46	-	-0.60	-0.57	-0.35	-0.61
$C_m @0$	-0.39	-	-0.53	-0.50	-0.27	-0.55
$C_L @0$	0.77	-	-	-	0.61	-
$C_{Di} @0$	0.02	-	-	-	0.01	-
$L/D@0$	44.78	-	-	-	45.68	-
$(L/D)_{max}$	-	-	-	-	45.68	-
$C_L @(L/D)_{max}$	-	-	-	-	0.61	-
$a@(L/D)_{max}$	-	-	-	-	0.00	-

Table 2.9 3D Properties at 30000 ft Altitude













Properties (Re=1850000)	Fx63_137sm 	S1210 	S1223rtl 	Fx74cl5140 	Eppler422 	S1223 
$C_L @3$	1.06	1.23	1.33	1.33	0.90	1.34
$C_{Di} @3$	0.02	0.03	0.04	0.04	0.02	0.04
$L/D@3$	36.67	32.03	27.19	27.64	38.50	27.73
$C_m @3$	-0.46	-0.55	-0.60	-0.57	-0.35	-0.61
$C_m @0$	-0.39	-0.48	-0.53	-0.50	-0.27	-0.55
$C_L @0$	0.77	-	1.05	-	0.61	1.07
$C_{Di} @0$	0.018	-	0.04	-	0.01	0.04
$L/D@0$	42.52	-	29.94	-	40.95	26.76
$(L/D)_{max}$	43.30	-	30.20	27.64	40.95	27.73
$C_L @(L/D)_{max}$	-	-	-	-	0.61	-
$a@(L/D)_{max}$	-	-	-	-	0.00	-

Table 2.10 3D Properties at 65000 ft Altitude

Properties (Re=700000)	Fx63_137sm	S1210	S1223rtl	Fx74cl5140	Eppler422	S1223
						
$C_L @3$	1.06	1	1	1	0.89	1
$C_{Di} @3$	0.03	0.04	0.05	0.05	0.02	0.05
$L/D@3$	35.2	30.32	26.04	25.25	34.87	26.75
$C_m @3$	-0.46	-0.55	-0.59	-0.57	-0.34	-0.61
$C_m @0$	-0.39	-0.48	-0.53	-0.5	-0.27	-0.55
$C_L @0$	0.77	0.94	1	1	0.60	1
$C_{Di} @0$	0.02	0.02	0.03	0.04	0.01	0.03
$L/D@0$	40.1	33.8	28.35	22.44	35.73	28.06
$(L/D)_{max}$	41	34	28.35	25.5	36.3	28.1
$C_L @(L/D)_{max}$	0.72	0.85	1.05	1.4	0.71	1.07
$a@(L/D)_{max}$	-1	-1	0	4	1	0

After all analysis, it is seen that Fx_63_137sm is the best alternative for Hybrid UAV, since it has the highest glide ratio, higher stall angle than other airfoils and high design lift coefficient.

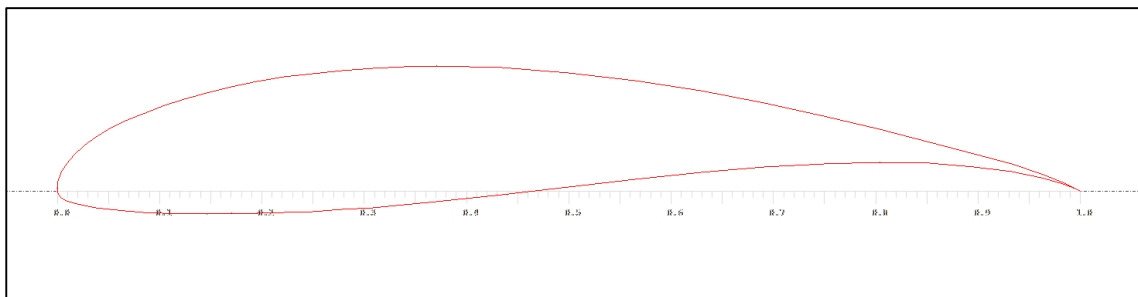


Figure 2.3 Fx_63_137sm Airfoil

2.7. Aspect Ratio

As mentioned before, HALE and solar airplanes have high aspect ratio. With such aspect ratio values, these airplanes resemble gliders, so it is appropriate to use gliders constants in Table 4.1 [1] to determine the aspect ratio.

$$AR = 0.19(L/D)_{max}^{1,3} \quad 2.14$$

Result of equation 2.14 is 23, but using average aspect ratio of the competitor aircrafts which is 24.5, is more convenient.

2.8. Thrust to Weight Ratio

Since there is no hybrid UAV design, it is not convenient to follow historical trend. Using general aviation aircraft design methodology is more convenient since Hybrid UAV uses turbofan engine during climb and cruise. Aircraft service ceiling is determined after solar energy and battery energy calculations are finished.

2.8.1. Thrust to Weight Ratio for a Level Constant-Velocity Turn

Equation 2.15 is used for verifying minimum thrust for an airplane to sustain loitering at service ceiling. For this calculation, Table 3.1 [3] is used.

$$\frac{T}{W} = q \left[\frac{C_{D,min}}{\left(\frac{W}{S}\right)} + K \left(\frac{n}{q}\right)^2 \frac{W}{S} \right] \quad 2.15$$

Table 2.11 Typical Aerodynamic Characteristics of Selected Classes of Aircraft [3]

Class	C _{Dmin}	C _{DTO}	C _{LTO}	Comment
Amphibious	0.040-0.055	0.050-0.065	0.7	Assumes flaps in T-O position.
Agricultural	0.035-0.045	0.045-0.055	0.7	Assumes flaps in T-O position.
Biplane	0.045-0.050	0.045-0.050	0.4	Assumes flaps in T-O position.
GA trainer	0.030-0.035	0.040-0.045	0.7	Assumes flaps in T-O position.
GA high-performance single	0.025-0.027	0.035-0.037	0.7	Assumes flaps in T-O position.
GA typical single, fixed gear	0.028-0.035	0.038-0.045	0.7	Assumes flaps in T-O position.
Turboprop commuter	0.025-0.035	0.035-0.045	0.8	Assumes flaps in T-O position.
Turboprop military trainer	0.022-0.027	0.032-0.037	0.7	Assumes flaps in T-O position.
Turbofan business jet	0.020-0.025	0.030-0.035	0.8	Assumes flaps in T-O position.
Modern passenger jetliner	0.020-0.028	0.030-0.038	0.8	Assumes flaps in T-O position.
1960s-70s passenger jetliner	0.022-0.027	0.032-0.037	0.6	Assumes flaps in T-O position.
World War II bomber	0.035-0.045	0.045-0.055	0.7	Assumes flaps in T-O position.
World War II fighter	0.020-0.025	0.030-0.035	0.5	Assumes flaps in T-O position.

2.8.2. Thrust to Weight Ratio for Desired Rate of Climb

The following equation is used for ascertaining the desired rate of climb. Where V_V is the desired rate of climb.

$$\frac{T}{W} = \frac{V_V}{V} + \frac{q}{\left(\frac{W}{S}\right)} C_{D,min} + \frac{K W}{q S} \quad 2.16$$

2.8.3. Thrust to Weight Ratio for a Desired Takeoff Distance

The following equation is for ascertaining to achieve desired takeoff distance.

$$\frac{T}{W} = \frac{(V_{lof})^2}{2\rho S_g} + q \frac{C_{D,TO}}{\left(\frac{W}{S}\right)} + \mu \left[1 - q \frac{C_{L,TO}}{\left(\frac{W}{S}\right)} \right] \quad 2.17$$

Where V_{lof} is lift-off speed which is taken as 1.1 times V_{stall} . S_g , is the desired takeoff distance, is taken as 2000 ft. The ground friction constant μ is taken as 0.4. Takeoff lift coefficient $C_{L,TO}$, is taken as 2, which is found from XFLR5.

2.8.4. Thrust to Weight Ratio for a Desired Service Ceiling

The following equation is used for verifying required thrust to weight ratio at service ceiling.

$$\frac{T}{W} = \frac{V_V}{\sqrt{\frac{2}{\rho_\infty} \sqrt{\frac{K}{3C_{D,min}} \frac{W}{S}}}} + 4 \sqrt{\frac{KC_{D,min}}{3}} \quad 2.18$$

2.8.5. Thrust to Weight Ratio for a Desired Cruise Speed

The following equation is used for verifying minimum thrust for airplane to sustain cruise at desired speed.

$$\frac{T}{W} = q \left[\frac{C_{D,min}}{\left(\frac{W}{S}\right)} + K \frac{1}{q} \frac{W}{S} \right] \quad 2.19$$

After all calculations thrust loading versus wing loading graph is drawn.

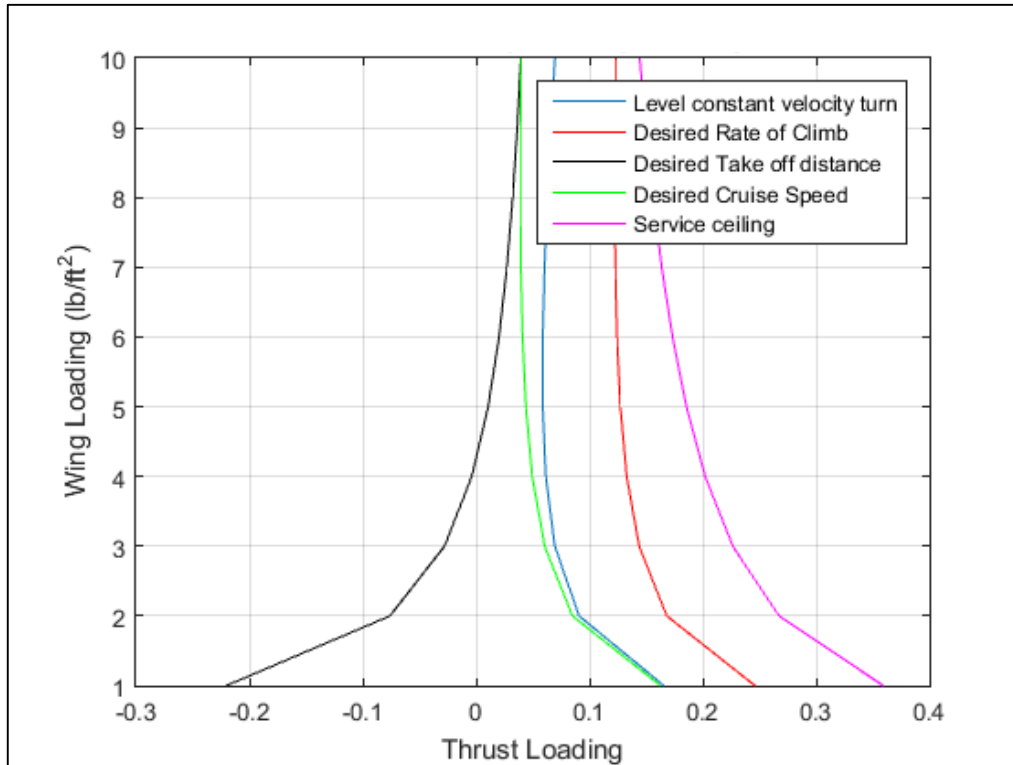


Figure 2.4 Thrust Loading vs. Wing Loading

After wing loading calculations thrust loading is chosen. According to first assumption, when wing loading is 5 lb/ft² then T/W becomes approximately 0.175.

2.9. Wing Loading

Wing loading is another crucial parameter for aircraft design since almost all performance characteristics depend on wing loading. Optimum wing loading is calculated by using aircraft's design requirements such as takeoff distance, landing distance, cruise speed, stall speed, instantaneous turn and sustained turn. The lowest wing loading is chosen after calculations since the lowest one satisfies all of the conditions. Wing loading calculations are performed with various velocity values, because observing the effects of the velocity changes on wing loading is useful when surveying performance parameters at different altitudes.

2.9.1. Takeoff Distance Wing Loading

In Turkey, aircraft's landing field is approximately 1 km (3280 ft) [47], which is taken for calculating the wing loading according to takeoff distance of the Hybrid UAV. TOP (Takeoff Parameter) is 300 for 3200 ft takeoff distance. Figure 2.5 is used for calculations. Takeoff distance can be found from the takeoff distance equation. [1]

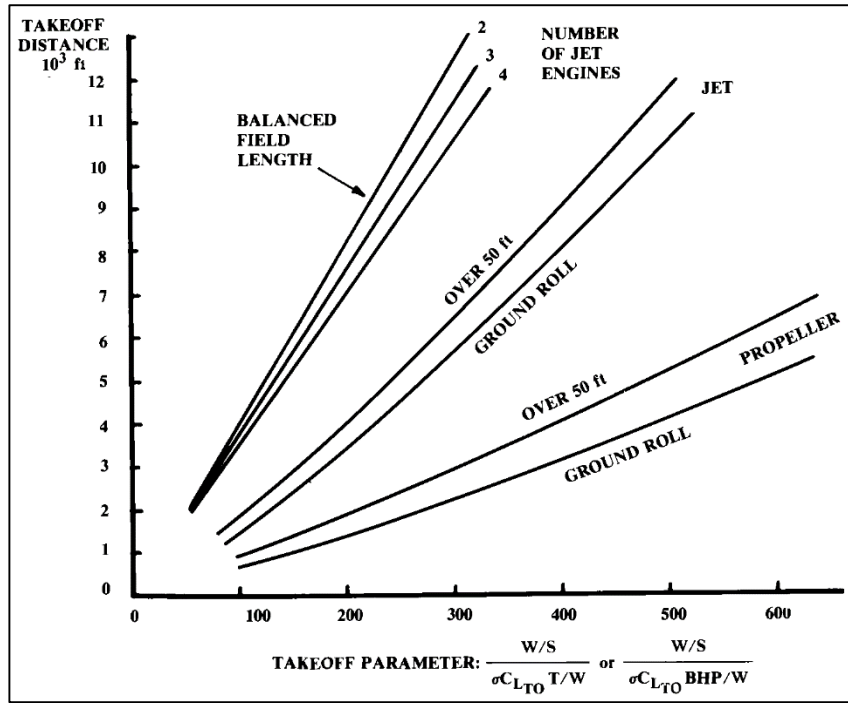


Figure 2.5 Takeoff Distance Estimation [1]

$$TOP(\text{takeoff parameter}) = \frac{W/S}{\left(\sigma C_{L,TO} \frac{T}{W}\right)} \quad 2.20$$

Where $\sigma=1$,

$$C_{L,TO} = \frac{C_{L,max}}{1.21} = 1.9935 \quad 2.21$$

Then according to equation 2.20 wing loading is found as 15 lb/ft².

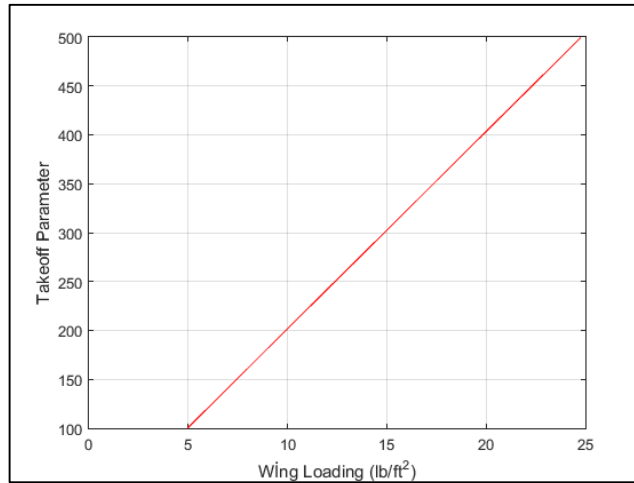


Figure 2.6 Wing Loading vs. Takeoff Parameter

2.9.2. Landing Distance Wing Loading

It is assumed that landing distance requirement is the same as the takeoff distance (3280 ft). Landing distance wing loading can be calculated as follows:

$$\text{Landing distance} = 80 \frac{W}{S} \sigma C_{L,max} + S_a \quad 2.22$$

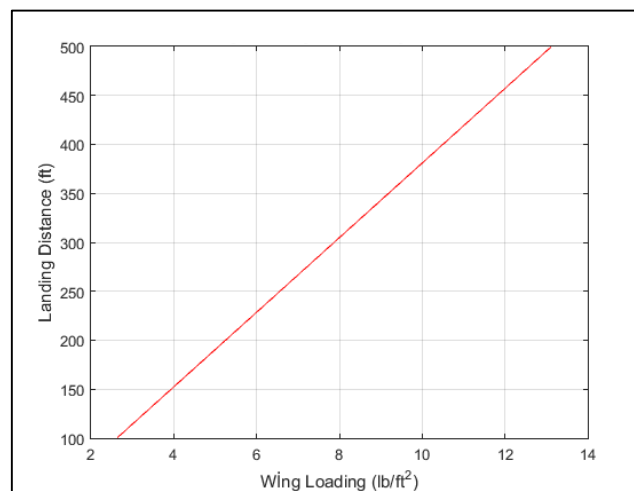


Figure 2.7 Wing Loading vs. Landing Distance

Wing loading according to takeoff distance is found as 24.5.

2.9.3. Cruise Speed Wing Loading

Parasite drag must be 3 times larger than induced drag for maximum range.

$$\frac{W}{S} = q_{\infty} \sqrt{\frac{C_{D,0}}{3K}} \quad 2.23$$

Where

$$K = \frac{1}{\pi e AR} \quad 2.24$$

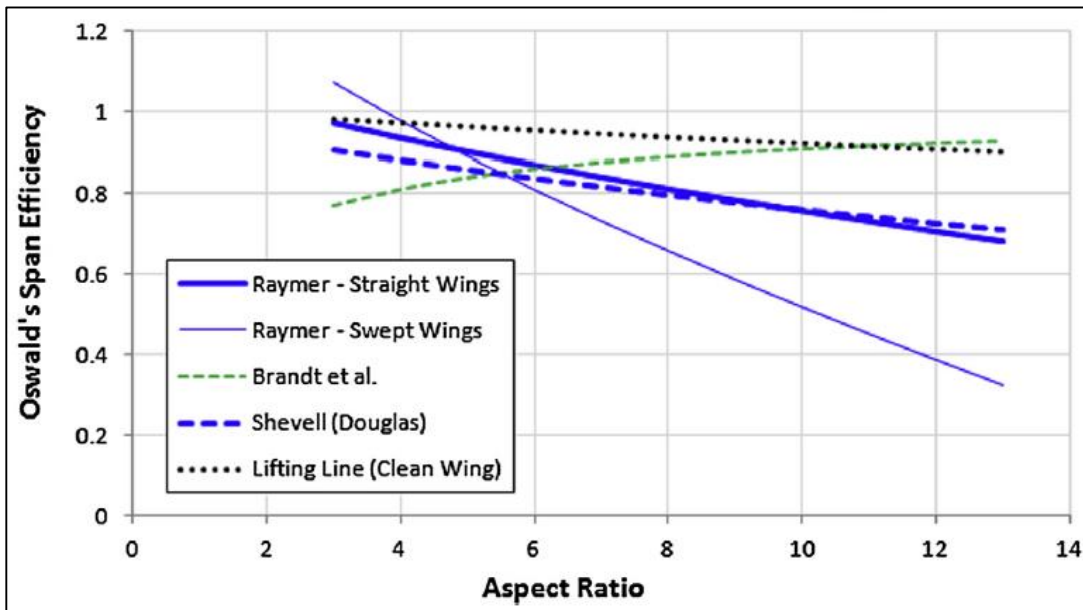


Figure 2.8 Oswald's Span Efficiency vs. Aspect Ratio [3]

There are six ways to predict e (the Oswald span efficiency factor) which are seen from Figure 2.8. For high aspect ratio wing, using lifting line method and Brandt method are more convenient. Span efficiency factor is found as 0.9 for 24.5 aspect ratio using average value of the two methods. $C_{D,0}$ is calculated using equation 2.25.[1]

$$C_{D,0} = \frac{S_{wet}}{S} C_{fe} \quad 2.25$$

C_{fe} is the skin friction coefficient which is a function of Reynolds number;

$$Re = \frac{\rho_{\infty} V c}{\mu} \quad 2.26$$

μ is the dynamic viscosity and c is the wing chord length. Average mean chord length of the competitor aircrafts is used for calculating Reynolds number which is found as 4 696 000. After finding Reynolds number C_{fe} is found as 0.08. Figure 2.9. S_{wet}/S is taken as 4 using Figure 2.10.

$$C_{D,0} = \frac{S_{wet}}{S} \times C_{fe} \quad 2.27$$

Equation 2.27 yields 0.032 zero lift drag coefficient.

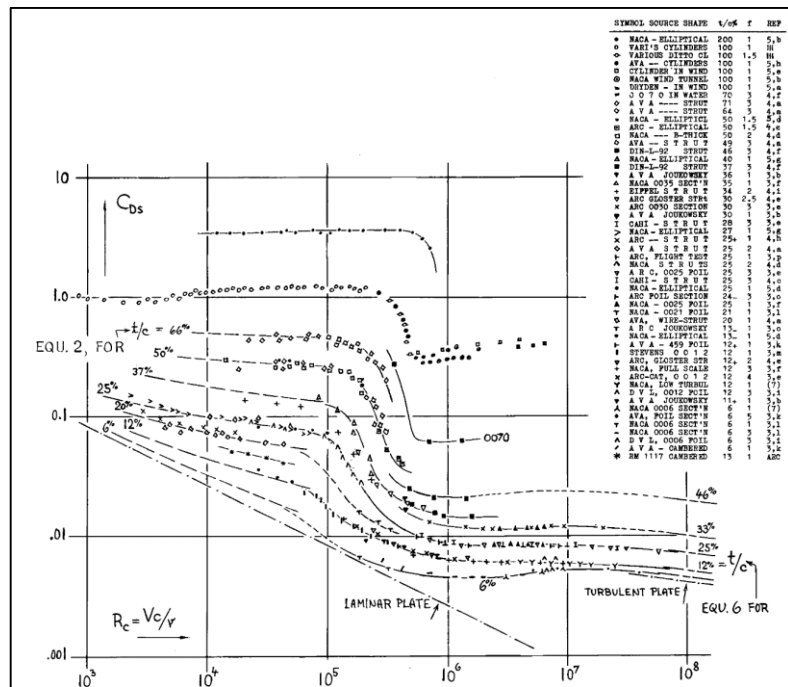


Figure 2.9 Skin Friction Coefficient vs Reynolds Number [30]

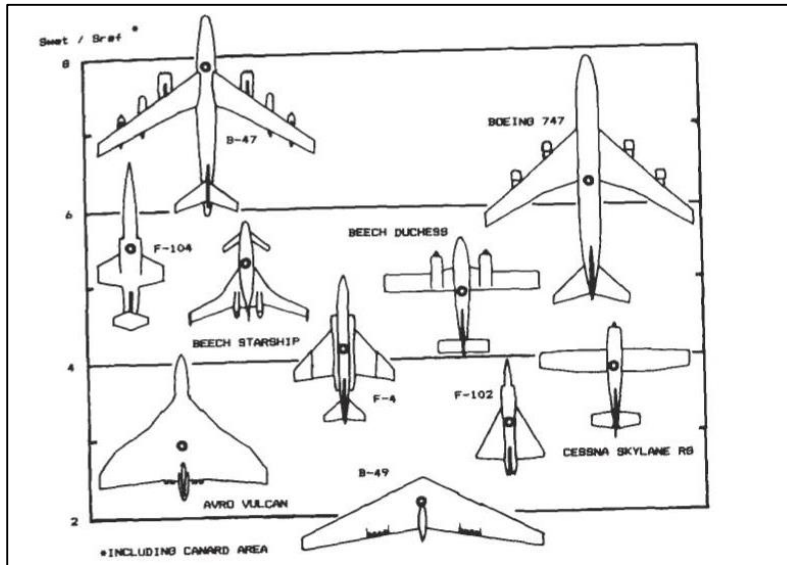


Figure 2.10 Wetted Area Ratios [1]

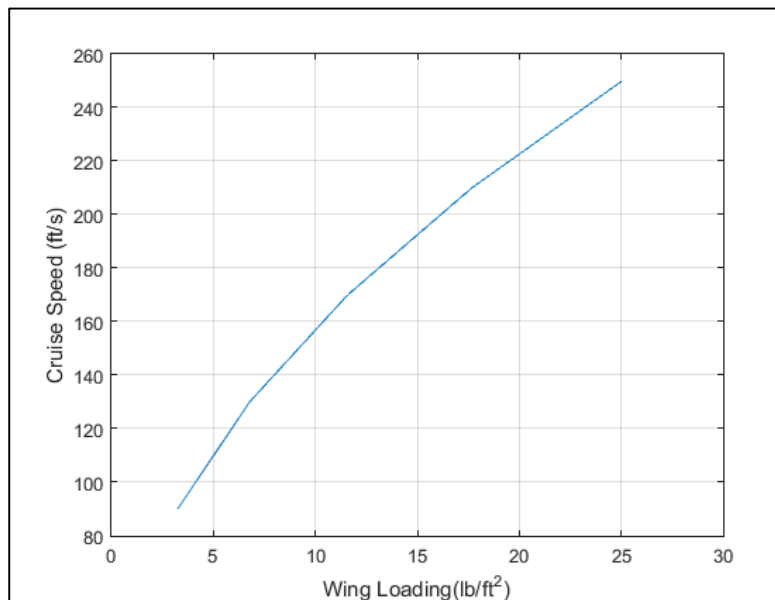


Figure 2.11 Wing Loading vs. Cruise Speed

Wing loading versus cruise velocity is given in Figure 2.11. Cruise velocity requirement is 110 ft/s, wing loading is read as 5.1 lb/ft² which is very close to the first assumption.

2.9.4. Stall speed Wing Loading

Stall speed wing loading is another important parameter which affects wing loading. In this part, sea level air density is used.

$$\frac{W}{S} = q_{\infty} C_{L,max} \quad 2.28$$

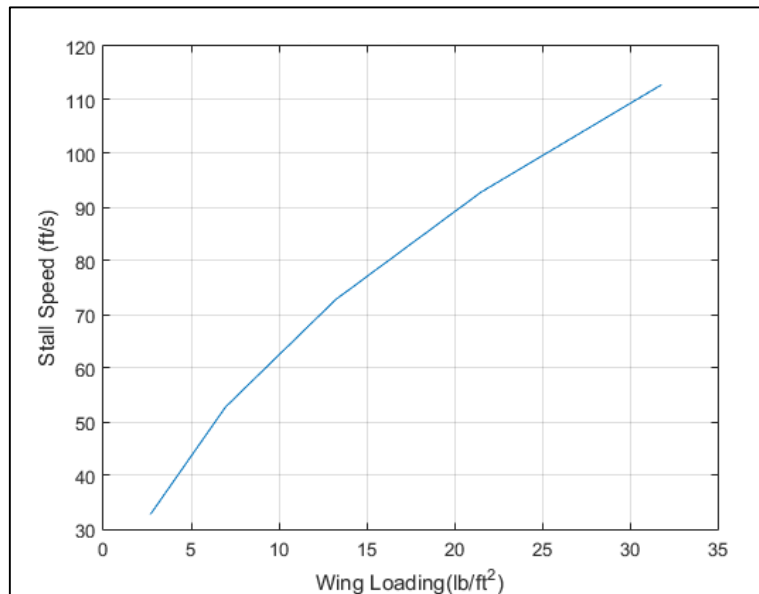


Figure 2.12 Wing Loading vs. Stall Speed

Stall requirement is 50 ft/s. Stall velocity wing loading constraint is 6.37 lb/ft² Fig. 3.12.

2.9.5. Instantaneous Turn and Sustained Turn Wing loading

Instantaneous turn wing loading is given in equation 2.29:

$$\frac{W}{S} = q_{\infty} \frac{C_{L,max}}{n} \quad 2.29$$

Sustained turn wing loading is given in equation 2.30:

$$\frac{W}{S} = \frac{\frac{T}{W} \pm \sqrt{\frac{T^2}{W^2} - 4n^2 3C_{D,0}K}}{\frac{2n^2 K}{q_\infty}} \quad 2.30$$

For $\frac{T}{W} = 0.175$, $C_{D,0} = 0.032$, $n = 1.5$, $K = 0.0153$, $V = 110 \frac{ft}{s}$ equation 2.30 yields a 16.3 lb/ft^2 wing loading and equation 2.29 yields a 7.9 lb/ft^2 wing loading.

It must be noted that since thrust loading has not been determined yet, initial guess is used [0.175].

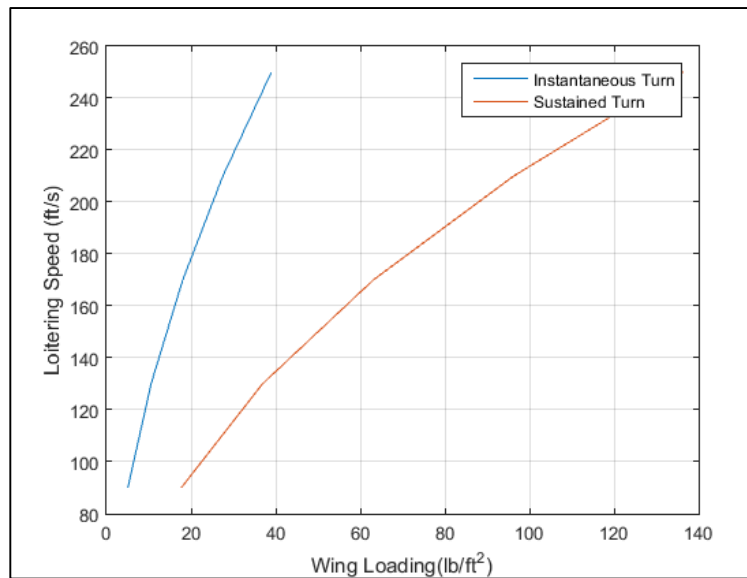


Figure 2.13 Wing Loading vs. Turning Equations

After all calculations, the lowest wing loading becomes 5.1 lb/ft^2 corresponding to the cruise velocity wing loading. Wing area can be determined by dividing first weight estimation by wing loading. The results of this calculation yields the wing planform area as 1775 ft^2 . Also, from Figure 2.4, 5.1 lb/ft^2 wing loading indicates 0.185 thrust loading. Required thrust can be calculated from following equation.

$$T = \frac{T}{W} \times W = 0.185 \times 9050 = 1674 \text{ lb}$$

In order to calculate the required thrust at sea level equation 2.31 is used.

$$\frac{T_{@30000}}{T_{@sea\ level}} = \left(\frac{\rho_{@30000}}{\rho_{@sea\ level}} \right)^{0,6} \quad 2.31$$

$$\frac{1674}{T_{required,@sea\ level}} = \left(\frac{0,000891}{0,00238} \right)^{0,6}$$

$T_{required,@sea\ level} = 3018\ lb$ Before choosing an appropriate engine it is essential to emphasize that it is convenient to choose an engine having a thrust value larger than 3018 lb. Selecting 2 units of FJ44-1 engine seems to be the best alternative, because of its lower specific fuel consumption than other small turbofan engines and relatively light weight [36]. It is a high bypass ratio engine. It was used on Scaled Composites/Beechcraft Triumph aircraft. Table 2.12 indicates the geometric and performance parameters of the engine.

Table 2.12 Specifications of FJ44-1A [36]

Specifications	
Firm	Williams International/Rolls-Royce
Specific fuel consumption (l/h)	0.4
Thrust (lbf)	1900
Dry weight (lb)	406
By-pass ratio	3.28
Overall length (in)	53.3
Approximate fan diameter (in)	20.9



Figure 2.14 FJ44-1 Engine [48]

Electric motor is chosen after performing required power analysis at 45000 ft altitude. Electric motors are relatively lightweight motors for instance a 10 kW electric motor is about 7.4 lb Therefore contributions of electric motor and propeller on center of gravity are taken in the solar propulsion contribution term.

2.10. Refined Weight Sizing Equations

Refined sizing equation is utilized after thrust loading and wing loading values are determined. Table 6.1 [1] is used for designing jet aircraft and Table 6.2 [1] is used for designing propeller driven aircraft. For hybrid case, refined weight equations most probably do not work since Hybrid UAV is a unique design including both jet engine and propeller engine. Since there is thrust loading term in the equation, jet transport aircraft case seems to be the best alternative relative to the other types, which are indicated in Table 6.1[1]. Using equations 2.2 to 2.11 with 2.32.

$$\frac{W_e}{W_0} = \left[a + b(W_0)^{c1}(A)^{c2} \left(\frac{T}{W} \right)^{c3} \left(\frac{W_0}{S} \right)^{c4} (M_{max})^{c5} \right] K_{vs} \quad 2.32$$

$$\frac{W_1}{W_0} = 0.97$$

$\frac{W_2}{W_1} = 1.0065 - 0.325M^2$, where Mach number is the climb Mach number which is 0.1206

$$\frac{W_3}{W_2} = 0.8646$$

Specific fuel consumption was taken as 0.4.

$\frac{W_4}{W_3} = 1$, it is assumed that during loiter only solar energy and battery energy is used.

$\frac{W_5}{W_4} = \frac{W_3}{W_2}$, cruise back

$\frac{W_6}{W_5} = 0.992$, descend

$\frac{W_7}{W_6} = 0.993$, landing and stop

$$\frac{W_7}{W_0} = \frac{W_7}{W_6} \frac{W_6}{W_5} \frac{W_5}{W_4} \frac{W_4}{W_3} \frac{W_3}{W_2} \frac{W_2}{W_1} \frac{W_1}{W_0} = 0.7229$$

$$\frac{W_f}{W_0} = 1.06 \left(1 - \frac{W_7}{W_0} \right) = 0.2937$$

Where K_{vs} is the sweep constant which is 1 for fixed swept.

$$a = 0.32, b = 0.66, C1 = -0.13, C2 = 0.3, C3 = 0.06, C4 = -0.05, C5 = -0.05$$

Empty weight fraction is found by using equations indicated above. After iterations W_0 becomes 6304 lb which is not a realistic value. Therefore, initial weight estimation found in Section 3.4, is used for oncoming calculations.

2.11. Geometry Sizing and Configuration

2.11.1. Fuel Volume

Fuel weight fraction is found as 0.223 in Section 3.4, gross weight is found as 9050 lb and fuel weight is calculated as 2020 lb. According to MILSPEC, density of JP-8/JET-A1 is 6.7 lb/gallon [1]. Then, fuel volume becomes 301.5 gallon (40 ft³). All fuel is stored in the wing integral fuel tanks, since wing is large enough for storage. Volume must be increased by 10% to account for the thick rubber of the bladder tanks.

$$V_{fuel,integral\ tanks} = 40\text{ft}^3$$

2.11.2. Fuselage Length and Diameter

Fuselage lengths are calculated by equation 2.33 using aircraft gross weights which are shown in Table 6.3 [1]. In order to verify equation 2.33, some common aircraft gross weights are used. Then, fuselage lengths which are calculated from equation 2.33 and exact fuselage lengths are compared. New constants (a and c) of equation 2.33 are shown in Table 2.13.

$$Fuselage\ length = aW_0c \qquad 2.33$$

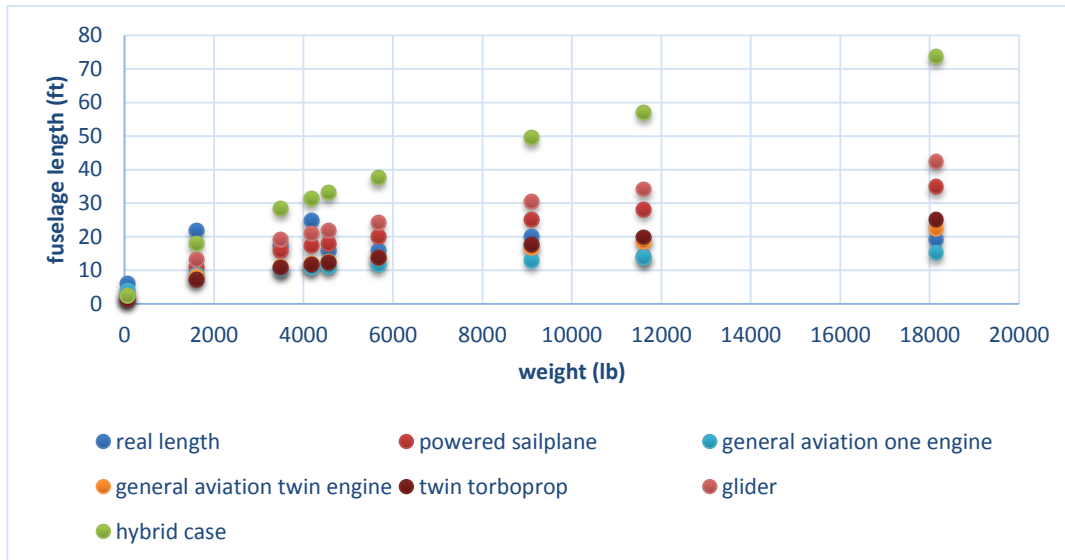
Table 2.13 Fuselage Length vs W_0 [1]

Fuselage length	a(ft)	a(m)	c
Sailplane	0.86	0.383	0.48
Sailplane(powered)	0.71	0.316	0.48
Homebuilt(metal/wood)	3.68	1.35	0.23
Homebuilt(composite)	0.05	1.28	0.23
General aviation single	4.37	1.6	0.23
General aviation twin	0.86	0.366	0.42
Agricultural	4.04	1.48	0.23
Twin Turboprop	0.37	0.169	0.51
Flying boat	1.05	0.439	0.4
Jet trainer	0.79	0.333	0.41
Jet fighter	0.93	0.389	0.39
Military cargo	0.23	0.104	0.5
Jet transport	0.67	0.287	0.43
Hybrid model	0.65	0.25	0.55

Table 2.14 Fuselage Length Comparison

Fuselage length (ft)	Sailplane	Sailplane (powered)	GA one engine	GA twin engine	Twin Turboprop	Exact length (ft)	hybrid case (ft)
Global Hawk	112.28	92.64	45.19	61.19	65.61	45.93	73.29
Condor	99.89	82.42	42.73	55.24	57.94	65.62	65.19
Phantom eye	71.70	59.16	36.45	41.33	40.74	52.49	46.82
Global Observer	68.67	56.65	35.70	39.80	38.91	82.02	44.82
Solar impulse	43.37	35.78	28.65	26.62	23.88	71.69	28.31
Lockheed martin u-2s	139.11	114.78	50.07	73.81	82.38	62.99	90.81
Hybrid UAV	74.2.	61.22	37.04	42.58	42.25	-	55.94

Table 2.14 is used for checking the fuselage length prediction model and constants indicated in Table 2.13, Competitor airplanes' weight values are used for checking model.



have long wingspan, have variable taper ratio in order to obtain elliptic lift distribution. Also it provides more wing area for solar cell placement. Taper ratio of 1 is better for solar panel placement. On the other hand, taper ratio of 0.5 is more convenient for attaining elliptic lift distribution on wing. Therefore taper ratio between 0.5 and 1 is the best alternative. Tip chord is assumed as 0.5 of the root chord. Using XFLR5 [33] wing geometry is constructed as shown in Figure 2.16. Taper ratio was calculated as 0.721. Mean chord length is calculated as 8.79 ft. Spanwise location of the mean chord is calculated as 49.32 ft. Raymer [1] wing geometry calculation methods are used for calculations.

$$C_{root,wing} = \frac{2S}{b(1 + \lambda)} = \frac{2 \times 1775}{208.53(1 + 0.721)} = 10.17 \text{ ft} \quad 2.35$$

$$C_{tip,wing} = \lambda C_{root,wing} = 5.184 \text{ ft} \quad 2.36$$

$$y_{mean} = \frac{b}{6} \left(\frac{1 + 2\lambda}{1 + \lambda} \right) = 49.32 \text{ ft} \quad 2.37$$

$$c_{mean,wing} = \frac{2}{3} C_{root,wing} \frac{1 + \lambda + \lambda^2}{1 + \lambda} = 8.79 \text{ ft} \quad 2.38$$

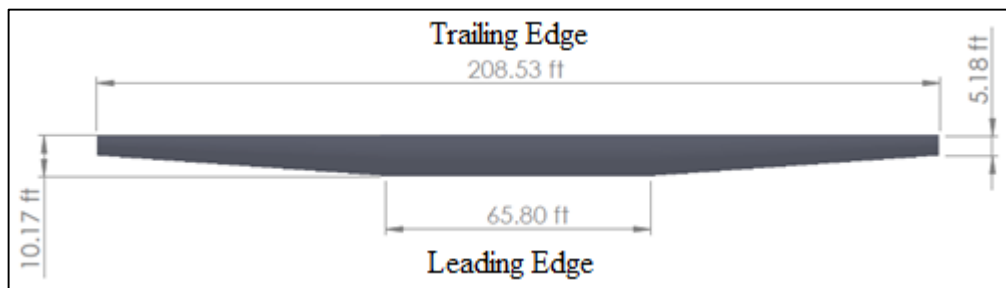


Figure 2.16 Wing Geometry

2.11.4. Tail Sizing

Selection of tail airfoil is the first step of the tail sizing. As chosen before, wing airfoil is Fx_63_137 sm airfoil. When choosing tail airfoil, thickness and the stall characteristics of the Fx_63_137 sm airfoil must be taken into account. Thickness of the tail airfoil should be as close as possible with wing airfoil. However stall angle should be higher than wing airfoil, because tails should not enter stall region before wing. Nasa/Langley Ls(1)-0013 is the best alternative for TUYGUN.

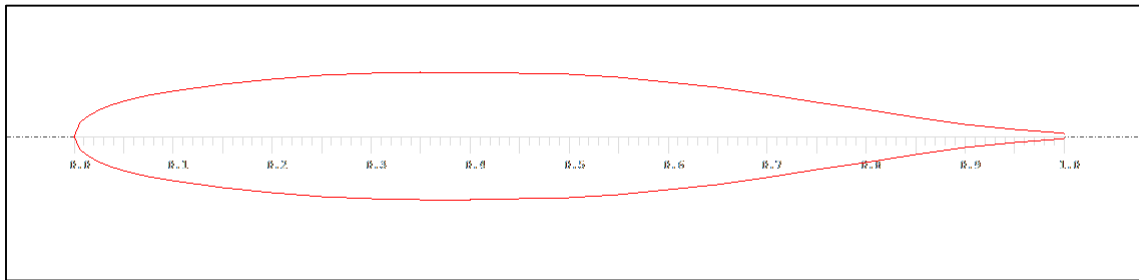


Figure 2.17 Nasa/Langley Ls (1)-0013 Airfoil

2.11.4.1. Horizontal Tail Sizing

T-tail configuration is used for tails because solar panels are used on the horizontal tail. Horizontal tail area can be determined from the equation 2.39.

$$S_{HT} = \frac{c_{HT} \bar{C}_W S_W}{L_{HT}} \quad 2.39$$

c_{HT} is the volume coefficient of the horizontal tail. Using volume coefficients of the competitor aircraft is convenient and are indicated in Table 2.15. Coefficients of ISR aircrafts are used for calculations.

Table 2.15 Tail Volume Coefficients [2]

Aircraft	Horizontal tail volume coefficient	Vertical tail volume coefficient
Lockheed Martin U-2S	0.34	0.014
Northrop Global Hawk	0.32	0.0186
Boeing Condor	0.53	0.012
ISR	0.34	0.014

$$S_{HT} = \frac{0.34 \times 8.79 \times 1775}{0.55 \times L_{fuselage}} = 168.84 \text{ ft}^2$$

Horizontal tail area is calculated as 168.84 ft². Aspect ratio of the horizontal tail is taken as 8 indicated in Table 4.3 [1]. Using equation 2.34, aspect ratio of the horizontal tail is calculated as 36.75 ft. Root chord and tip chord of the tails can be calculated using aspect ratio of the tail and taper ratio of the wing. Λ is the taper ratio of the horizontal tail, which is taken as 0.5. Using equations 2.35, 2.36, 2.37, 2.38 horizontal tail geometry is determined.

$$C_{root,HT} = 6.13 \text{ ft}$$

$$C_{tip,HT} = \lambda C_{HT} = 3.06 \text{ ft}$$

$$y_{mean,HT} = 8.17 \text{ ft}$$

$$c_{mean,HT} = 4.76 \text{ ft}$$

2.11.4.2. Vertical Tail Sizing

Vertical tail surface area can be determined as Raymer's [1] vertical tail geometry calculation model.

$$S_{VT} = \frac{c_{VT} b_W S_W}{L_{VT}} \tag{2.40}$$

$$S_{VT} = \frac{0.014 \times 208.53 \times 1775}{0.55 \times L_{fuselage}} = 168.85 \text{ ft}^2$$

Aspect ratio of the horizontal tail is 1.8[1]. Taper ratio of the vertical tail Λ , is 0.5.

$$b_{VT} = (AR_{VT} \times S)^{0.5} = (1.8 \times 168.85)^{0.5} = 17.43 \text{ ft}$$

$$C_{root,VT} = \frac{2S}{b(1+\lambda)} = \frac{2 \times 168.85}{17.43(1+0.5)} = 12.11 \text{ ft}$$

$$C_{tip,VT} = \lambda C_{VT} = 7.26 \text{ ft}$$

$$y_{mean} = \frac{b}{6} \left(\frac{1+2\lambda}{1+\lambda} \right) = 46.34 \text{ ft}$$

$$c_{mean,VT} = \frac{2}{3} C_{root,VT} \frac{1+\lambda+\lambda^2}{1+\lambda} = 8.08 \text{ ft}$$

2.11.5. Control Surface Sizing

The main control surfaces are ailerons, elevators and rudders. Flaperons are decided to be used on Hybrid UAV. Solar panels are used on wing and more wing area means more solar panels. Figure 6.3 [1] and Table 6.5 [1] are used for control surface sizing.

$$c_{flaperon} = 0.2c_{mean,wing} = 1.76 \text{ ft} \quad 2.41$$

$$b_{flaperon} = 0.4b_{wing} = 83 \text{ ft} \quad 2.42$$

$$S_{flaperon} = 143.6 \text{ ft}^2$$

$$c_{elevator} = 0.3c_{mean,ht} = 1.43 \text{ ft} \quad 2.43$$

$$c_{rudder} = 0.36c_{mean,vt} = 2.91 \text{ ft} \quad 2.44$$

2.11.6. Engine Dimensions and Weight

Chosen engine is 2 units of FJ44-1 which have a 950 lb dry weight and 1352 lb total weight and 3800 maximum thrust at sea level. Length of the engine is 41.9 inch, diameter

of the engine is 20.9 inch, specific fuel consumption is 0.4/h, and mass flow rate of the engine is 78 lb/s

2.11.7. Capture Area

Inlet area calculations are as follows, from Figure 10.17 [1].

$$\frac{\text{capture area}}{\text{mass flow}} = \frac{0.025\text{sqft}}{\text{lb/s}}$$

$$A_{inlet} = 158 \times 0.025 = 3.95 \text{ ft}^2$$

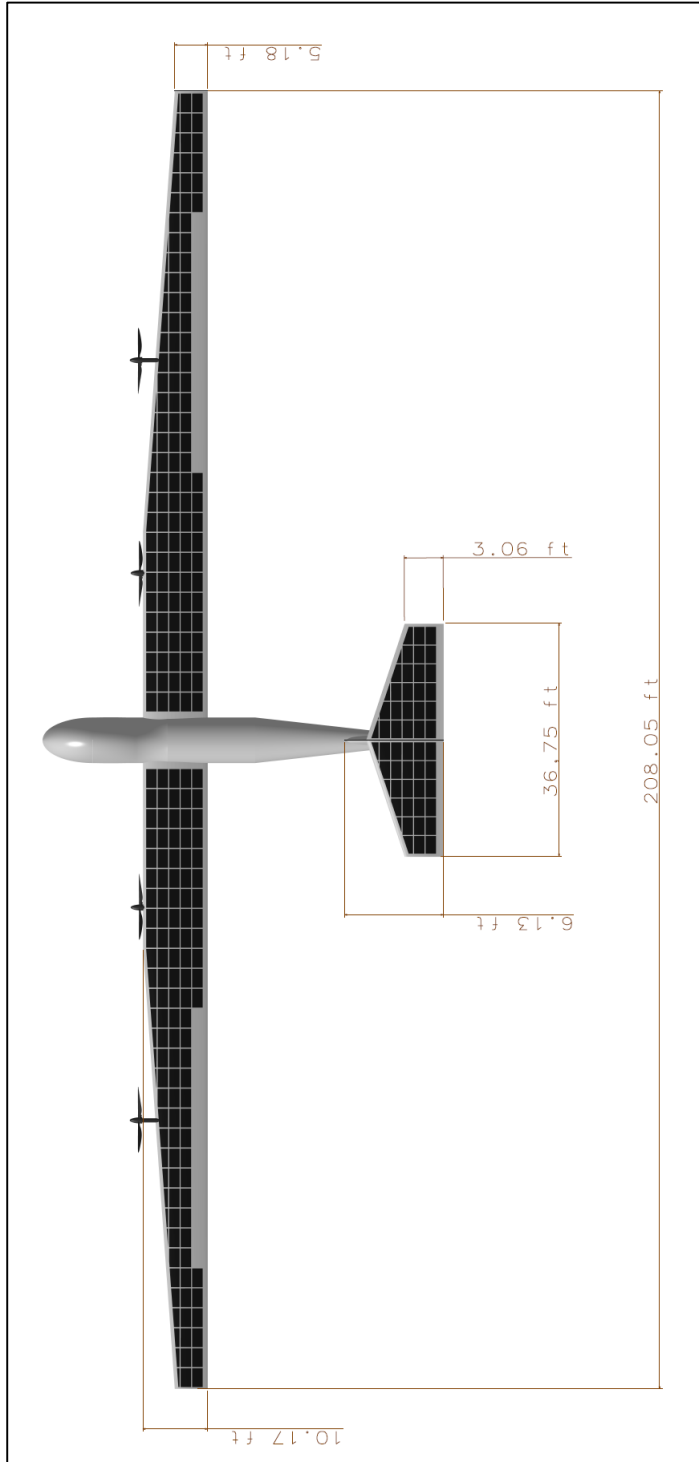


Figure 2.18 Top View of TUYGUN

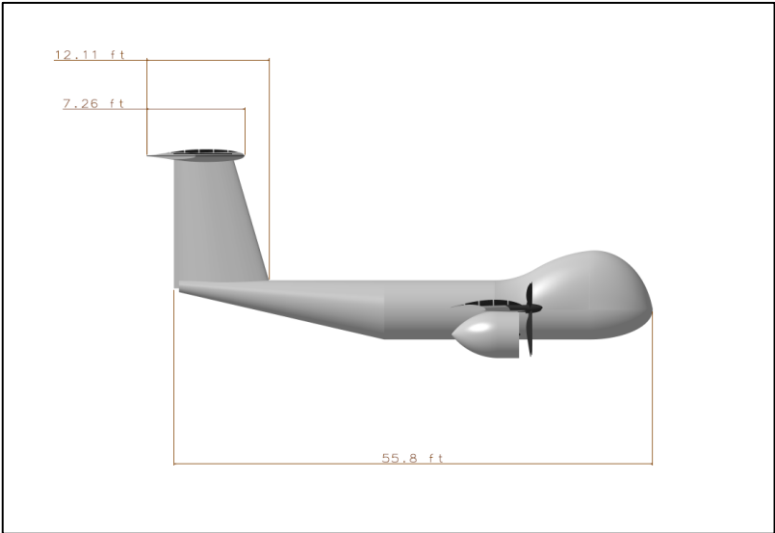


Figure 2.19 Side View of TUYGUN

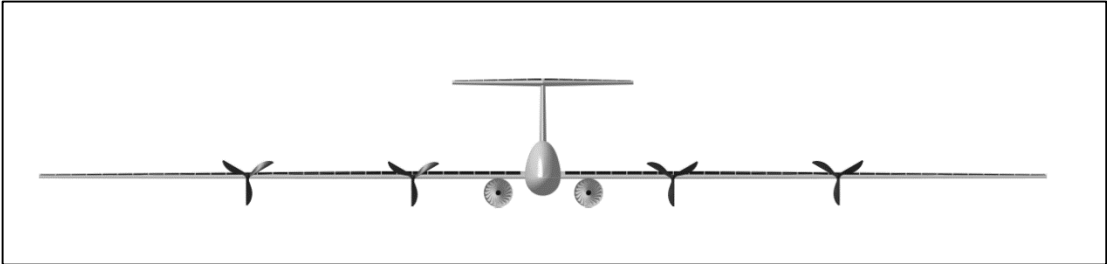


Figure 2.20 Front View of TUYGUN



Figure 2.21 Isometric View of TUYGUN

2.12. Preliminary Center of Gravity Estimation, Landing Gear Placement and Sizing

2.12.1. Weights of Major Components

Prediction of components weight is the major difficulty for HALE aircraft. Wingspan is very long and wing area is very high so standard equations do not work. Leland and Nicolai's [2] weight prediction model is the best choice for calculating fuselage, wing and tail weights.

2.12.1.1. Wing Weight

Wing weight calculation method is illustrated in equation 2.45 [2]

$$W_{wing} = 96.948 \left[\left(\frac{W_{takeoff} N}{10^5} \right)^{0.65} \left(\frac{AR}{\cos \lambda \frac{1}{4}} \right)^{0.57} \left(\frac{S_{wing}}{100} \right)^{0.65} \left(\frac{1 + \lambda}{\frac{2t}{c}} \right)^{0.61} \left(\frac{V_e}{500} \right)^{0.5} \right]^{0.993} \quad (1) \quad 2.45$$

Where N is the ultimate load factor, $\cos \lambda \frac{1}{4}$ is the quarter-chord sweep, λ is the wing taper ratio, t/c is the wing thickness ratio and V_e is the cruise speed in knots. Then

$$W_{wing} = 96.948 \left[\left(\frac{9050 \times 2}{10^5} \right)^{0.65} \left(\frac{24.5}{\cos 0} \right)^{0.57} \left(\frac{1775}{100} \right)^{0.65} \left(\frac{1 + 0.721}{2 \times 0.137} \right)^{0.61} \left(\frac{65.76}{500} \right)^{0.5} \right]^{0.993} = 2302.98 \text{ lb}$$

For advanced composite aircraft wing weight can be reduced by 20% then [2] wing weight becomes 1842.4 lb.

2.12.1.2. Fuselage Weight

Fuselage weight calculation method is illustrated as follows.

$$W_{fuselage} = 200 \left[\left(\frac{W_{takeoff} N}{10^5} \right)^{0.286} \left(\frac{L}{10} \right)^{0.857} \left(\frac{W_m + D_m}{10} \right) \left(\frac{V_e}{100} \right)^{0.338} \right]^{1.1} \quad 2.46$$

Where D_m is the fuselage maximum depth in feet, L is the fuselage length in feet, W_m is the fuselage maximum width in feet. Then

$$W_{fuselage} = 200 \left[\left(\frac{9050 \times 2}{10^5} \right)^{0.286} \left(\frac{55.8}{10} \right)^{0.857} \left(\frac{6.52 + 8.2}{10} \right) \left(\frac{65.76}{100} \right)^{0.338} \right]^{1.1} = 775.66 \text{ lb}$$

For advanced composite aircraft fuselage weight can be reduced by 25% then fuselage weight becomes 581.75 lb.

2.12.1.3. Horizontal Tail Weight

Horizontal tail weight calculation method is illustrated as follows.

$$W_{horizontal,tail} = 127 \left[\left(\frac{W_{takeoff} N}{10^5} \right)^{0,87} \left(\frac{S_h}{100} \right)^{1,2} \left(\frac{L_t}{10} \right)^{0,483} \left(\frac{b_h}{t_{ht}} \right)^{0,5} \right]^{0,458} \quad 2.47$$

L_t is the distance from wing one-fourth mean aerodynamic chord to tail one-fourth mean aerodynamic chord. b_h is the horizontal tail span, t_{hr} is the horizontal tail maximum root thickness in inches. Then

$$\begin{aligned} W_{horizontal,tail} &= 127 \left[\left(\frac{9050 \times 2}{10^5} \right)^{0,87} \left(\frac{168.84}{100} \right)^{1,2} \left(\frac{4.7642}{10} \right)^{0,483} \left(\frac{36.75}{12 \times 0.137} \right)^{0,5} \right]^{0,458} \\ &= 167 \text{ lb} \end{aligned}$$

For advanced composite aircraft tail weight can be reduced by 25% [2] then horizontal tail weight becomes 125.33 lb.

2.12.1.4. Vertical Tail Weight

Vertical tail weight calculation method is illustrated as follows.

$$W_{vertical,tail} = 98.5 \left[\left(\frac{W_{takeoff} N}{10^5} \right)^{0,87} \left(\frac{S_v}{100} \right)^{1,2} \left(\frac{b_v}{t_{vt}} \right)^{0,5} \right] \quad 2.48$$

$$W_{vertical,tail} = 98.5 \left[\left(\frac{9050 \times 2}{10^5} \right)^{0,87} \left(\frac{168.85}{100} \right)^{1,2} \left(\frac{17.4338}{12 \times 0.137} \right)^{0,5} \right] = 136 \text{ lb}$$

For advanced composite aircraft tail weight can be reduced by 25% [2] then $W_{vertical,tail}$ is calculated as 101.96 lb.

2.12.1.5. Landing Gear Weight

Landing gear weight can be calculated statistically. From Table 15.2 [1]

$$W_{landing\ gear} = 0.057 \times W_{gross} = 515\ lb \quad 2.49$$

For advanced composite aircraft landing gear weight can be reduced by 8% then landing gear weight becomes 474.59 lb.

2.12.1.6. All Else Weight

All else empty can be calculated by the same approach with landing gear, From Table 15.2 [1]

$$W_{all\ else} = 0.1 \times W_{gross} = 0.1 \times 9050 = 905\ lb \quad 2.50$$

2.12.1.7. Fuel Weight

As calculated before $\frac{W_f}{W_0} = 0.226$. Then fuel weight becomes 218.15 lb.

2.12.1.8. Solar Panels and Propulsion Weight

Solar panel weight can be calculated by area rules.

$$W_{solar\ panels} = solar\ area \times 1 \frac{kg}{m^2} = 165.55\ lb \quad 2.51$$

Since there is no weight equation of avionics and propulsion, average mass/power ratio of the modern solar aircraft are used.

Table 2.16 Mass to Power Ratio and Propulsive Efficiency of Solar Powered Airplanes

[4]

Designer of the project	Type	Mass to Power Ratio	Propulsive Efficiency
Rizzo	60m HALE	9.92 lb/kW	68.0%
Youngblood	84m HALE	11.25 lb/kW	-
Hall	100m HALE	14.3 lb/kW	80.3%
Brandth	61m HALE	31 lb/kW	76.2%
Colozza	80m HALE	12.1 lb/kW	80.0%

For the design, it is convenient to use 16.92 lb/kW mass to power ratio which is the average value of the competitors. According to first estimation of the required thrust, it is calculated that solar propulsion system needs approximately 45-50 kW power during loiter. Average solar propulsive weight is about 756-844 lb for 45 and 50 kW respectively. Using average value of two cases (45 and 50 kW), weight of the solar propulsion is calculated as 800 lb.

Finally total weight of the aircraft is calculated as follows;

$$\begin{aligned}
 &W_{wing} + W_{fuselage} + W_{horizontal,tail} + W_{vertical,tail} + W_{landing\ gear} + W_{all\ else} \\
 &\quad + W_{fuel} + W_{solar\ panels} + W_{solar\ propulsion}
 \end{aligned}
 \tag{2.52}$$

$$W_{gross} = 10128\ lb$$

Empty weight becomes 8881.4 lb.

2.12.2. Center of Gravity Estimation

Weight and x and y location of the components can be seen from Table 2.17 and Table 2.18, respectively.

Table 2.17 Horizontal Center of Gravity Estimation

Components	Weight (lb)	c.g. of Components	Location of x_{cg} (ft)	$W * x_{c.g}$ (lb.ft)
Wing+solar panels	2205.93	0.40 of Mean Chord	18.16	33455.85
Payload	2204.62	front of the fuselage	8	17600
Fuselage	581.74	0.45 of its Length	25.11	14607.73
Turbofan engine	1157	Under the wing	15	17355
Avionics instruments	905	-	22.32	20199.6
Landing gear	474.582	0.85 of the Distance Between the Nose and Rear Wheel	27.9	13240.83
Vertical tail	101.95	0.40 of its Mean Chord	49.86	5084.44
Horizontal tail	125.22	0.40 of its Mean Chord	52.94	6629.60
Fuel	2018.15	c.g. of the Aircraft	16.83	33975.04
Solar avionics and electric engine	363.54	c.g. of the Aircraft	16.83	6120.24

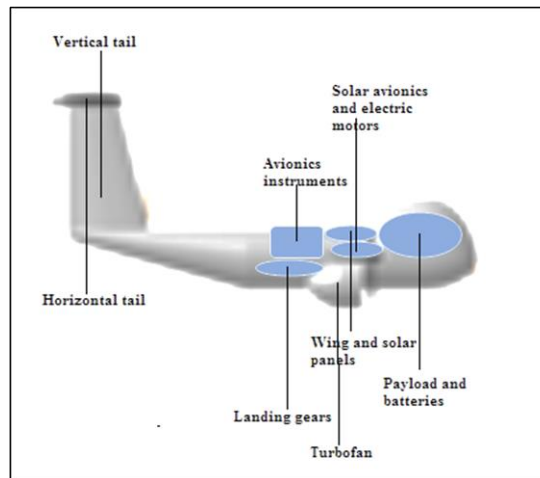


Figure 2.22 Location of Parts and Instruments

Table 2.18 Vertical Center of Gravity Estimation

Components	Weight (lb)	c.g. of Components	Location of y_{cg} (ft)	$W*y_{c.g}$ (lb.ft)
Wing+solar panels	2205.93	Height of the Mean Chord	0	0
Payload	2204.62	0.50 of Nose Height	2,25	4961.25
Fuselage	581.75	0.50 of its Diameter	2	1163.5
Turbofan engine	1157	0.50 of its Height	7.604	8797.83
Avionics instruments	905	0.50 of Nose Height	2.25	2262.5
Landing gear	474.582	0.50 of its Height	-3	-1423.74
Vertical tail	101.96	Height of the Mean Chord	6.469	659.58
Horizontal tail	125.22	Height of vertical tail minus mean Chord	17.43	2812
Fuel	2018.15	Same as Fuselage	2.5	4960
Solar avionics and electric engine	363	Height of the Mean Chord	16.834	6110.24
All else empty	1842.39	Same as Fuselage	2.5	4605.97

After all calculations, horizontal center of gravity is found as 17.6 ft from nose and vertical center of gravity is found as 4.62 ft from bottom edge of the fuselage

CHAPTER 3

PERFORMANCE ANALYSIS

The purpose of the performance analysis is to ensure whether the design satisfies the requirements or not. This part includes estimation of C_{Lmax} , $C_{L\alpha}$, α_{CLmax} , and C_{D0} of the designed aircraft and $(L/D)_{max}$. Raymer's [1] performance prediction equations are used for this chapter.

3.1. Estimation of $C_{L\alpha}$

Lift curve slope can be estimated as follows:

$$C_{L\alpha} = \frac{2\pi AR}{2 + \sqrt{4 + \frac{AR^2 \beta^2}{\eta^2} \left(1 + \frac{\tan^2 \Lambda_{max,t}}{\beta^2}\right)}} \left(\frac{S_{exposed}}{S_{ref}}\right) (F) \quad 3.1$$

Where $\beta^2 = 1 - M_\infty^2$

Here, M_∞ is taken as the design Mach number which was obtained considering the maximum velocity at 30000 ft.

$$V_{max(30000ft)} = 250ft/s, \quad a_{(30000ft)} = 994.8ft/s$$

Airfoil efficiency η can be calculated by equation 3.2.

$$\eta = \frac{c_{l\alpha}}{2\pi/\beta} = 0.9967 \quad 3.2$$

$\Lambda_{max,t}$ is the sweep angle of the wing at the chord location where the airfoil thickness is maximum.

$$\Lambda_{max,t} = \tan^{-1} \left(\frac{\frac{c_{root} - c_{tip}}{2} - 0.351 \times (c_{root} - c_{tip})}{\frac{b}{2}} \right) \quad 3.3$$

$$\Lambda_{max,t} = \left(\frac{\frac{10,17 - 5,184}{2} - 0.351 \times (10,17 - 5,184)}{\frac{208}{2}} \right) = 0.00542 \text{ rad} = 0.31 \text{ deg}$$

Exposed planform area can be obtained by subtracting the area of the wing intersecting with fuselage from wing planform area.

Diameter of the fuselage (d_f) at the wing section is 8.2 ft

Wetted area calculation of the fuselage is as follows:

$$S_{exposed} = S_{ref} - \left(2 \times c_{root} - (d_f \times \tan\Lambda) \right) \times \frac{d_f}{2} \quad 3.4$$

$$S_{exposed} = 1775 - \left(2 \times 5.184 - (8.2 \times \tan 2.5^\circ) \right) \times \frac{8.2}{2} = 1766 \text{ ft}^2$$

$$\frac{S_{exposed}}{S_{ref}} = \frac{1766}{1775} = 0.995$$

Fuselage lift factor can be calculated as follows:

$$F = 1.07 \left(1 + \frac{d_f}{b} \right)^2 \quad 3.5$$

$$F = 1.07 \times \left(1 + 8,2/208 \right)^2 = 1.156$$

Aspect ratio of the wing; AR=24.5

Finally,

$$C_{L\alpha} = \frac{2\pi \times 24,5}{2 + \sqrt{4 + \frac{(24,5)^2(0,9967)^2}{(0,9967)^2} \left(1 + \frac{\tan^2 0,745}{0,9967^2}\right)}} (0,995)(1,156)$$

$$C_{L\alpha} = 7.1955/rad = 0.1256/deg$$

$c_{l\alpha} = 2\pi/rad = 7.2421/rad$ for the airfoil or infinite wing. $C_{L\alpha} = 7.1955/rad$ is slightly lower than that value which is reasonable. Due to the induced effect, lift curve slope of the finite wing is supposed to be smaller.

3.2. Estimation of C_{Lmax}

The maximum lift coefficient of aircraft without high lift devices can be calculated as follows:

$$C_{Lmax} = 0.9C_{lmax} \cos \Lambda_{c/4} \frac{S_{exposed}}{S_{ref}} F + \Delta C_{L,max} \quad 3.6$$

$$\Lambda_{c/4} = 0.0218 \text{ rad} = 1.251^\circ$$

$$\Delta C_{L,max} = 0.9 \left(\Delta C_{l,max} \frac{S_{flaperon}}{S_{ref}} \cos \Lambda_{HL} \right)$$

$$\Delta C_{L,max} = 0.9 \left(2.185 \frac{143.6 \text{ ft}^2}{1775 \text{ ft}^2} \cos 0^\circ \right) = 0.16 \quad 3.7$$

Maximum lift coefficient of FX63-137sm airfoil:

$$C_{Lmax} = 0.9(2.1) \cos 1.251^\circ (0.995)(1.156) \text{ (without flaperon)}$$

$$C_{Lmax} = 2.17$$

$$C_{Lmax,tekeoff} = 2.33 \text{ (with flaperon)}$$

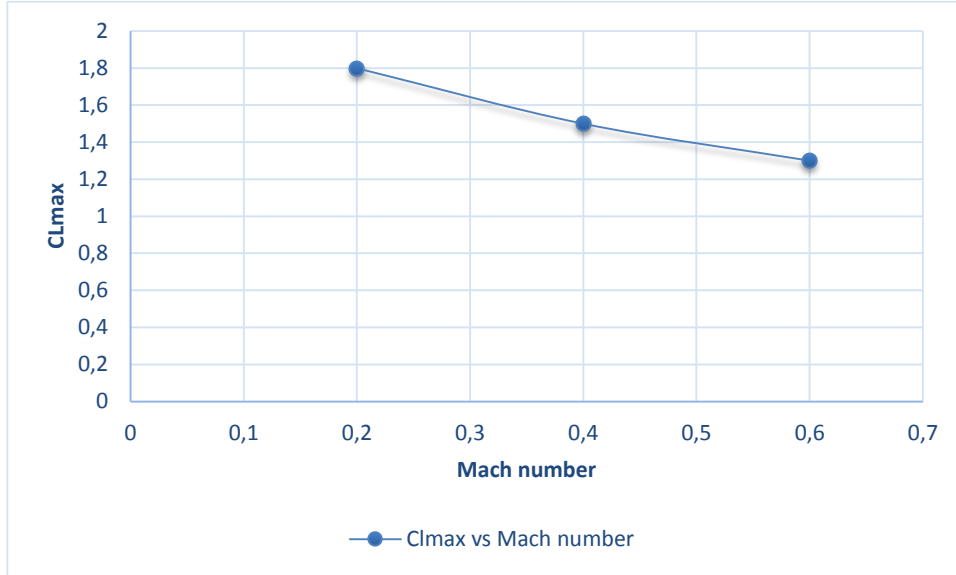


Figure 3.1 C_{Lmax} vs M

Figure 3.1 indicates the maximum lift coefficient variations with Mach number

Maximum lift coefficient decreases due to reduction of the Mach number correction factor with velocity, Figure 12.10 [1].

3.3. Estimation of $\alpha_{C_{Lmax}}$

The angle of attack for the maximum lift is defined in the following equation:

$$\alpha_{C_{Lmax}} = \frac{C_{Lmax}}{C_{L\alpha}} + \alpha_{L0} + \Delta\alpha_{C_{Lmax}} \quad 3.8$$

This equation is valid for high aspect ratio wings. α_{L0} in the equation can be approximated by the airfoil zero-lift angle. The third term $\Delta\alpha_{C_{Lmax}}$ is a correction for nonlinear effects of vortex flow.

$\alpha_{L0} = -7.5^\circ$ For the FX63-137 sm airfoil

In order to find $\Delta\alpha_{C_{Lmax}}$, firstly, leading edge sharpness parameter (Δy) has to be defined. The leading edge sharpness parameter is the vertical separation between the points on the upper surface that are 0.15% and 6% of the airfoil chord from the leading edge.

Here, $y_{0.015c} = 0.0239$ and $y_{0.06c} = 0.0463$

$$\Delta y = y_{0.06c} - y_{0.015c} = 0.0463 - 0.0239 = 0.0224 \text{ (2.24\%)}$$

From Fig. 12.10 [1], which is for Mach-number correction for subsonic maximum lift of high aspect ratio wings, $\Delta\alpha_{C_{Lmax}} = 0.592 \text{ deg}$ is obtained considering leading edge sharpness and leading edge sweep angle.

$$\alpha_{C_{Lmax}} = \frac{2.17}{0.1256} + (-7.5) + 0.592 = 10.4^\circ$$

Maximum lift coefficient of the wing is 2.17 which is enough for takeoff.

3.4. Estimation of the Parasite Drag Coefficient C_{D_0}

Subsonic parasite drag coefficient can be estimated by using the component build-up method and its equation is given below:

$$C_{D_0} = \frac{\sum C_{fc} FF_c Q_c S_{wet,c}}{S_{ref}} C_{D_{misc}} + C_{D_{L\&P}} \quad 3.9$$

Where

C_f : Skin friction factor

FF : Form factor (shape factor)

Q : Interference factor

$C_{D_{misc}}$: Miscellaneous drag

$C_{D_{L\&P}}$: Leakages and protuberances drag

In order to calculate skin friction coefficient, C_f , Reynolds number should be found in order to find the flow type.

If Reynolds number is greater than 1000000, flow is fully turbulent and skin friction coefficient for fully turbulent flow is as follows;

$$C_f = \frac{0.455}{(\log Re)^{2.38}(1 + 0.144M)^{0.65}} \quad 3.10$$

As mentioned before, parasite drag coefficient is estimated by build-up method. Calculations are completed for three different altitudes which are sea level, 20000ft and 30000ft. In calculations, maximum velocity is used because the aim of this part is to calculate the maximum parasite drag which increases with velocity.

At sea level;

$$\rho_\infty = 0.002377 \text{ slug/ft}^3, \quad \mu_\infty = 3.737 \times 10^{-7} \text{ lbs/ft}^2$$

$$a_\infty = 1116.5 \text{ ft/s} \quad \text{and} \quad M = 0.098$$

At 30000ft altitude;

$$\rho_\infty = 0.000891 \text{ slug/ft}^3, \quad \mu_\infty = 3.11 \times 10^{-7} \text{ lb/ft.s} \quad \text{and}$$

$$a_\infty = 994.66 \text{ ft/s} \quad \text{and} \quad M = 0.08$$

Firstly, parasite drag coefficient at 30000ft altitude is calculated.

3.4.1. Wing Parasite Drag

First of all, Reynolds number of the wing is determined. After determination of flow type, skin friction coefficient and form factor are determined. Wing drag calculations are as follows:

$$Re_{wing} = \frac{\rho_{\infty} V_{max} \bar{c}}{\mu_{\infty}} = \frac{(0.000891)(250)(10,17)}{(3.11 \times 10^{-7})} = 2.31 \times 10^6$$

This result shows flow is fully turbulent. Then using equation 3.8:

$$C_{f,wing} = \frac{0.455}{(\log(2.31 \times 10^6))^{2.38} (1 + 0.144(0.08))^{0.65}} = 0.0038$$

$$FF_{wing} = \left(1 + \frac{0.6}{(x/c)_m} \left(\frac{t}{c} \right) + 100 \left(\frac{t}{c} \right)^4 \right) (1.34M^{0.18} (\cos \Lambda_m)^{0.28}) \quad 3.11$$

$$FF_{wing} = \left(1 + \frac{0.6}{0.3} (0.137) + 100(0.137)^4 \right) (1.34(0.08)^{0.18} (\cos 2.5^\circ)^{0.28}) = 1.1747$$

$$S_{wet,wing} = S_{exposed, wing} \left[1.977 + 0.52 \left(\frac{t}{c} \right) \right] \quad 3.12$$

$$S_{wet,wing} = (1766)[1.977 + 0.52(0.137)] = 3636 ft^2$$

Interference factor of the wing is taken 1.2 [1]

3.4.2. Fuselage Parasite Drag

At first, Reynolds number of fuselage is determined. After determination of flow type skin friction coefficient, fineness ratio and form factor are determined. Fuselage parasite drag calculations are as follows:

$$Re_{fuselage} = \frac{\rho_{\infty} V_{max} l}{\mu_{\infty}} = \frac{(0.000891)(250)(55.8)}{(3.11 \times 10^{-7})} = 1.28 \times 10^7$$

Since Reynolds Number is greater than 1000000, flow over the fuselage is fully turbulent.

$$C_{f,fuselage} = \frac{0.455}{(\log(1.28 \times 10^7))^{2.38} (1 + 0.144(0.08))^{0.65}} = 0.0029$$

$$FF_{fuselage} = \left(1 + \frac{60}{f^3} + \frac{f}{400} \right) \quad 3.13$$

Where f is fineness ratio and defined as;

$$f = \frac{l}{d} \quad 3.14$$

$$f = \frac{l}{\sqrt{\left(\frac{4}{\pi}\right) A_{max}}} = 6.8049$$

$$FF_{fuselage} = \left(1 + \frac{60}{(6.8049)^3} + \frac{6,8049}{400}\right) = 1.2074$$

3.4.3. Horizontal Tail Drag

Firstly, Reynolds number of horizontal tail is determined. After determination of flow type, skin friction coefficient and form factor are determined. Horizontal tail drag calculations are as follows:

$$Re_{horizontal\ tail} = \frac{\rho_{\infty} V_{max} \bar{c}}{\mu_{\infty}} = \frac{(0.000891)(250)(4.7642)}{(3.11 \times 10^{-7})} = 1,092 \times 10^6$$

It shows that flow is fully turbulent. Then using equation 3.8, 3.9 and 3.10:

$$C_{f, horizontal\ tail} = \frac{0.455}{(\log(1.092 \times 10^6))^{2.38} (1 + 0.144(0.08))^{0.65}} = 0.0044$$

$$FF_{horizontal\ tail} = \left(1 + \frac{0.6}{(x/c)_m} \left(\frac{t}{c}\right) + 100 \left(\frac{t}{c}\right)^4\right) (1.34M^{0.18} (\cos\Lambda_m)^{0.28})$$

$$FF_{ht} = \left(1 + \frac{0.6}{0.3} (0.13) + 100(0.13)^4\right) (1.34(0.08)^{0.18} (\cos 2.5^\circ)^{0.28}) = 1.0969$$

$$S_{wet, ht} = S_{exposed, ht} \left[1.977 + 0.52 \left(\frac{t}{c}\right)\right] = (168.84)[1.977 + 0.52(0.137)] = 345.21 ft^2$$

3.4.4. Vertical Tail Drag

At first Reynolds number of vertical tail is determined. After determination of flow type skin friction coefficient and form factor are determined. Vertical tail drag calculations are as follows:

$$Re_{vertical\ tail} = \frac{\rho_{\infty} V_{max} \bar{c}}{\mu_{\infty}} = \frac{(0.000891)(250)(10,81)}{(3.11 \times 10^{-7})} = 2,266 \times 10^6$$

It shows that flow is fully turbulent.

$$C_{f,vertical\ tail} = \frac{0.455}{(\log(2.266 \times 10^6))^{2.38}(1 + 0.144(0.08))^{0.65}} = 0.0039$$

$$FF_{vertical\ tail} = \left(1 + \frac{0.6}{(x/c)_m} \left(\frac{t}{c}\right) + 100 \left(\frac{t}{c}\right)^4\right) (1.34M^{0.18} (\cos\Lambda_m)^{0.28})$$

$$FF_{vt} = \left(1 + \frac{0.6}{0.3} (0.137) + 100(0.137)^4\right) (1.34(0.08)^{0.18} (\cos 2.5^\circ)^{0.28}) = 1.0961$$

$$S_{wet,vt} = S_{exposed,vt} \left[1.977 + 0.52 \left(\frac{t}{c}\right)\right] = (345.23)[1.977 + 0.52(0.13)] = 345.23ft^2$$

Afterwards, $C_{D,0}$ calculations is performed. In order to calculate $C_{D,0}$, miscellaneous drag is determined and then zero lift drag coefficient is calculated.

3.4.5. Miscellaneous Drag, Landing Gear Drag Calculation and Total Zero Lift Drag Calculation

Miscellaneous drag is the additive drag of the components which are, antennas, sharp corners, inlets outlets etc. Calculations are performed from Table 12.8. [1]:

$$C_{D,0LP} = C_{D,0cruise} \times 0.1 \quad 3.15$$

$$C_{D,0LG} = \frac{\left(\frac{D}{q} \times 3\right)(1.2)(1.07)}{S_{ref}} \quad 3.16$$

$$C_{D,0LG} = \frac{(0.3 \times 3)(1.2)(1.07)}{1775} = 0,00065$$

$$C_{D,0cruise} = \frac{(\sum C_{fc} FF_C Q_c S_{wet,c})_{30000ft}}{S_{ref}} = 0.014 \quad 3.17$$

Miscellaneous drag is added to the total cruise parasite drag. $C_{D,0LG}$ is the landing gear parasite drag.

3.5. Zero Lift Drag Coefficient of Aircraft at Different Altitudes.

Some calculations have been done for sea level, 20000 ft and 45000 ft altitude. Landing gear parasite drag coefficient is taken into account at sea level.

Table 3.1 $C_{D,0}$ at Sea Level

Sea Level	Re	C_f	FF	$C_{D,0}$
Wing	5.13E+06	0.0033	1.11	0.008600
Fuselage	2.84E+07	0.0026	1.21	0.000245
Vertical Tail	5.03E+06	0.0034	1.10	0.000625
Horizontal Tail	2.42E+06	0.0038	1.10	0.000913
Total zero lift drag coefficient				0.0129

Table 3.2 $C_{D,0}$ at 20000 ft Altitude

20000ft	Re	C_f	FF	$C_{D,0}$
Wing	3.07E+06	0.0037	1.11	0.001900
Fuselage	1.70E+07	0.0028	1.21	0.001046
Vertical Tail	3.02E+06	0.0037	1.10	0.000718
Horizontal Tail	1.45E+06	0.0042	1.10	0.009736
Total zero lift drag coefficient				0.0134

Table 3.3 $C_{D,0}$ at 45000 ft Altitude

45000ft	Re	C_f	FF	$C_{D,0}$
Wing	1.25E+06	0.0043	1.12	0.01146
Fuselage	6.95E+06	0.0032	1.21	0.00084
Vertical Tail	1.23E+06	0.0043	1.10	0.00123
Horizontal Tail	5.96E+05	0.0049	1.10	0.00217
Total zero lift drag coefficient				0.0157

Drag and lift values are estimated at four different altitudes. Also optimum endurance velocity and cruise velocity at different altitudes are determined which are shown in Figure 3.2, Figure 3.3, Figure 3.4, Figure 3.5, Figure 3.6.

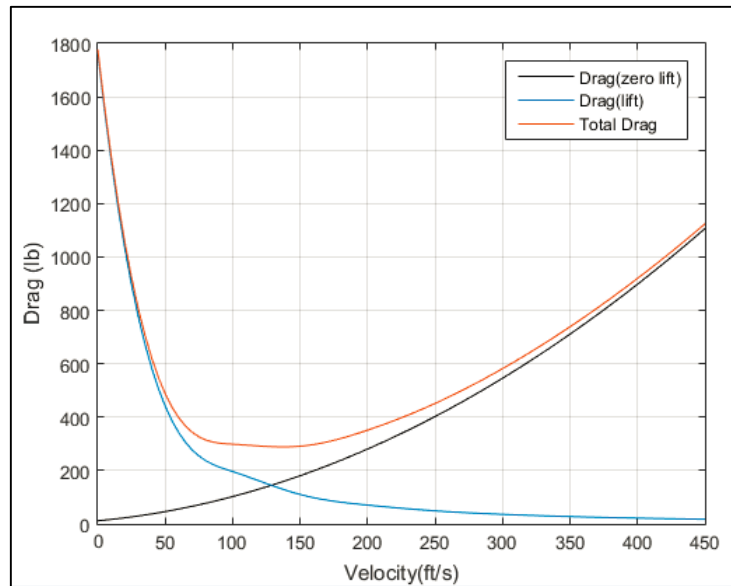


Figure 3.2 Drag vs. Velocity

3.6. Required Power and Velocity Calculations

During loiter, airplane uses solar energy and battery energy so power required curve is needed in order to find the minimum power needed and the optimum flight velocity. as can be seen in Figure 3.3 at 20000 ft altitude minimum power required for loiter is 32.73 kW, and the optimum velocity is of loiter 80 ft/s. At 30000 ft altitude minimum power required for loiter is 39.19 kW and the optimum velocity for loiter is 90 ft/s. At 45000 ft altitude minimum power required for loiter is 53.88 kW, and the optimum velocity for loiter is 120 ft/s. 10% excess power was added to the calculations to account for the power requirement of avionics and payload. Available solar power and battery power are calculated later.

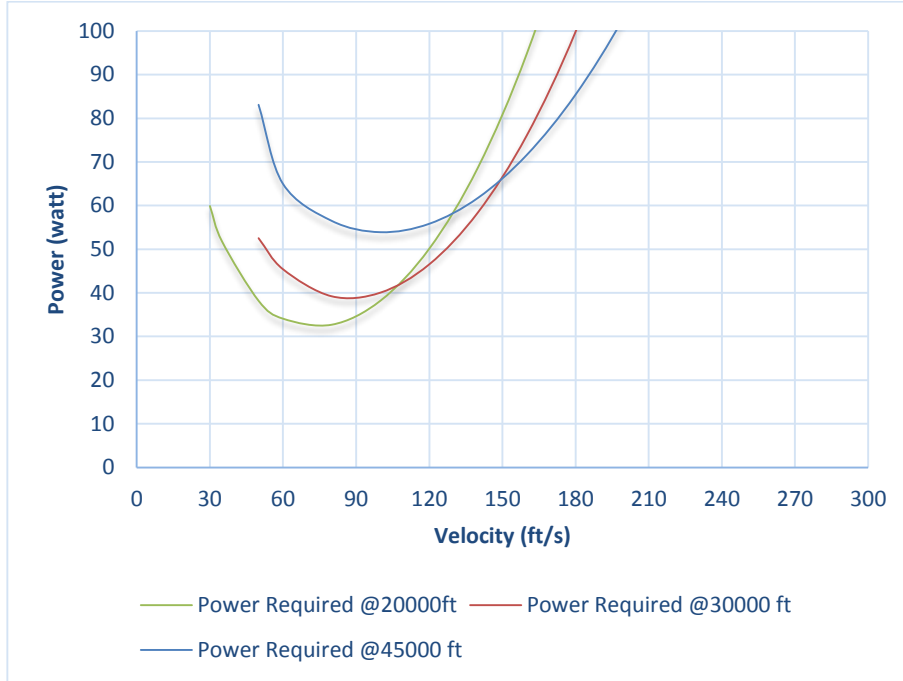


Figure 3.3 Power Required vs Velocity

3.7. Electric Engine Selection and Propeller Sizing

As mentioned in Chapter 3 electric motor can be chosen after power required analysis. At 45000 ft altitude required power is estimated as 53.8 kW. JM2 electric engine is the best alternative for TUYGUN. It has 15kW continuous shaft power. 4 piece of JM2 with 4 propeller provides 56 kW continuous shaft power which is enough for design.

Table 3.4 JM2 Engine Specifications [51]

Specifications	
Firm	Joby Motors
Power (kW)	15-19
Weight (lb)	8.82
Continuous Torque(ftlbs)	39.1
Nominal RPM	2500
Diameter (in)	7.88



Figure 3.4 JM2 Electric Motor [51]

There is no equation to find propeller diameter for electric engines. Solar Impulse has totally 30 kW power plant and its diameter is 11.5 ft. After literature review, it is observed that the most suitable propeller diameter for such engines is about 13.1 ft. Pitch of the propeller is estimated as 40 in.

3.8. Thrust and Velocity Calculations at Different Altitudes

Aim of the thrust versus velocity study is to predict the optimum range velocity at different altitudes. However, finding maximum velocity is also predicted by the intersection of the available power and required power curves.

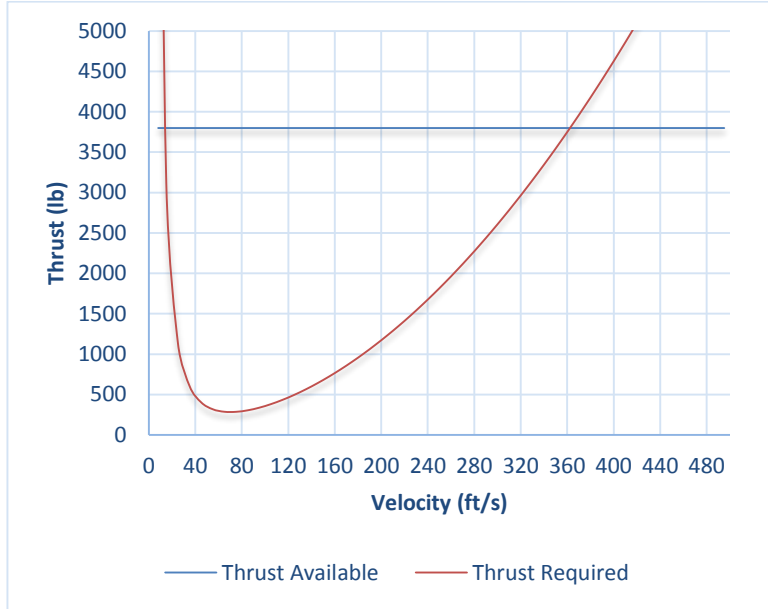


Figure 3.5 Thrust Required and Thrust Available vs. Velocity at Sea Level

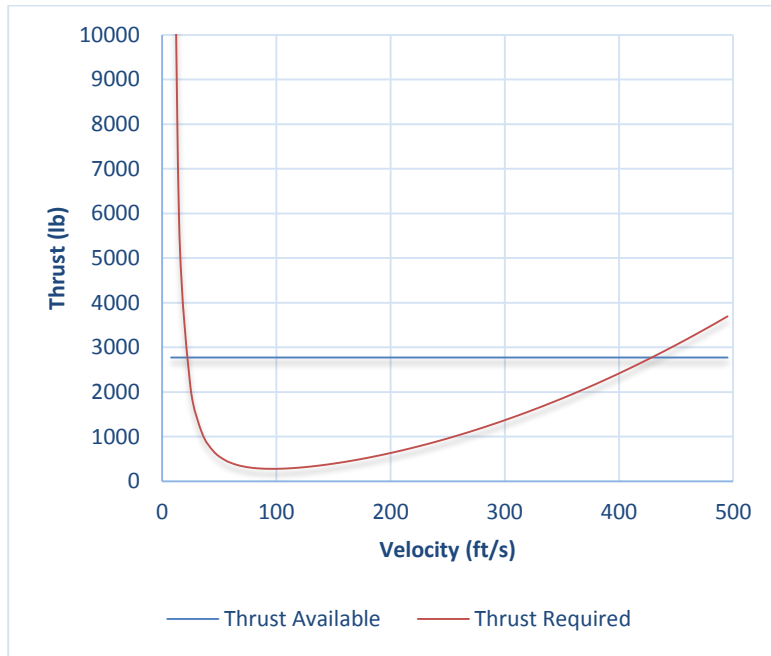


Figure 3.6 Thrust Required and Thrust Available vs Velocity at 20000 ft

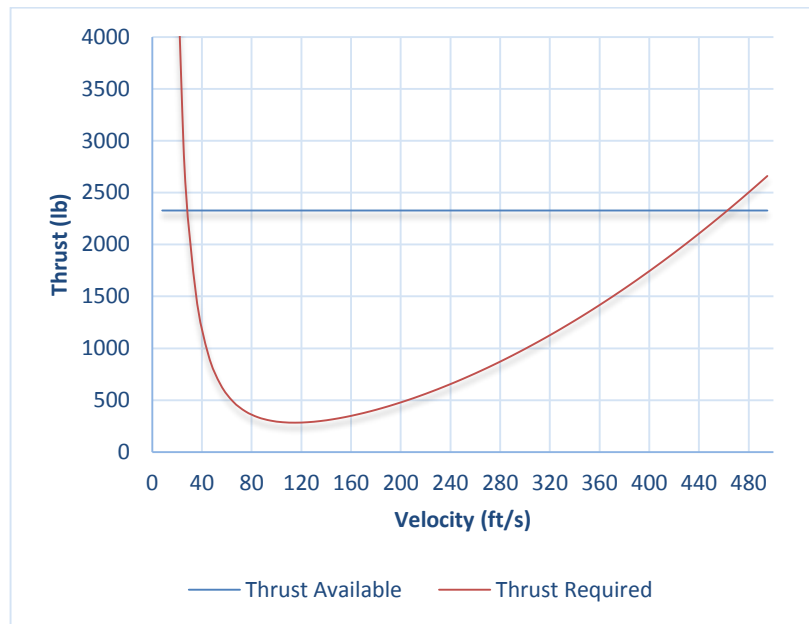


Figure 3.7 Thrust Required and Thrust Available vs Velocity at 30000 ft

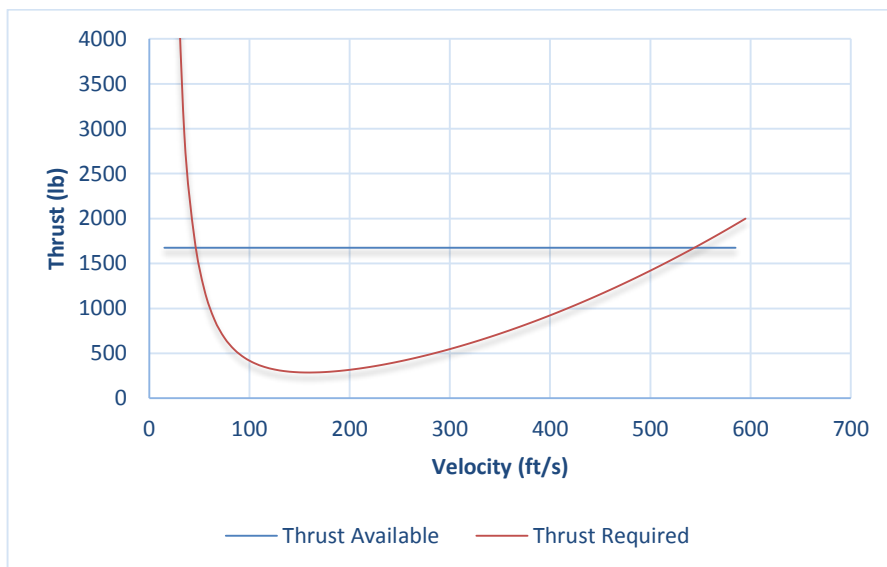


Figure 3.8 Thrust Required and Thrust Available vs Velocity at 45000 ft

As mentioned before, maximum velocity of the aircraft can be found from the intersection of power required and power available curves. As a result;

V_{\max} @ sea level = 358 ft/s

V_{\max} @ 20000 ft = 440 ft/s

V_{\max} @ 30000 ft = 460 ft/s

V_{\max} @ 45000 ft = 540 ft/s

Another important figure is lift to drag ratios variations with velocity. Figure 3.8 indicates the optimum loiter and cruise velocity at 30000 ft. Maximum $C_L^{3/2}/C_D$ indicates the optimum velocity for loitering. Maximum C_L/C_D indicates the optimum velocity for cruise. According to calculations, optimum velocity for endurance is calculated as 80 ft/s and the optimum velocity for cruise is calculated as 120 ft/s. $C_L^{1/2}/C_D$ ratio is used for calculating required power as a function of velocity.

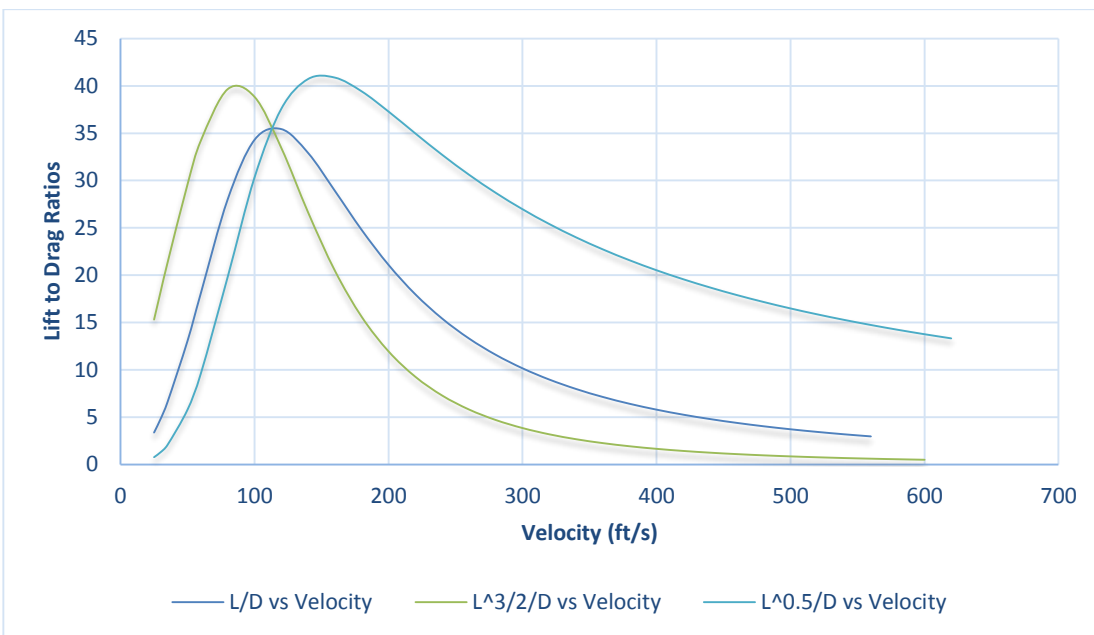


Figure 3.9 Lift to Drag Ratios vs Velocity at 30000 ft

3.9. Rate of Climb, Service and Absolute Ceilings

Rate of climb of the aircraft is calculated by using equation 3.18;

$$(R/C) = \left(\frac{\text{excess power}}{W} \right) = TV_{\infty} - DV_{\infty} \quad 3.18$$

Thrust available is known and it is calculated for different altitudes, Δh is taken as 5000 ft. Equation 3.19 is used for turbofan engines;

$$\left(\frac{T}{T_{sea\ level}} \right) = \left(\frac{\rho}{\rho_{sl}} \right)^{0.6} \quad 3.19$$

Then using constant velocity cruise conditions equation;

$$T = D = \frac{1}{2} \rho_{\infty} V_{\infty}^2 C_D S \quad 3.20$$

Now, rate of climb for different altitudes is given in Table 3.5.

Table 3.5 Rate of Climb for Different Altitudes

Altitude (ft)	Rate of Climb (ft/s)
0	39.26
5000	35.85
10000	32.73
15000	29.73
20000	26.91
25000	24.26
30000	21.78
35000	19.46
40000	16.96
45000	14.69
50000	12.73
55000	11.04
60000	9.55
65000	8.29
70000	7.14
75000	6.21
80000	5.38
85000	4.64

When finding service and absolute ceilings it is assumed that the relation between altitude and R/C is linear. Using this assumption; absolute ceiling where $\frac{R}{C} = 0$ and service ceiling where $\frac{R}{C} = 100 \text{ ft/min}$ are found as follows:

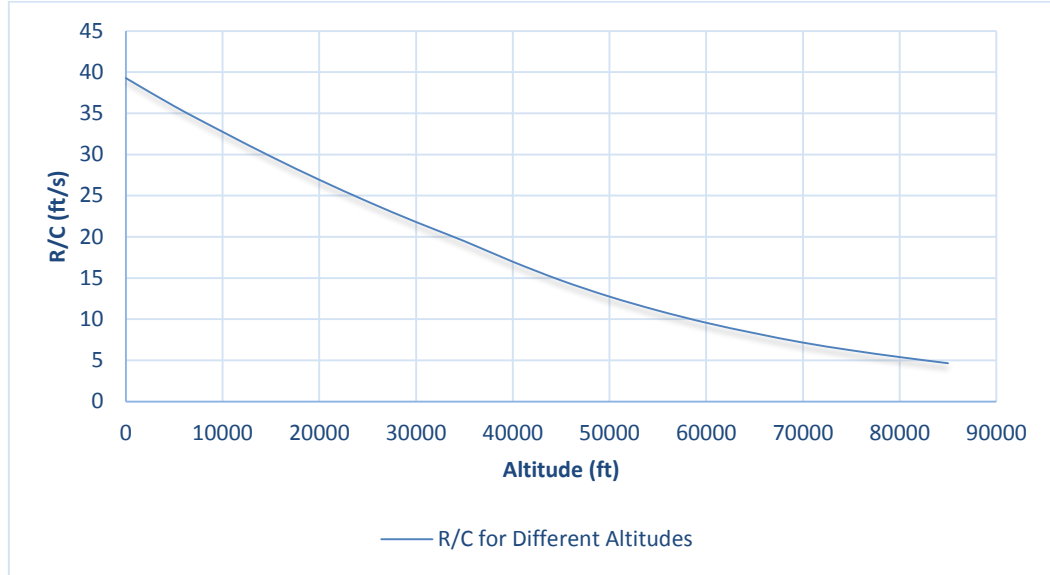


Figure 3.10 Rate of Climb for Different Altitudes

R/C curve is drawn, then using the definition of absolute:

$$\text{Absolute ceiling} = 97563 \text{ ft.}$$

3.10. Time to Climb

Time to climb can be calculated using the following assumption;

$$t = \sum \left[\frac{\Delta h}{(R/C)_{max}_i} \right] \quad 3.21$$

Equation is derived using the property of integral operator. R/C values for different altitudes are known already. From this information $1/(R/C)$ can be found. Then;

Table 3.6 Time to Climb for Certain Altitudes

Altitude	Time to Climb (min)
15000	6.41
20000	12.39
30000	23.01
45000	51.06

3.11. Maximum Range of Aircraft at 30000 ft

Range for the jet airplanes can be found using the equation 5.153 [36].

$$R = \frac{2}{C} \left(\frac{L}{D} \right)^{0.5} \sqrt{\frac{2}{\rho_{\infty} S}} (W_2^{0.5} - W_3^{0.5}) \quad 3.22$$

$$\frac{L}{D} max = \sqrt{\frac{1}{4C_{D,0} K}} \quad 3.23$$

$$\frac{L}{D} max = \sqrt{\frac{1}{4 \times 0.014 \times 0.0144}} = 35.6$$

Then range is found as 3569000 ft (588.96 nm) which is greater than 500 nm. So, range requirement is satisfied.

3.12. Ground Roll for Takeoff

The ground roll for takeoff can be calculated as follows;

$$S_g = \frac{W/S}{\sigma C_{L,max} T/W} \quad 3.24$$

$$TOP = \frac{\frac{10128}{1775}}{1 \times 0.002377 \times 2.17 \times 0.105} = 126$$

Using Figure 2.5, takeoff distance is read as 1000 ft.

3.13. Ground Roll and Total Distance for Landing

In order to calculate ground roll for landing; equation 8.28 [36] is used.

$$S_{landing} = 80 \frac{W}{S} \frac{1}{\sigma C_{L,max}} \quad 3.25$$

$$S_{landing} = 1061 \text{ ft}$$

3.14. Gliding (unpowered) Flight

In order to calculate horizontal distance after engine stops, equation 5.126 [36] is used:

$$\tan(\theta_{min}) \frac{1}{(L/D)_{max}} \quad 3.26$$

Using triangular equalities, θ_{min} can be calculated. Height of the airplane is known.

Horizontal distance can be found using following equation:

$$(L/D)_{max} = 35.6, \theta_{min} = 1.61 \text{ degree Then,}$$

Horizontal distance is found as 1067615 ft (175 nm) the corresponding velocity is:

$$V_{\infty} = \sqrt{\frac{2}{\rho_{\infty}} 5.7 \frac{1}{2.17} \cos \theta} = 76 \text{ ft/s} \quad 3.27$$

$$\text{Time to land : } t = \frac{\sqrt{R^2 + H^2}}{V_{\infty}} \quad 3.28$$

$$t = \frac{\sqrt{1067615^2 + 30000^2}}{76} = 234 \text{ min}$$

All performance parameters of the aircraft are found. The results of the performance parameters show that; the aircraft satisfies all the requirements of the mission profile. After performing accurate estimations of the performance parameters, it is seen that stall speed requirements are satisfied at different altitudes. During takeoff and landing; aircraft can fly safely. Also all cruise mission requirements are satisfied.

3.15. Maneuverability and V-n Diagrams

3.15.1. V vs. n_{max} Chart

Velocity vs. n_{max} chart is basically constrained with two factors which are, C_{Lmax} for low flight velocities and thrust available (T_A) for higher flight velocities, which is shown in the equation below. Maximum load factor for a sustained level turn at any velocity is given as follows:

$$n_{max} = \left\{ \frac{1/2 \rho_{\infty} V_{\infty}^2}{K(W/S)} \left[\left(\frac{T}{W} \right)_{max} - \frac{1}{2} \rho_{\infty} V_{\infty}^2 \frac{C_{D0}}{(W/S)} \right] \right\}^{1/2} \quad 3.29$$

For low velocities the expression for n_{max} can be calculated as follows:

$$n_{max} = \frac{1}{2} \rho_{\infty} V_{\infty}^2 \frac{C_{Lmax}}{W/S} \quad 3.30$$

All calculations are performed at 30000 ft altitude.

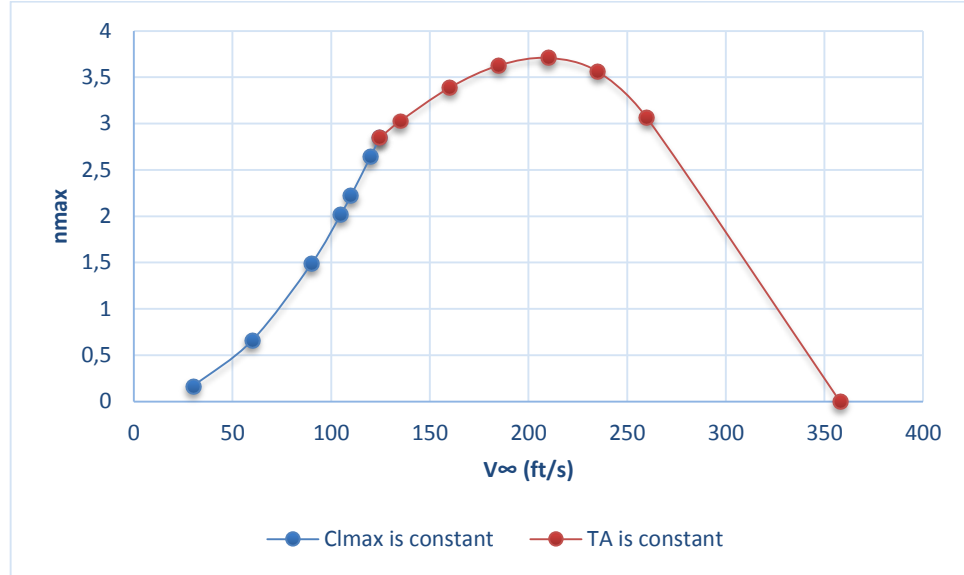


Figure 3.11 Maximum Load Factors vs Velocity at 30000 ft

3.15.2. Minimum Turn Radius

The equations giving the minimum turn radius, its corresponding velocity and the load factor are shown below. A sample calculation at sea level is also shown.

$$V_{\infty(Rmin)} = \sqrt{\frac{4K(W/S)}{\rho_{\infty}(T/W)}} \quad 3.31$$

$$V_{\infty(Rmin)} = \sqrt{\frac{4(0.0144)(5,7)}{(0.002377)(0.105)}} = 56 \text{ ft/s}$$

$$n_{(Rmin)} = \sqrt{2 - \frac{4Kcdo}{(T/W)^2}} \quad 3.32$$

$$n_{(Rmin)} = \sqrt{2 - \frac{4(0.0144)(0.014)}{(0.105)^2}} = 1.388$$

$$R_{(min)} = \frac{4K(W/S)}{g\rho_{\infty}/\left(\frac{T}{W}\right)^2 \sqrt{1 - \frac{4KC_{D0}}{(T/W)^2}}} = 101 \text{ ft} \quad 3.33$$

3.15.3. Maximum Turn Rate

Equations for the maximum turn rate calculations are illustrated in equation 3.34 and 3.36.

$$V_{\infty(wmax)} = \left[\frac{2(W/S)}{\rho_{\infty}} \right]^{0.5} \left(\frac{K}{C_{D,0}} \right)^{0.25} = 108 \text{ ft/s} \quad 3.34$$

$$n_{(wmax)} = \left(\frac{T/W}{\sqrt{KC_{D,0}}} - 1 \right)^{0.5} = 2.53 \quad 3.35$$

$$\omega_{max} = g \sqrt{\frac{\rho_{\infty}}{W/S} \left[\frac{T/W}{2K} - \left(\frac{C_{D,0}}{K} \right)^{0.5} \right]} = 0.694 \text{ rad/s} \quad 3.36$$

3.15.4. V-n Diagram

In the V-n diagram, the aerodynamic and structural constraints of the aircraft are plotted. Lines and their illustrations are listed below.

- n_{max} line: Aerodynamic limit on the load factor is imposed by $C_{L,max}$.
- Red line: Positive ultimate load factor (intersection in V_{∞} vs. n_{max} diagram).
- Blue line: High speed limit. At flight velocities which is higher than this limit, the dynamic pressure increases more than the design limit of the aircraft.
- Green line: Stall limit for negative lift.
- Purple line: Negative ultimate load factor
- Yellow line: Never exceed speed.

Corner velocity is the maneuverability point, which is very important for an aircraft.

$C_{L,max}$ and n are maximum at this point. Corner velocity is given as:

$$V^* = \sqrt{\frac{2n_{max}}{\rho_{\infty} C_{Lmax}} \frac{W}{S}} \quad 3.37$$

Velocities smaller than V^* ; any structural damage is not possible to the aircraft. The calculated value is shown below.

$$V^* = 139.41 \text{ ft/s}$$

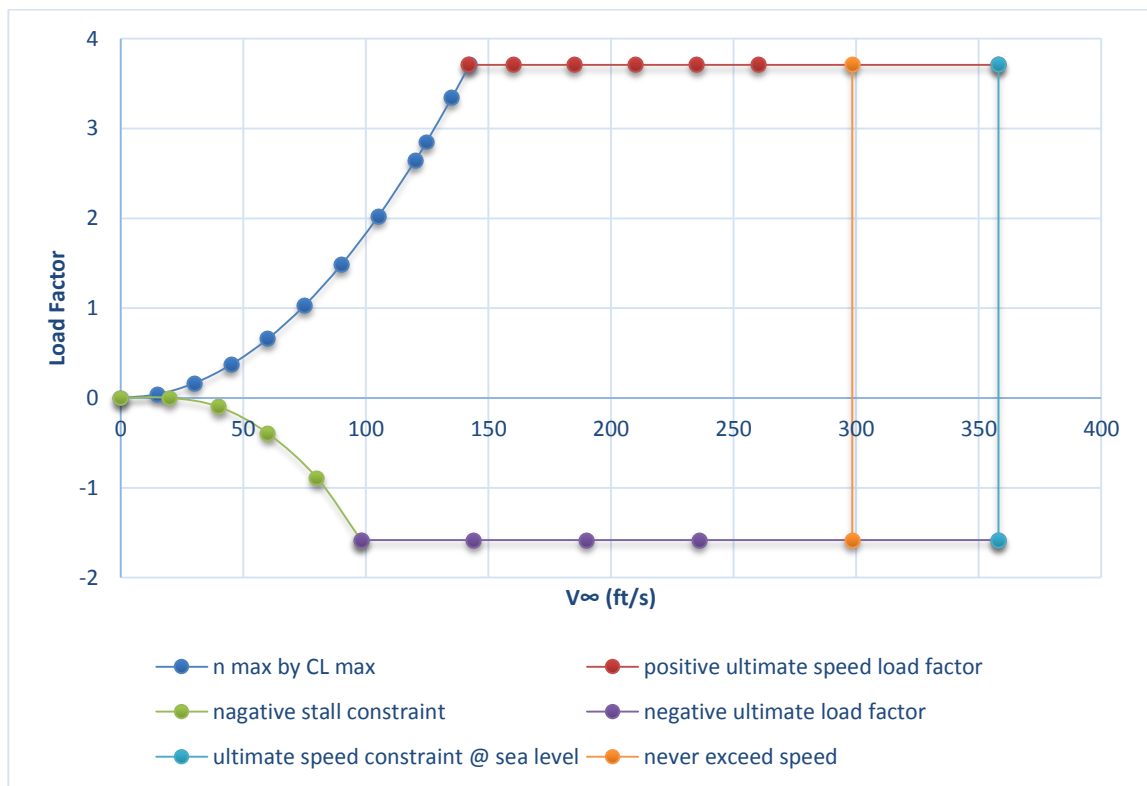


Figure 3.12 V-n Diagram

3.16. Longitudinal Stability Analysis

Longitudinal stability calculations shows the aircraft tendency to remain level flight. First of all, aircraft pitching moment is calculated. Then neutral point of the aircraft, where pitching moment is equal to zero, is calculated.

3.16.1. Neutral Point

3.16.1.1. Wing Term

Aerodynamic center of the wing is at 25% of mean aerodynamic center of the wing. X_{acw} is found as 20.1 ft.

$$C_{L\alpha} = \frac{2\pi \times AR}{2 + \sqrt{4 + \frac{AR^2 \beta^2}{\eta^2} \left(1 + \frac{\tan^2 \Lambda}{\beta^2}\right)}} \left(\frac{S_{exp}}{S_{ref}}\right) (F) \quad 3.38$$

$$\bar{x}_{acw} = \frac{x_{acw}}{\bar{c}} = \frac{20.1}{8.79} = 2.29 \quad 3.39$$

Wing factor F is calculated by using equation 3.40.

$$F = 1.07 \left(1 + \frac{d}{b}\right)^2 = 1.07 \left(1 + \frac{10.07}{208}\right)^2 = 1.073 \quad 3.40$$

As calculated before, for wing at cruise Mach number (clean), is found as 0.0805

$$\beta^2 = 1 - M^2 = 0.994, C_{L\alpha} = 7.1955/rad = 0.1256deg^{-1}$$

3.16.1.2. Fuselage Term

Fuselage terms for neutral point calculation is as follows. K_f is taken as 0.03 for position for the quarter root chord from Figure 16.14 [1].

$$C_{m\alpha fus} = \frac{K_f W_f^2 L_f}{c S_w} \quad 3.41$$

Where,

$W_f = \text{maximum width of fuselage} = 8.2 \text{ ft.}$

$L_f = \text{Length of the fuselage} = 55.8 \text{ ft}$

$S_w = \text{Wing area} = 1775 \text{ ft}^2$

Substituting the above values in the equation, $C_{m\alpha, fus} = 0.0063 \text{ deg}^{-1} = 0.36 \text{ deg}^{-1}$.

3.16.1.3. Horizontal Tail Term

Aerodynamic center of the horizontal tail is at $X_{ach} = 50.41 \text{ ft}$ from the nose.

$$\bar{x}_{ach} = \frac{\bar{x}_{ach}}{\bar{c}} = \frac{50.41}{4.76} = 10.59$$

Same calculations are performed for horizontal tail as for wing with its corresponding properties, aspect ratio is 8, exposed wing area is 163.2 ft², reference wing area is 165 ft², and lift curve slope is 5.73 rad⁻¹.

$$\eta_h = \frac{C_{l\alpha}}{2\pi/\beta} \quad 3.42$$

$$\eta_h = \frac{5.73}{2\pi/0.994} = 0.907$$

Using equation 3.43 lift curve slope horizontal tail is found;

$$C_{L\alpha h} = \frac{2\pi AR}{2 + \sqrt{4 + \frac{AR^2 \beta^2}{\eta^2} \left(1 + \frac{\tan^2 \Lambda_{max,t}}{\beta^2}\right)}} \left(\frac{S_{exposed}}{S_{ref}}\right) (F) \quad 3.43$$

$$\begin{aligned} C_{L\alpha h} &= \frac{2\pi 8}{2 + \sqrt{4 + \frac{8^2 0.994^2}{0.907^2} \left(1 + \frac{\tan^2 0.3}{0.994^2}\right)}} \left(\frac{163.4}{164}\right) (1.073) \\ &= 4.2 \text{ rad}^{-1} = 0.073 \text{ deg}^{-1} \end{aligned}$$

$\frac{\partial \varepsilon}{\partial \alpha}$ is the wing trailing vortex contributions to the downwash of the tail.

$$\frac{\partial \varepsilon}{\partial \alpha} = 4.44 \left[K_A K_\lambda K_H (\cos \Lambda_{c/4})^{0.5} \right]^{1.19} \quad 3.44$$

Where, $\frac{\partial \varepsilon}{\partial \alpha}$ is the wing trailing vortex contributions to the downwash of the tail.

3.16.1.4. Aspect Ratio Factor

Aspect ratio factor is found as follows [1].

$$K_A = \frac{1}{AR} + \frac{1}{1 + AR^{1.7}} = 0.039 \quad 3.45$$

3.16.1.5. Taper Ratio Factor

Taper ratio factor are found as follow [1].

$$K_\lambda = \frac{10 - 3\lambda}{7} = \frac{10 - 3 \times 0.5}{7} = 1.214 \quad 3.46$$

3.16.1.6. Horizontal Tail Location Factor

Horizontal tail location factor calculations are as follows:

$$K_H \frac{1 - \frac{h_b}{b}}{\sqrt[3]{\frac{2I_H}{b}}} = \frac{1 - \frac{34.59}{208}}{\sqrt[3]{\frac{2 \times 30.1}{208}}} = 1.26 \quad 3.47$$

Where h_b and I_H are the horizontal and vertical distances between tail mean aerodynamic quarter chord location and wing mean aerodynamic quarter chord location. Then

$$\frac{\partial \varepsilon}{\partial \alpha} = 4.44 [0.039 \times 1.214 \times 1.26 \times \cos(0.3)^{0.5}]^{1.19} = 0.151$$

Neutral point calculations are as follows.

$$\bar{X}_{np} = \frac{C_{L\alpha} \bar{X}_{acw} - C_{m_{cgus}} + \eta_h \frac{S_h}{S_w} C_{L_{\alpha h}} \frac{\partial \alpha_h}{\partial \alpha} \bar{X}_{ach}}{C_{L\alpha} + \eta_h \frac{S_h}{S_w} C_{L_{\alpha h}} \frac{\partial \alpha_h}{\partial \alpha}} \quad 3.48$$

$$\bar{X}_{np} = \frac{7.2 \times 2.29 - 0.36 + 0.907 \times \frac{165}{1775} \times 10.59 \times (1 - 0.151)}{7.2 + 0.907 \times \frac{165}{1775} \times 10.59 \times (1 - 0.151)} = 2.13$$

$$X_{np} = 18.8 \text{ ft}$$

3.16.2. Determination of Static Margin

Static margin can be calculated using 4.48.

$$K_n = \bar{X}_{np} - \bar{X}_{cg} \quad 3.49$$

Where, center of gravity is 17.6 ft (from the nose) calculated before

$$K_n = \frac{18.8 - 17.6}{8.7} = 0.097 = 9.7\%$$

$$C_{ma} = -C_{La} K_n = -0.6984 \text{ rad}^{-1} \quad 3.50$$

3.17. Landing Gear Placement and Sizing

3.17.1. Landing Gear Configuration

Tricycle landing gear is the best choice for TUYGUN. It has two main wheels located at aft of the c.g. and the auxiliary wheel located at forward of the c.g. Thanks to the tricycle landing gear, aircrafts become stable on the ground and can land at a fairly large ‘crab’ angle. For heavy aircrafts tricycle landing gear may have more than one wheel.

3.17.2. Landing Gear Placement

Since wingspan of the TUYGUN is very high, it is convenient to use two landing gears under wing tips. Also front landing gear is assumed as 5 ft from the nose of the aircraft, and it is located at midway of the fuselage. The main landing gear is located at midway of the mean chord of the wing. The station of main landing gear, mean aerodynamic chord and c.g. of wing is stated below.

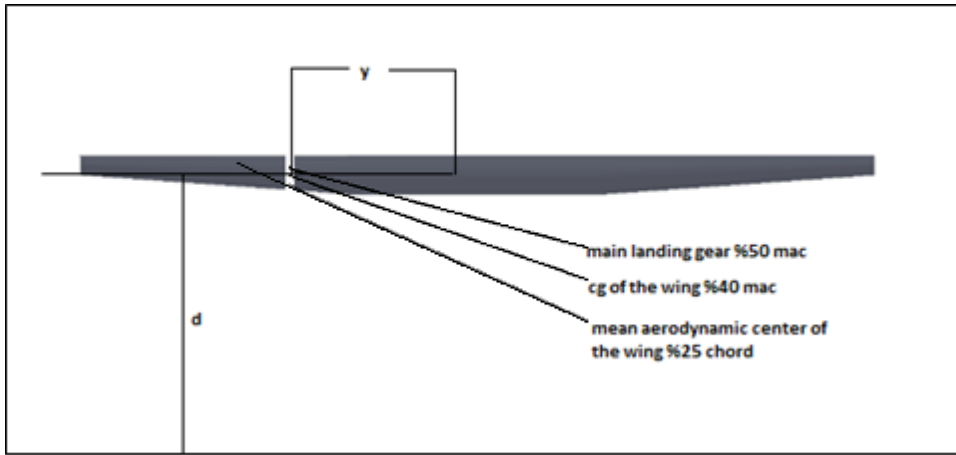


Figure 3.13 Aerodynamic Properties of the Wing

Distance d is (landing gear cg position from the nose of the fuselage) 18.16 ft. From the geometry the location of main landing gear is found as follows:

$$x_{xlg} = 18.16 + (0.50 - 0.25)\bar{c} = 20.34 \text{ ft}$$

In other words main landing gear is located at $55.8 - 20.34 = 35.46$ ft away from rear end of the fuselage.

\bar{y} is found before as 49.32 ft and $\alpha_{C_{Lmax}}$ is found as 17° before then;

$$\tan\theta_{static,taildown} = \frac{H_2}{35.46} = \tan 17^\circ \quad H_2 > 11.15 \text{ ft}$$

Where H_2 is the fuselage tip back height, H_1 is the height of the cg from ground. The tip back angle is the maximum aircraft nose-up attitude with the tail touching the ground and

the strut fully extended. It should be 15° or higher in order to prevent fuselage tipping back.

$$\tan\theta_{tip,back} = \frac{0.81}{H_2} = \tan 15^\circ$$

$$\tan\theta_{tipback} = \frac{0.81}{H_1} = \tan 15^\circ \text{ So } H_1 < 3.01 \text{ ft}$$

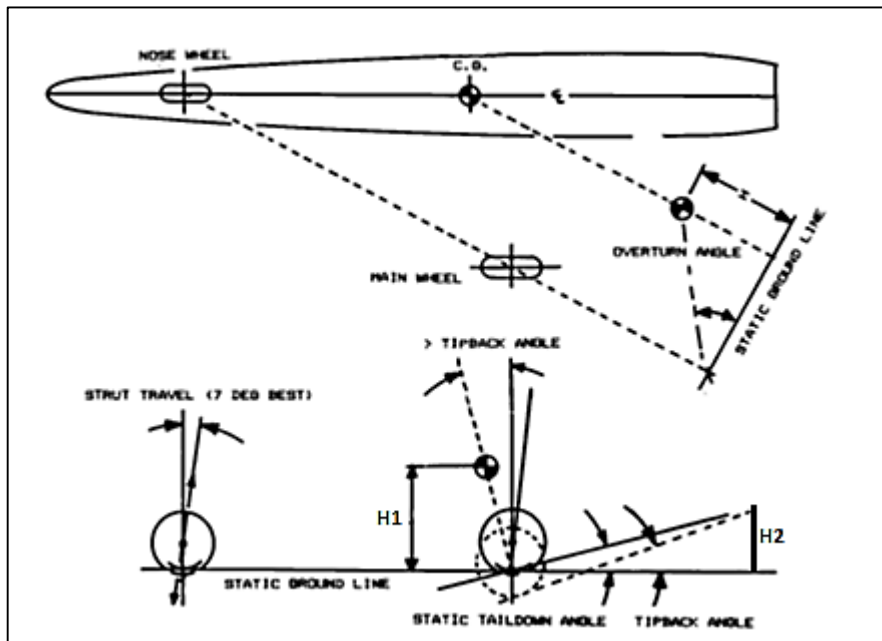


Figure 3.14 Properties of Landing Gear [1]

Information about the sizes of the wheels can be obtained by calculating the load acting on the nose and main landing gears. Moments are taken from the nose;

$$2F_m(x_m + x_n) = W_o x_n \quad 3.51$$

$$2F_m(0.81 + 18.8) = 10137 \times 18.8$$

$$F_m = 4859 \text{ lb}$$

$$F_n(x_m + x_n) = W_o x_n \quad 3.52$$

$$F_n(0.81 + 18.8) = 10137 \times 0.81$$

$$F_n = 420lb$$

Wheel diameters and widths are found from the Table 11.1 [1] for general aviation aircraft.

Wheel diameter and width of the nose landing gear:

- $Diameter_n = 1.51F_n^{0.349} = 12.41 \text{ in}$ $Width_n = 0.715F_n^{0.312} = 4.7 \text{ in}$

Wheel diameter and width of the main (rear) landing gear:

- $Diameter_r = 1.51F_r^{0.349} = 29.13 \text{ in}$, $Width_r = 0.7150F_r^{0.312} = 10.1 \text{ in}$

CHAPTER 4

ENERGY BALANCE FOR LOITERING

In this chapter, energy required and energy available diagrams are drawn using real time simulation. Energy balance diagram shows the power needed for flight, solar irradiance and battery power. Main aim is to obtain 48 hours of endurance or more. By defining payload weight main aim is to carry about 550 lb payload, the remaining 1654 lb belonging to the battery. Total solar panel area is taken as $1615ft^2$. Wing area is $1775ft^2$, horizontal tail area is $160ft^2$. It is assumed that usable wing area for solar panels is $1506ft^2$. Solar panels are not used on the regions on the wing which have high curvature and the control surfaces. Also using same assumptions, solar panel area on horizontal tail is estimated as $108ft^2$.

4.1. Solar Irradiance

Duffie J. A., Beckman W. A [32] solar irradiance model is used for illustrating daily solar energy obtained. Model is based on day number (1 January represents 1, 31 December represents 365), pressure, solar irradiance constant, and latitude. Location of city of Ankara is used for simulating endurance.

Table 4.1 Representation of Solar Irradiance Constant

Constant	Representation
d	Day of the year
ϕ	Latitude
P	Pressure
h	Hour
G_{sc}	Radiation constant
P₀	Pressure at sea level
g	The acceleration of gravity
δ	Declination
τ	Atmospheric transmittance for beam radiation
v	Extraterrestrial radiation

$$v^2 = \left(1 + 0.033 \times \cos \frac{360 \times d}{365}\right) \quad 4.1$$

$$\delta = 23.45 \times \sin\left(\frac{360 \times (284 + d)}{365}\right) \quad 4.2$$

$$P_s = G_{sc} \times A_s \times v^2 \times (\sin\delta \times \sin\phi + \cos((h - 12) \times 15) \times \cos\delta \times \cos\phi) \quad 4.3$$

$$\tau = \frac{p}{p_0} \times (\sqrt{1229 + (614 \times \cos(\phi - \delta))^2} - 614 \times \cos(\phi - \delta)) \quad 4.4$$

$$A_s = 0.5 \times (e^{-0.65 \times \tau} + e^{-0.095 \times \tau}) \quad 4.5$$

A_s represents the solar radiation per area. If all calculations are made for 21 June Ankara namely 40° North, following solar irradiance graph is obtained.

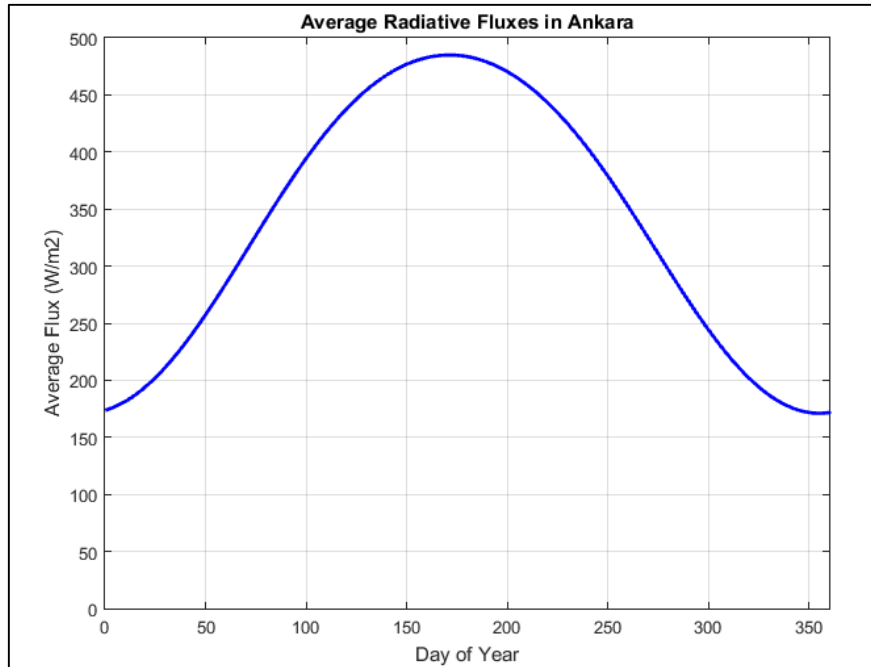


Figure 4.1 Average Annual Solar Radiation Fluxes of Ankara

Area under the curve gives the total solar energy. In Ankara sun rises at 4.50 am and sets at 19.50 pm as seen from Figure 4.1. Annual solar radiation for city of Ankara is showed in Figure 4.2. Radiation fluxes of June 21 is approximately 3 times higher than radiation fluxes of 21 December. Therefore it is expected that endurance reduces dramatically on winter for solar powered aircrafts

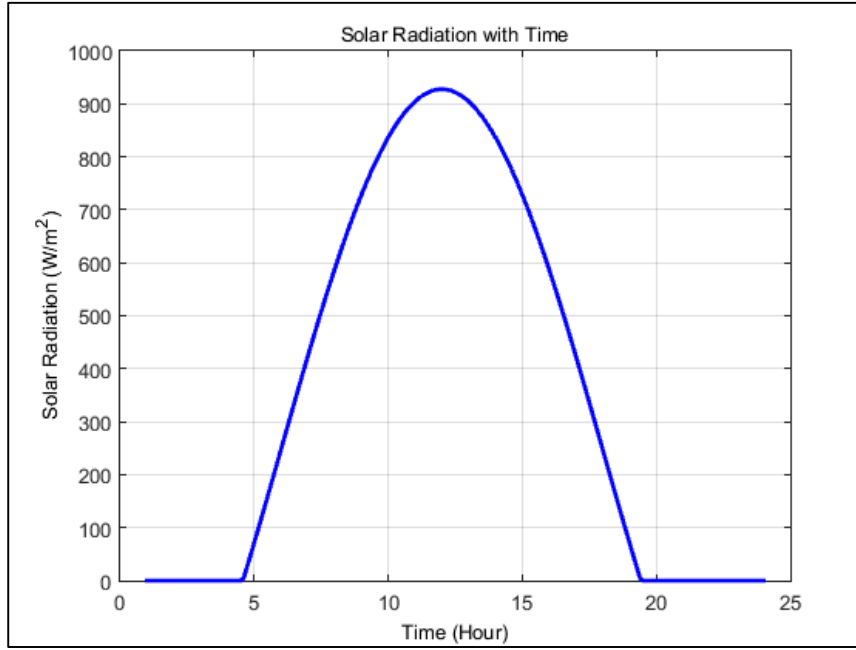


Figure 4.2 Solar Radiation of Ankara on June 21

4.2. Solar Energy Calculation

Total energy gained from solar radiation is calculated by equation 4.6;

$$E_{elec,tot} = \frac{I_{max} \times T_{day}}{\pi/2} \times A_s \eta_{wthr} \eta_{sc} \eta_{cbr} \eta_{mppt} \quad 4.6$$

Where

η_{wthr} is the weather efficiency namely if there is a clear sky or dark sky. It is assumed that the sky is clear.

η_{sc} is the solar cell efficiency taken as 0.3.

η_{cbr} is the wing camber efficiency taken as 0.9. It is calculated by using wing upper surface slope. It is calculated by taking both oncoming airfoil upper surface coordinate data and calculating its slope. Solar panels are not used on area having high slope. η_{mppt} (Sunlight conversion system efficiency) is taken as 0.95.

Table 4.2 Efficiency of Solar Instruments

Instruments	Efficiency
Cell configuration	0.93%
MPPT	0.97%
MPPT tracking	0.95%
Charge/Discharge	0.986%
Propeller	0.8%
Electric Motor	87%
Gearbox	95%

4.3. Required Energy Calculation

Required energy is calculated before conceptual design phase. Power required analysis is performed in order to simulate loitering phase. During simulation, the flight efficiencies are assumed as constant. Also it is assumed that aircraft fly at clear sky. Wind is assumed as steady; there is no gust. During simulations, batteries are taken as fully charged before takeoff.

4.4. Battery Energy Calculation

Battery is one of the most important phenomena for solar powered aircraft. When determining battery properties, Solar Impulse's battery technology is used since Solar Impulse designers use the most cost and energy efficient batteries. In addition, specific energy of the batteries is greater than 572 Wh/lb, which means they are efficient enough and available for Hybrid UAV. There are very important parameters about batteries of Solar Impulse given from official website. There are 4 pieces of 41 kWh lithium-ion batteries and total 52 kW power plant on Solar Impulse. Each battery weighs 348 lb 5 identical batteries are used for this thesis study and simulation. Also it is assumed that excess solar energy is stored in the batteries. Battery charge and discharge efficiencies are taken as 0.986 [4].

4.5. Real Time Simulation

Theory of real time simulation is based on energy balance of the system. Aircraft takes off with fully charged batteries. Until flying up to the mission area and altitude, turbofan engine is used. Then solar irradiance energy and battery energy are used. If required power becomes greater than the available power, simulation stops. Optimum takeoff time is found by trying different times of the day. For instance, On June 21 maximum endurance occurs when aircraft starts loitering at 24.00. On the other hand, On December 21(shortest daytime) maximum endurance time occurs when aircraft starts loitering at 06.00 am. Simulation is performed for 2 additional different days of the year which are 21 March, 23 September. Solar radiation on equinoxes are same. Differences are sunrise and sunset times. Simulations are performed for each day in order to show the optimum loitering hours.

4.6. Methods for Reconstructing Solar Cycle

Major advantage of the hybrid system is the possibility of reconstructing the solar cycle. One way is to fill excess fuel to the aircraft in order to attain to the point where required power is equal to the solar power obtained from solar panels. After reaching that point, cycle restarts.

Another method is the unpowered gliding method. In other words, if required energy becomes more than available solar and battery energy, aircraft starts unpowered gliding in order attain to the point where required power is equal to the solar power obtained from solar panels. For instance when aircraft loiters at 45000 ft with 40% efficient solar cells on June 21, approximately 4 hours are needed to reach to that point. After 4 hours of unpowered gliding, solar cycle restarts at 5000 ft altitude at 11.00 am.

4.7. Simulations of Various Cases

First case is the lowest altitude case. At 20000 ft aircraft needs 32 kW power in order to sustain loitering. As mentioned before, 4 different days of the year are used for illustrating loitering time.

4.7.1. Simulations for 30% Efficient Solar Cells

Firstly, simulations are performed by 30% efficient solar cells.

4.7.1.1. 20000 ft, June 21, 30% Efficient Solar Cells

The longest daytime of the year in the northern hemisphere occurs on 21 June. Sun rises at 04:50 am. Aircraft start loitering at 24:00. All simulations are performed for location of Ankara (40° latitude).

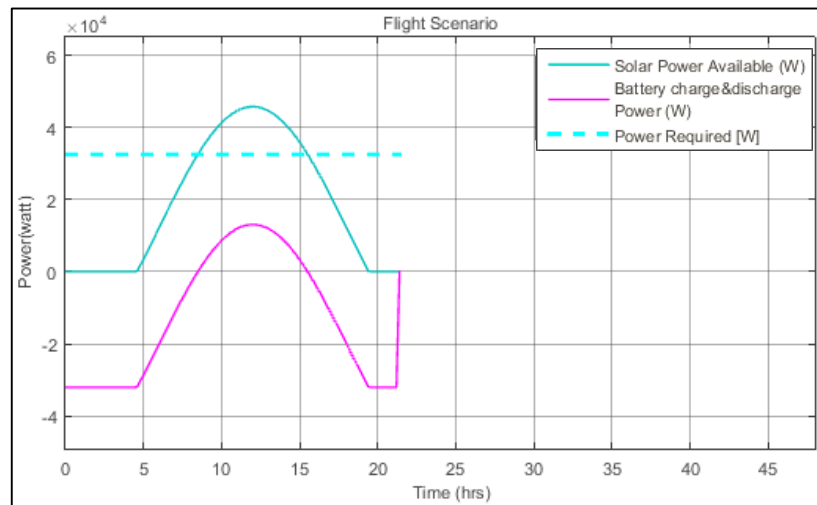


Figure 4.3 Energy Balance Diagram with 30% efficient solar cells on June 21

As mentioned before, when required power is less than battery power and solar powered gained from sun simulation stops. For this case, simulation stops after 21.3 hours loitering. Figure 4.3. Reconstruction method suggests that, firstly, the time between simulation stops (A) and the point, where the power gained from sun is equal to the required power (B), is calculated. There are 9.5 hours between point (A) and point (B), Figure 4.4.

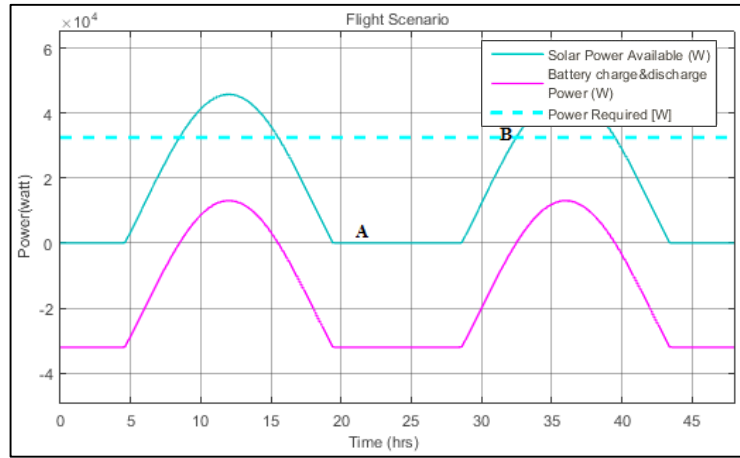


Figure 4.4 Required Time Calculation for Reconstructing Solar Cycle Diagram with 30% Efficient Solar Cells on June 21

9.5 hours loitering flight must be sustained by turbofan engine in order to reconstruct the solar cycle. Secondly, weight estimation equation is used in order to find required fuel by assuming that aircraft fly only by turbofan. Weights are estimated again with iteration method. Using equations 2.2 to 2.12 and 4.7:

$$\frac{W_1}{W_0} = 0.97, \text{ engine start, taxi and takeoff, historical trend was used.}$$

$$\frac{W_2}{W_1} = 1.0065 - 0.325M^2$$

$$\frac{W_3}{W_2} = \exp\left(\frac{-Rc_t}{V(L/D)}\right), \text{ then } \exp\left(\frac{-6076100 \times 1.11 \times 10^{-4}}{2 \times 110 \times (35)}\right) = 0.9228$$

Specific fuel consumption was taken as 0.4.

$$Endurance = \exp\left(-\frac{Ec_t}{L/D}\right) \quad 4.7$$

$$\frac{W_4}{W_3} = e^{\frac{Ec_t}{L/D}} = 0.8971, \text{ where endurance is 9.5 hours.}$$

$$\frac{W_5}{W_4} = \frac{W_3}{W_2}, \text{ cruise back}$$

$$\frac{W_6}{W_5} = 0.992, \text{ descend}$$

$$\frac{W_7}{W_6} = 0.993, \text{ landing and stop}$$

$$\frac{W_7}{W_0} = \frac{W_7}{W_6} \frac{W_6}{W_5} \frac{W_5}{W_4} \frac{W_4}{W_3} \frac{W_3}{W_2} \frac{W_2}{W_1} \frac{W_1}{W_0} = 0.7387$$

$$\frac{W_f}{W_0} = 1.06 \left(1 - \frac{W_7}{W_0} \right) = 0.277$$

Also $\frac{W_4}{W_0} = \frac{W_4}{W_3} \frac{W_3}{W_2} \frac{W_2}{W_1} \frac{W_1}{W_0} = 0.789 W_0$ is calculated as

$$W_0 = \frac{W_{payload}}{1 - 2.75(W_0)^{-0.18} - \frac{W_f}{W_0}}$$

12000 lb. after iteration. Then W_4 is calculated as 9468 lb.

$$\frac{W_3}{W_0} = \frac{W_3}{W_2} \frac{W_2}{W_1} \frac{W_1}{W_0} = 0.88 \quad W_3 = 10560 \text{ lb}, \text{ during 9.5 hours loiter}$$

$10560 - 9468 = 1092$ lb fuel is consumed.

If 1092 lb. excess fuel added to the tanks before takeoff, solar cycle can be reconstructed and endurance becomes 48 hours. But it is too heavy for aircraft to fill in such an excess fuel before takeoff. Therefore optimizing excess fuel method does not work for these conditions.

4.7.1.2. 20000 ft, March 21, 30% Efficient Solar Cells

With same conditions except the day condition, simulations are performed and following results are obtained. Sun rises at 05:50 am and the maximum endurance occurs when aircraft starts loitering at 05:50 am. Loitering lasts 17.1 hours.

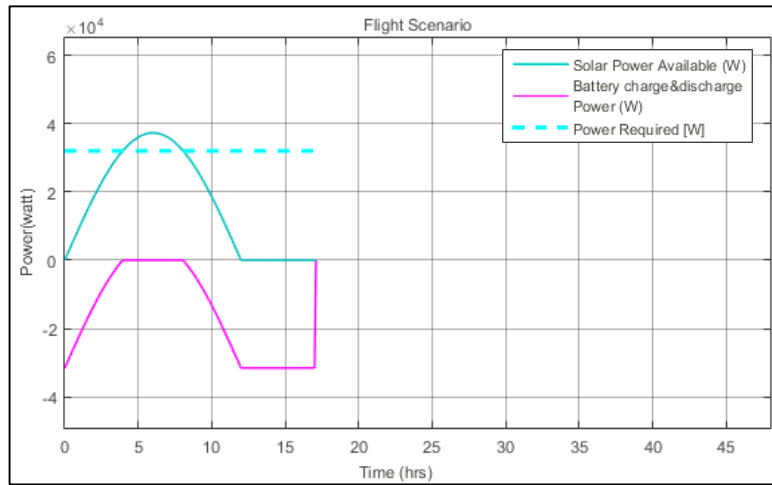


Figure 4.5 Energy Balance Diagram with 30% Efficient Solar Cells on March 21

As seen from Figure 4.5, loitering endurance is 17.2 hours. Time needed for reconstructing the solar cycle is 10.2 hours. Using equations 2.2 to 2.12 and 4.7 excess fuel is calculated as 1209 lb. It does not make sense to reconstruct solar cycle for these conditions.

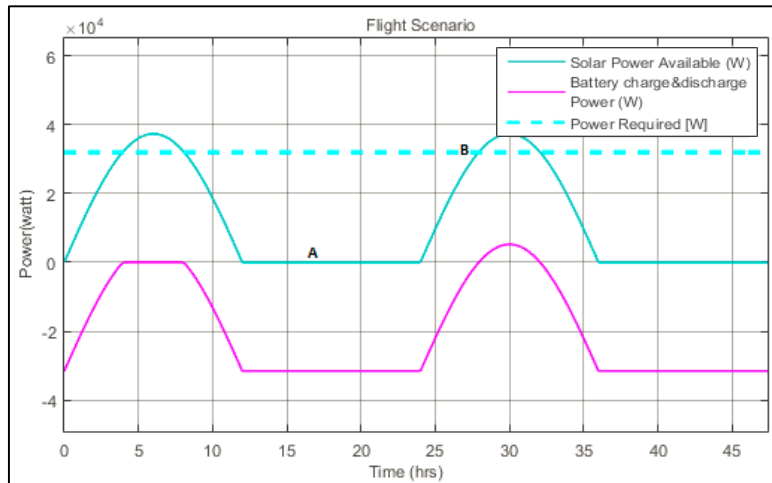


Figure 4.6 Required Time Calculation for Reconstructing Solar Cycle Diagram with 30% Efficient Solar Cells on March 21

4.7.1.3. 20000 ft, September 23, 30% efficient solar cells

23 September flight conditions gives approximately same results with 21 March as seen from Figure 4.7. Airplane starts loitering at 04:00 am.

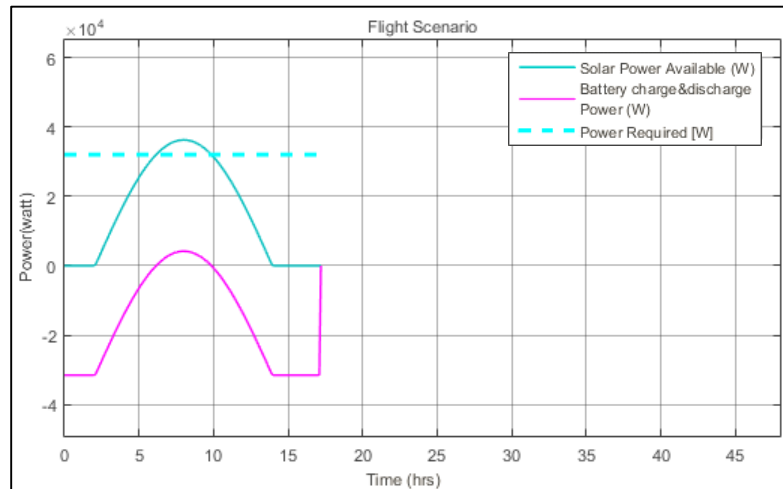


Figure 4.7 Energy Balance Diagram with 30% Efficient Solar Cells on September 23

4.7.1.4. 20000 ft, December 21, 30% Efficient Solar Cells

On December 21, namely shortest daytime in the year, hybrid airplane endurance time is relatively short due to less solar irradiance. Endurance is approximately 12.3 hours when aircraft starts loitering at 07:00 am. Available power never becomes equal to the required power. Therefore optimizing excess fuel method does not work.

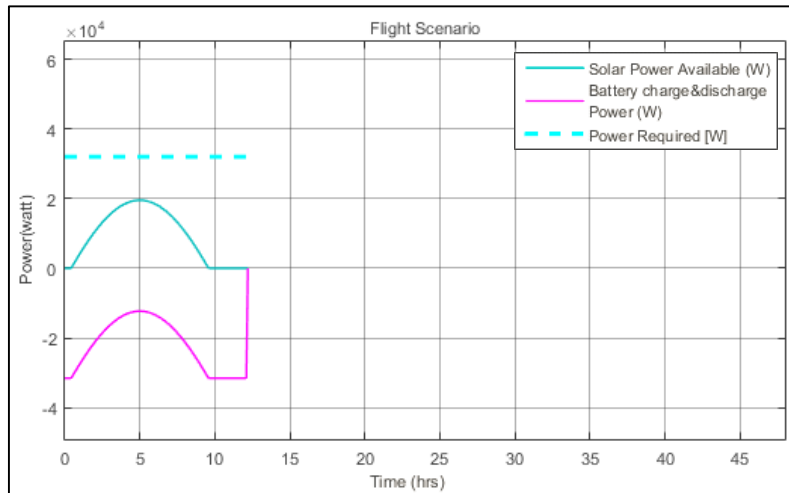


Figure 4.8 Energy Balance Diagram with 30% Efficient Solar Cells at December 21

4.7.2. Simulations for 40% Efficient Solar Cells

After 30% efficient solar cells simulations, it is observed that 40% efficient solar cells are more suitable for the current design. As mentioned before, these solar cells are really expensive for solar aircraft. Currently, solar powered aircrafts use 22% efficient solar cells. Developments state that 10 years later 40% efficient solar cells might be used for solar powered aircraft technology. Following simulations are done by using 40% efficient solar cells.

4.7.2.1. 20000 ft, June 21, 40% Efficient Solar Cells

As seen from Figure 4.9, maximum endurance becomes 26.6 hours when aircraft starts loitering at 22:00 pm.

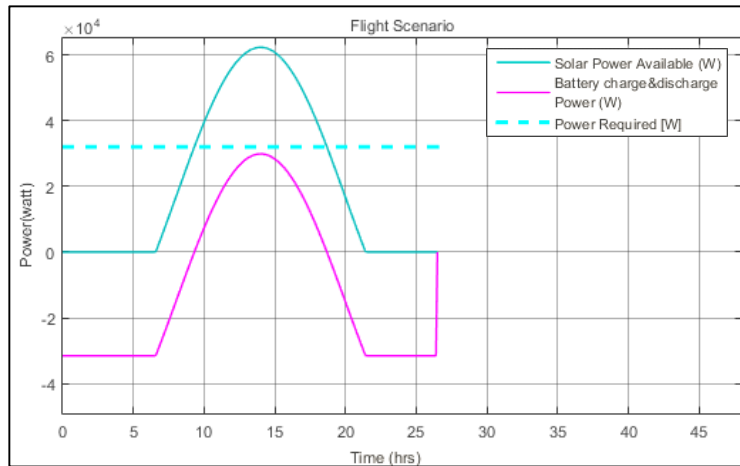


Figure 4.9 Energy Balance Diagram with 40% Efficient Solar Cells on June 21

There are 5.5 hours between the times when the simulation ends (A) and solar power available which is equal to the power required (B)

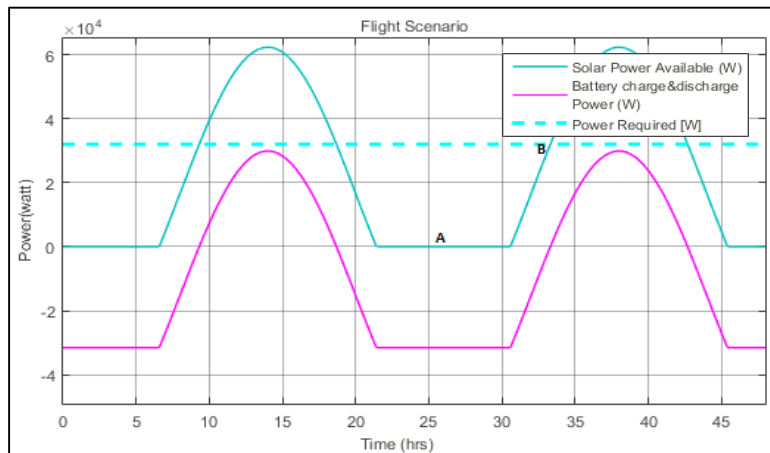


Figure 4.10 Required Time Calculation for Reconstructing Solar Cycle Diagram with 40% Efficient Solar Cells on June 21

Time needed for reconstructing the solar cycle is 5.5 hours. Using Weight equations 2.2 to 2.12 and 4.7 gross weight calculated as 10620 lb, $W_3 = 9346 \text{ lb}$, $W_4 = 9010 \text{ lb}$. During 5.5 hours loiter, $9346 - 9010 = 336 \text{ lb}$ fuel is consumed. If 336 lb. excess fuel

is added to the tanks before takeoff, solar cycle can be reconstructed and endurance becomes 67 hours.

4.7.2.2. 20000 ft, March 21, 40% Efficient Solar Cells

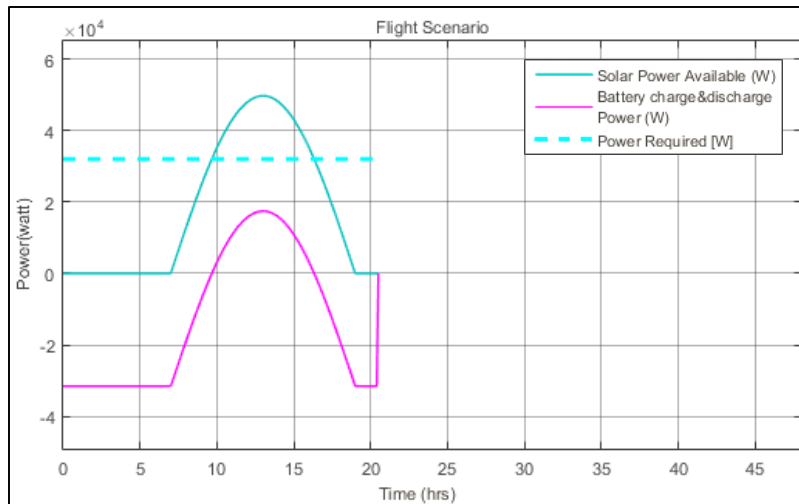


Figure 4.11 Energy Balance Diagram with 40% Efficient Solar Cells on March 21

As seen from Figure 4.11 loiter endurance is calculated as 20.6 hours when aircraft starts loitering at 23:00, There are 6.25 hours between the time when the simulation ends (A) and solar power available which is equal to the power required (B) as illustrated in Figure 4.11.

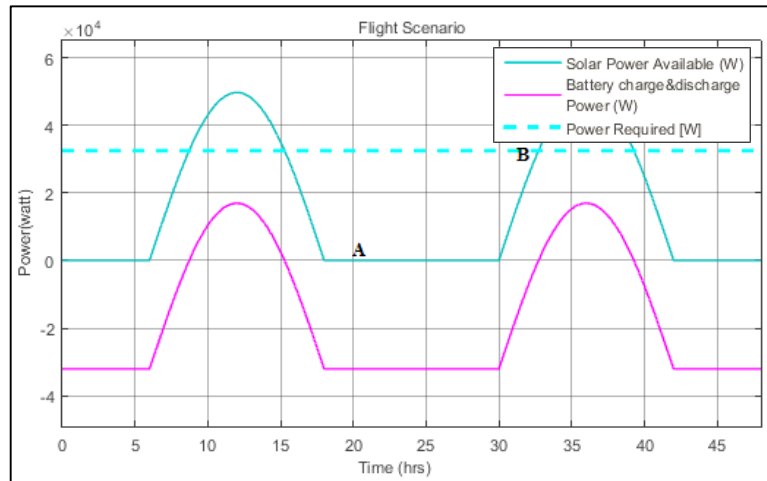


Figure 4.12 Required Time Calculation for Reconstructing Solar Cycle Diagram with 40% Efficient Solar Cells on March 21

Time needed for reconstructing the solar cycle is 13 hours. Using Weight equations 2.2 to 2.12 and 4.7, gross weight is calculated as 12729 lb, W_3 is calculated as 11201 lb. W_4 is calculated as 9836 lb. During 13 hours loiter, $1201 - 9836 = 1365$ lb fuel is consumed. If 1365 lb excess fuel is added to the tanks before takeoff, solar cycle can be reconstructed which is irrelevant to add such an excess fuel since it is too heavy to be used for current design.

4.7.2.3. 20000 ft, September 23, 40% Efficient Solar Cells

When airplane starts loitering at 23:00, approximately same results are obtained as for 21 March.

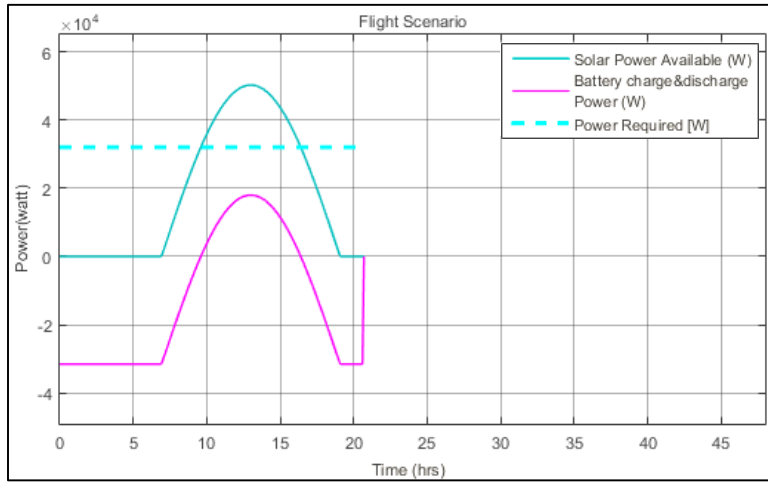


Figure 4.13 Energy Balance Diagram with 40% Efficient Solar Cells on September 23

4.7.2.4. 20000 ft, December 21, 40% Efficient Solar Cells

On December 21 maximum endurance is 13.5 hours when aircraft starts loitering at 06:00 am. However available power never becomes equal to the required power. Therefore optimizing excess fuel does not work.

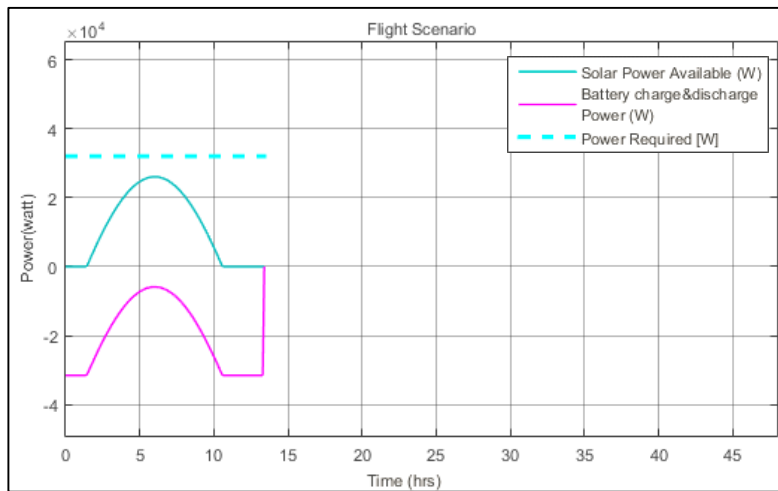


Figure 4.14 Energy Balance Diagram with 40% Efficient Solar Cells on December 21

4.7.2.5. 30000 ft, June 21, 40% Efficient Solar Cells

Same simulations were performed for 30000 ft altitude. At 30000 ft required power of aircraft is 39.7 kW. On June 21, maximum endurance of the aircraft is 21.3 hour when aircraft starts loitering at 01.00 am.

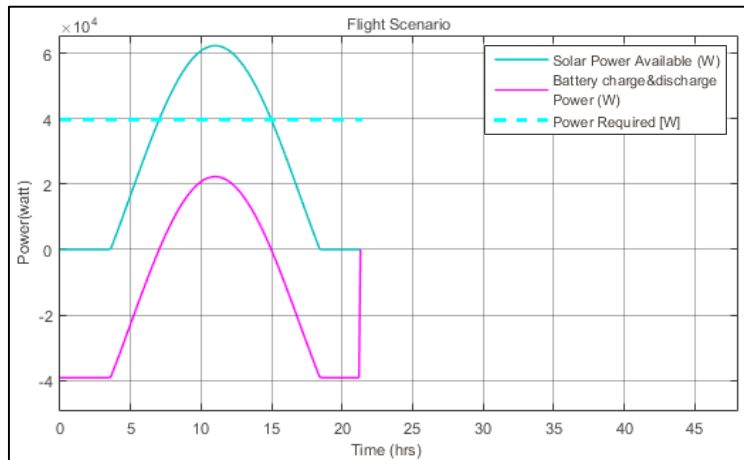


Figure 4.15 Energy Balance Diagram with 40% Efficient Solar Cells on June 21 at 30000 ft

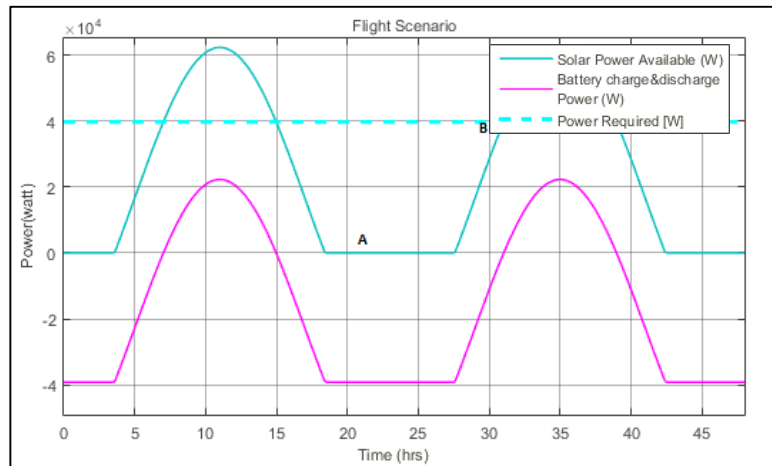


Figure 4.16 Required Time Calculation for Reconstructing Solar Cycle Diagram with 40% Efficient Solar Cells on June 21

Time needed for reconstructing the solar cycle is 10.2 hours. Using Weight equations 2.2 to 2.12 and 4.7 gross weight is calculated as 11786 lb, W_3 is calculated as 10371 lb W_4 is calculated as 9366 lb. During 10.2 hours loiter 10371 – 9366 = 1005 lb fuel is consumed. If 1005 lb excess fuel is added to the tanks before takeoff, solar cycle can be reconstructed but it is irrelevant to add such an excess fuel since it is too heavy to be used for current design.

4.7.2.6. 30000 ft, March 21, 40% Efficient Solar Cells

Maximum endurance is 16.6 hours when aircraft starts loitering at 04:00 am.

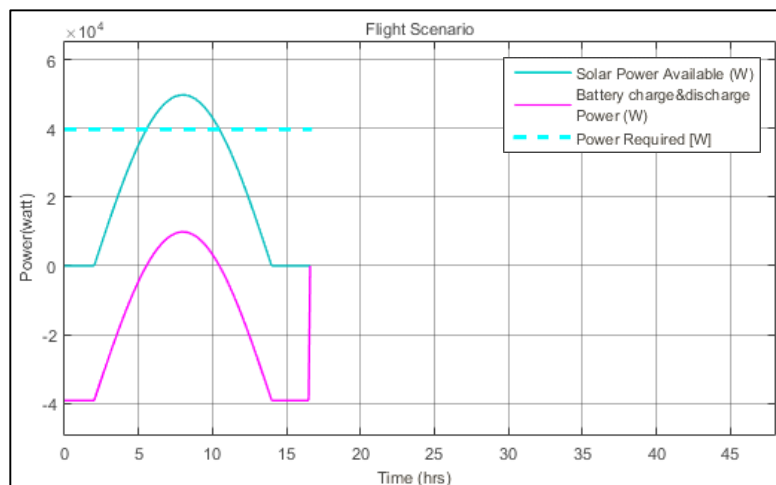


Figure 4.17 Energy Balance Diagram with 40% Efficient Solar Cells on March 21 at 30000 ft

Time needed for reconstructing the solar cycle is approximately 13 hours. Excess fuel is found as 1365 lb. If 1365 lb excess fuel was added to the tanks before takeoff, solar cycle can be reconstructed but it also seems to be irrelevant to fill in such an excess fuel before takeoff.

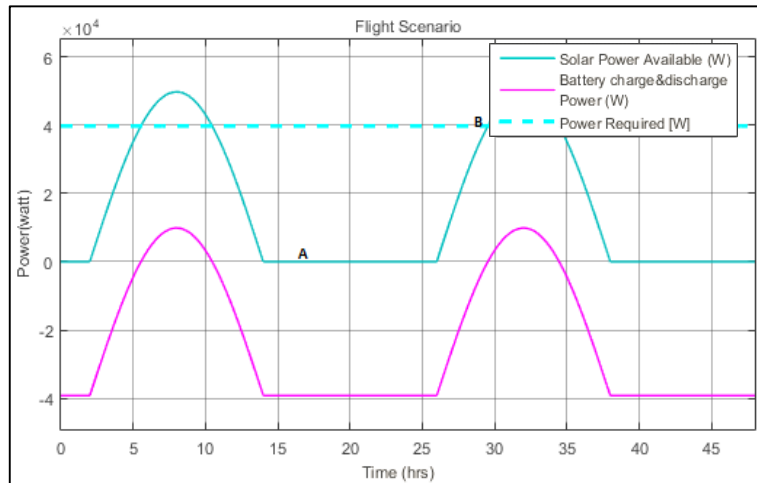


Figure 4.18 Required Time Calculation for Reconstructing Solar Cycle Diagram with 40% Efficient Solar Cells on March 21

4.7.3. 30000 ft, September 23, 40% Efficient Solar Cells

Aircraft endurance is approximately same as 21 March when aircraft starts loitering at 04:00 am.

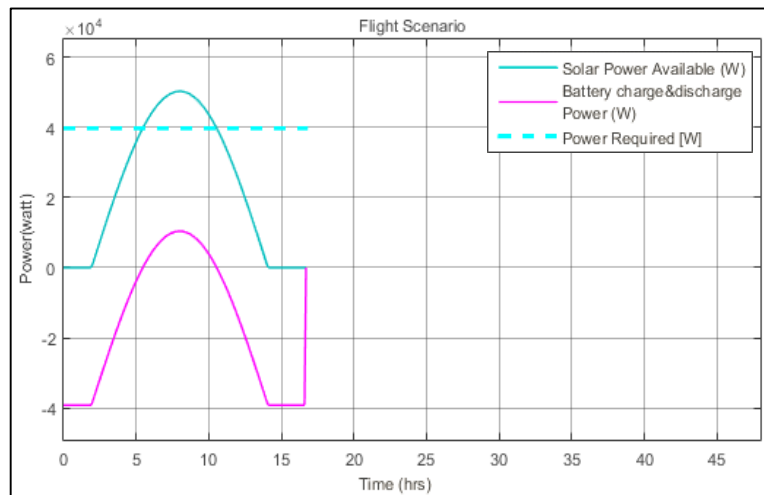


Figure 4.19 Energy Balance Diagram with 40% Efficient Solar Cells on September 23 at 30000 ft

4.7.4. 30000 ft, December 21, 40% Efficient Solar Cells

On December 21 maximum endurance is 11 hours when aircraft starts loitering at 07:00 am. However available power never becomes equal to the required power. Therefore optimizing excess fuel does not work.

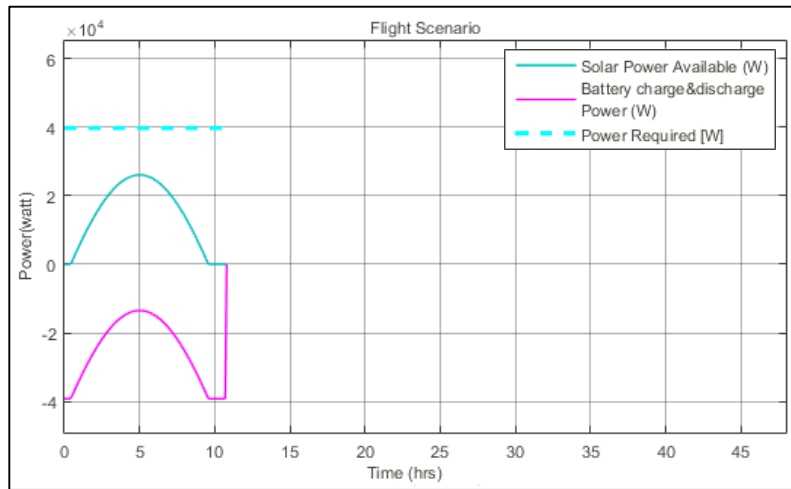


Figure 4.20 Energy Balance Diagram with 40% Efficient Solar Cells on December 21 at 30000 ft

4.7.5. 45000 ft, June 21, 40% Efficient Solar Cells

At 45000 ft required power is calculated as 53.88 kW. However solar power gained from sun decreases when altitude increases. Therefore endurance is approximately %30 lower than 30000 ft. Endurance is found as 17 hours on June 21 when airplane starts loitering at 04.00 am.

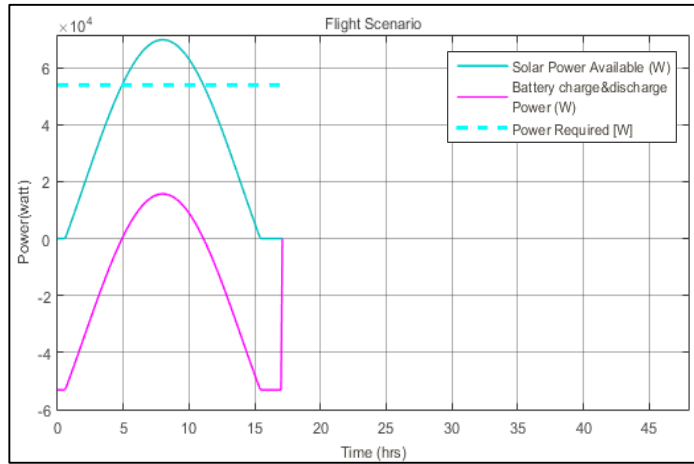


Figure 4.21 Energy Balance Diagram with 40% Efficient Solar Cells on June 21 at 45000 ft

Time needed for reconstructing the solar cycle is approximately 11 hours. Excess fuel is found as 1102 lb. If 1365 lb excess fuel is added to the tanks before takeoff, solar cycle is reconstructed which is irrelevant to add such an excess fuel to the aircraft.

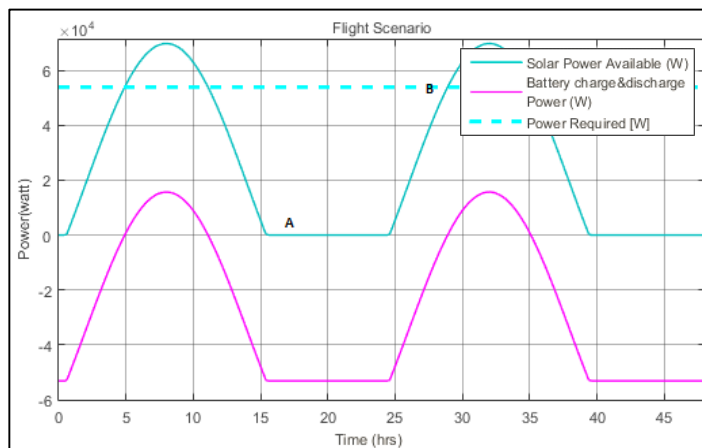


Figure 4.22 Required Time Calculation for Reconstructing Solar Cycle Diagram with 40% Efficient Solar Cells on June 21 at 45000 ft

4.7.6. 45000 ft, March 21, 40% Efficient Solar Cells

Maximum endurance is found as 13 hours when aircraft starts loitering at 06:00 am.

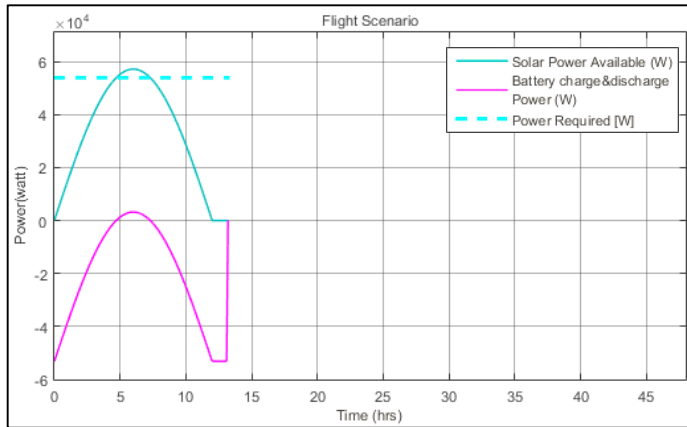


Figure 4.23 Energy Balance Diagram 40% Efficient Solar Cells on March 21 at 45000 ft

Time needed for reconstructing the solar cycle is approximately 15.2 hours. Excess fuel is found as 1680 lb. If 1680 lb excess fuel was added to the tanks before takeoff, solar cycle can be reconstructed but it seems to be irrelevant to fill in such an excess fuel before takeoff.

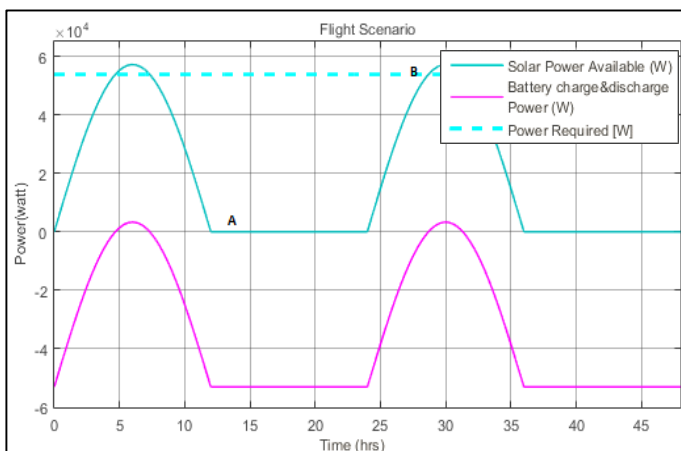


Figure 4.24 Required Time Calculation for Reconstructing Solar Cycle Diagram with 40% Efficient Solar Cells on March 21 at 45000 ft

4.7.7. 45000 ft, September 23, 40% Efficient Solar Cells

Aircraft endurance on September 23 is approximately same as March 21 when aircraft starts loitering at 05:00 am.

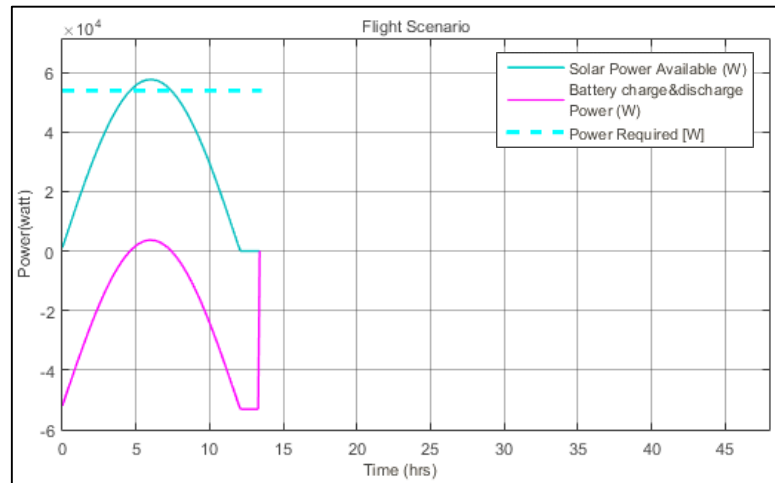


Figure 4.25 Energy Balance Diagram with 40% Efficient Solar Cells on September 23 at 45000 ft

4.7.8. 45000 ft, 21 December, 40% Efficient Solar Cells

On December 21 maximum endurance is 8 hours when aircraft starts loitering at 09:00 am. However available power never becomes equal to the required power. Therefore optimizing excess fuel does not work.

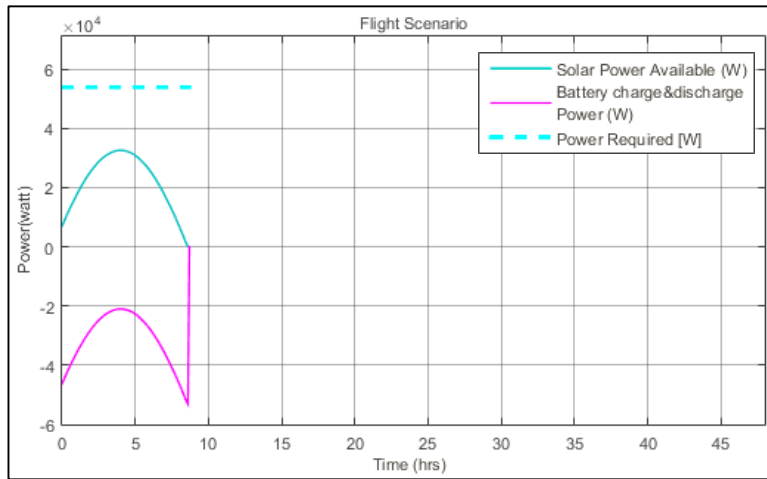


Figure 4.26 Energy Balance Diagram with 40% Efficient Solar Cells on December 21 at 45000 ft

4.7.9. 45000 ft, June 21, 40% Efficient Solar Cells with Batteries Having 328 kWh Energy Density

In near future, through battery energy densities doubling, continuous flight may be possible. Figure 4.27 shows Hybrid UAV loiter simulation at 45000 ft, with 40% efficient solar panels and batteries having 328 kWh energy density.

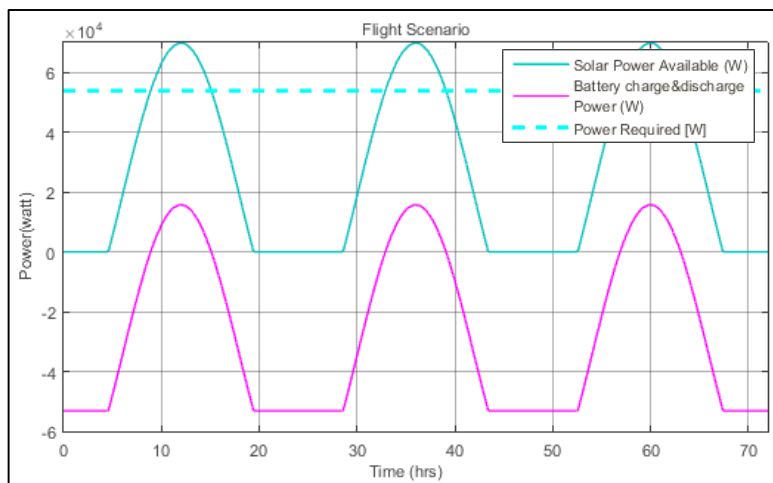


Figure 4.27 Energy Balance Diagram for Continuous Flight

CHAPTER 5

COST ANALYSIS

In this chapter, cost analysis of the TUYGUN is performed. It is assumed that 10 units of aircraft are produced. DAPCA-IV model is used for calculations. RDT&E and flyaway costs of TUYGUN are found. Model uses costs of 1999. Therefore, prices is updated in accordance to inflation rates in the US to calculate the 2016 prices. Raymer [1] describes the modified DAPCA IV cost model as indicated in Equations 5.1-5.9. DAPCA IV model does not include solar cells. Therefore cost of solar cells are added. Reduction in the cost of solar cells power per kW is taken into account. Figure 5.1 indicates the cost of solar cells per kW. During cost of solar cell calculations current price of the 30% efficient solar cells is taken as \$30000 per m², current price of the 40% efficient solar cells is taken as \$90000 per m² [54]

As mentioned in Chapter 1, thanks to technological developments, cost of solar power per Watt tends to decrease, and the availability of the solar cells tends to increase. Therefore, when estimating aircraft cost, it is important to take into account the reduction in the cost of solar power. Using historical trend of the reduction in the cost of solar power, annual reduction rate is estimated as 20%, Figure 5.1.

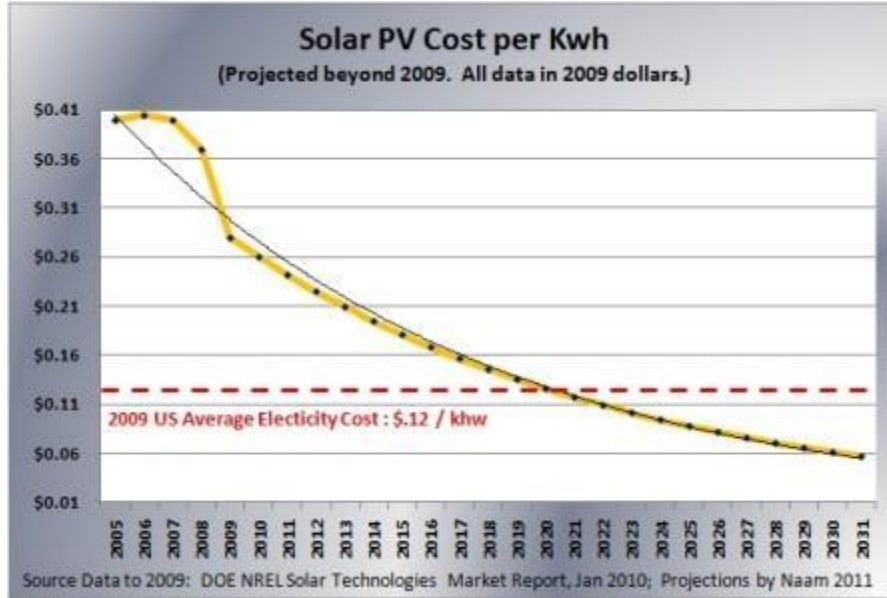


Figure 5.1 Yearly PV System Costs and Prediction per kW [53]

RDT&E + flyaway cost

$$= H_e R_e + H_t R_t + H_m R_m + H_q R_q + C_d + C_f + C_m + C_{eng} N_{eng} + C_{avionics} \quad 5.1$$

$$H_e : \text{Engineering Hours} = 4.86 W_e^{0.777} V^{0.894} Q^{0.163} \quad 5.2$$

$$W_e : \text{empty weight (lb)}, \quad W_e = 10128 \text{ lb}$$

$$V : \text{Maximum speed (knots)}, \quad V = 272 \text{ knots}$$

$$Q : \text{Production number}, \quad Q = 10$$

$$H_e = 4.86(10128)^{0.777} (272)^{0.894} (10)^{0.163},$$

$$H_e = 1378928 \text{ hours } R_e = 86 \text{ \$/h}$$

5.3

$$H_t : \text{Tooling Hours} = 5.99 W_e^{0.777} V^{0.696} Q^{0.263},$$

$$H_t = 704881 \text{ hours}, R_t = 88 \text{ \$/h}$$

$$H_m: \text{Manufacturing Hours} = 7.37W_e^{0.82}V^{0.484}Q^{0.641}, \quad 5.4$$

$$H_m = 937777 \text{ hours}, R_m = 73 \text{ \$/h}$$

$$H_q: \text{Quality Control Cost} = 0.133H_m, \quad 5.5$$

$$H_q = 124724 \text{ hours}, R_q = 81 \text{ \$/h}$$

$$C_d: \text{Development Support Cost} = 66W_e^{0.63}V^{1.3} \quad 5.6$$

$$C_d = 32311847$$

$$C_f: \text{Flight Test Cost} = 1807.1W_e^{0.325}V^{0.282}FTA^{1.21} = 8415735 \quad 5.7$$

$$\text{Number of Flight Test Aircraft : } FTA = 2$$

$$C_m: \text{Manufacturing material cost} = 16W_e^{0.932}V^{0.621}Q^{0.799}, \quad 5.8$$

$$C_m = \$16,032,761$$

$$C_{eng}: \text{Engine production cost} \quad 5.9$$

$$= 2251(0.043T_{max} + 243.35M_{max} + 0.969T_{turbine\ inlet} - 2228)$$

$$T_{max} = 3800 \text{ lb}$$

Turbine inlet temperature is assumed as 1200°C.

$$T_{turbine\ inlet} \approx 1200^\circ\text{C} = 2651.67^\circ\text{R}$$

$$C_{eng} = \$488,108 \text{ (per engine)}$$

$$N_{eng} = (2 + 1)Q, \text{ (1 engine for spare)}$$

Using DAPCA IV model, the cost of 30% efficient solar cells, and 40% efficient solar cells quantity versus total cost per aircraft is calculated.

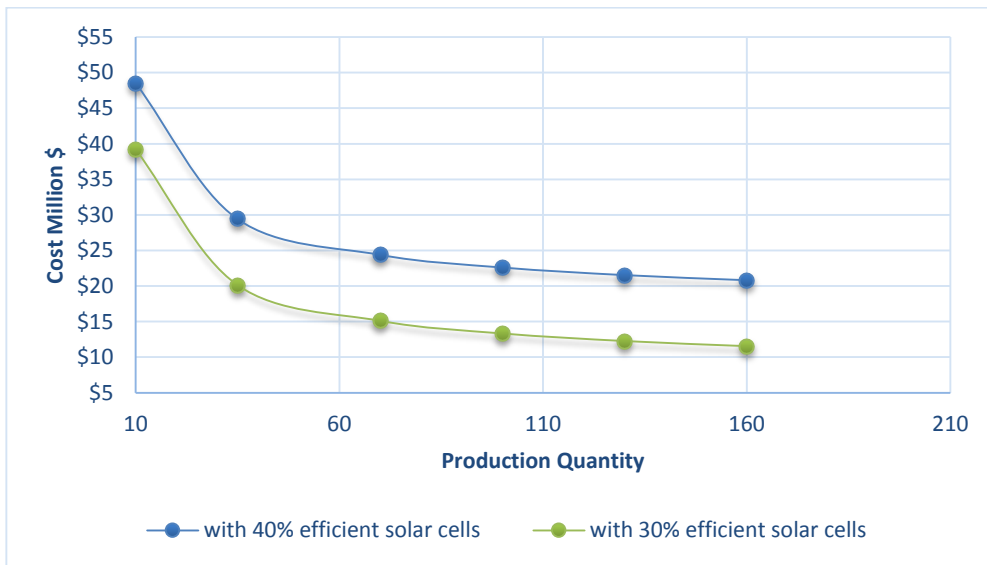


Figure 5.2 Production Quantity vs Total Cost per Aircraft with 30% and 40% Efficient Solar Cells

Another trade-off study is performed by using the annual reduction rate of the solar cells power and its effects on aircraft overall cost Figure 5.3.

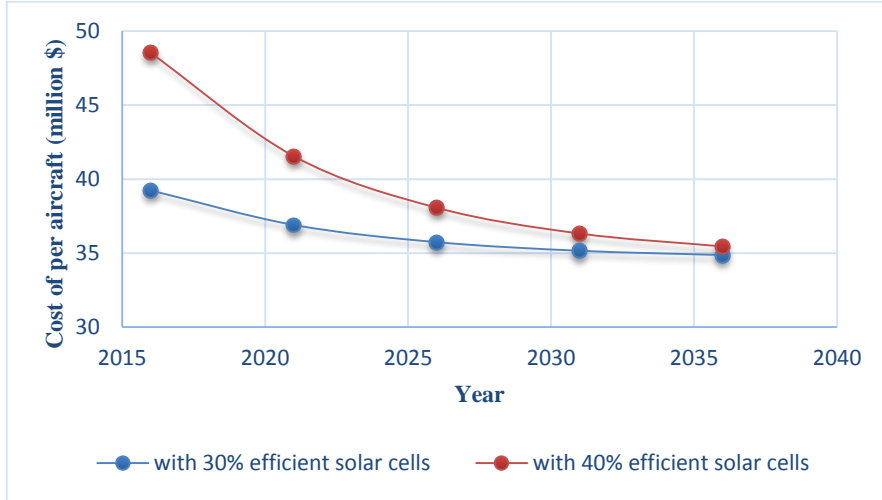


Figure 5.3 Annual Reduction in the Cost of TUYGUN Thanks to Decreasing in Solar Cell Prices

Aircraft production cost is estimated as \$ 34.5 million without solar cells, \$ 39.5 million with 30% efficient solar cells and \$ 48.3 million with 40% efficient solar cells. 10 years later, in 2026, cost of the aircraft with %40 efficient solar cells is estimated as \$ 38 million.

As a result, solar powered aircraft designers should regard the cost reduction rate when both designing their aircraft and estimating the cost.

CHAPTER 6

CONCLUSION

This thesis is a combination of a conceptual design of a turbine engine HALE UAV and a solar powered UAV. Within this aspect, this study is unique. Conventional conceptual designs of a UAV having turbine engines do not work for HALE UAV designs, because high aspect ratio and large wing area lead to wrong weight and performance results. Therefore, new design principles must be developed especially about prediction of weight and performance equations, which include the aspect ratio term. Hence, some assumptions are made while predicting wing weight and span efficiency factor. Also when estimating gross weight, batteries are assumed as payload.

At first, the design was done for 65000 ft altitude, but after calculations, it was seen that designing a hybrid UAV with 550 lb payload to operate at such a high altitude is not feasible. 550 lb payload weight is a challenging requirement for the design, since, lift reduces dramatically at higher altitudes. Approximately 140 kW power is needed for sustaining loiter at 65000 ft, but available solar power is limited for the current size. Therefore, service ceiling must be lowered. Then, calculations are made for 30000 ft altitude since it is the minimum HALE category aircraft altitude.

Airfoil selection is one of the most crucial factor for high altitude aircraft. It is observed from the literature that airfoils which have higher glide ratios are more convenient for HALE category aircrafts. Especially the airfoils whose design lift coefficient is higher

than 1.3 are the most preferable ones. Before analyzing the airfoils, almost all low speed high lift airfoils are examined. When choosing a suitable airfoil, 2D analysis and 3D analysis are performed by XFLR5. Panel method is chosen for selecting airfoils during conceptual design phase. Modified FX 63-137 airfoil is the best alternative among all the other options. The major advantage of the airfoil is higher gliding ratio which makes the aircraft aerodynamically more efficient. Another important parameter of the Modified FX 63-137 is the relatively flat upper surface which is very crucial for gaining sun lights efficiently.

Stability is another important design parameter for HALE category aircraft. Aircraft must be as stable as possible in order to loiter efficiently. As observed from design, center of gravity is very close to the nose of the fuselage since batteries and payload are located near the nose of the fuselage.

The second part of the study is about loitering performance. Loitering performance is simulated for 4 different days of the year, (21 March, 21 June, 23 September and 21 December) for 2 different solar cell efficiencies (30% and 40%) and 3 different altitudes, (20000 ft, 30000ft, and 45000 ft). As a result, the longest endurance occurred with 40% efficient solar cells, at 20000 ft altitude and on 21 June when the solar irradiance is maximum. After simulations it is seen that maximum endurance is 27.4 hours without excess fuel. Main aim of the project is to attain 48 hours loitering endurance. Therefore a method called excess fuel calculation is used. Filling excess fuel to TUYGUN before takeoff is the best option in order to reconstruct the solar cycle and reach minimum 48 hour loitering endurance. Method suggests that excess fuel, calculated using weight prediction model, can be used for predicting the fuel in order to find the fuel consumed for reaching the point where required power is equal to the solar power available obtained from solar cells. After excess fuel method is performed, it is observed that this method is suitable only when aircraft flies on June 21, at 20000 ft, 40% efficient solar cells. After the solar cycle is reconstructed, TUYGUN reaches 67 hour endurance.

When performing trade off study, solar cell efficiency is taken 40%. This value is really high for the current technology since this type of solar cells are very expensive. But technological development rate indicates that ten years later %40 efficient solar cells may be available for solar powered aircrafts. Another trade off study is done for battery technology. When performing simulations, 164 kWh batteries are used [20]. It can be easily said that 10 years later, batteries will have higher energy density than recent ones. As simulated before batteries which have 328 kWh energy density may make continuous flight dream true.

Main drawbacks of solar HALE UAV with higher payloads are inadequate climb rates and very limited maximum speed. It may take a long time for attaining desired region or fly away from region. Hybrid UAV satisfies relatively high maximum speed and rate of climb thanks to its turbofan engines.

Continuous flight of solar airplanes depend mainly on the sunlight. Endurance reduces dramatically during winter since, nights are longer and available sunlight is limited. Because of that reason, solar aircraft projects and studies are tested during summertime. During winter, it is recommended that TUYGUN to use turbofan engine only by subtracting battery and filling fuel to the battery space. In addition sun angle is another crucial parameter for available solar power calculations. Sun angle must be taken into account during calculations. Solar irradiance equation includes the latitude of the region, which indicates the angle of the sunlight. For instance, at higher latitudes daytime is longer, on the other hand, sunlight angle is lower which makes solar radiance inefficient during summer.

After design and simulations, performance parameters are found as shown in Table 6.1 UAV Performance Results. All design requirements are met.

Table 6.1 UAV Performance Results

Parameter	Value
Landing Distance	1061 ft
Takeoff distance	1000 ft
L/D max	35.3
Maximum endurance@30000 ft	21.3 h
Maximum endurance@20000 ft (without excess fuel)	26.6 h
Maximum Endurance with excess fuel	67 h.
MaximumRange@30000ft	588 nm
MaximumRange@20000ft	545 nm
Maximum endurance velocity@30000ft	100 ft/s
Maximum endurance velocity@20000ft	80 ft/s
Maximum range velocity @30000ft	145 ft/s
Maximum range velocity @20000ft	93 ft/s
Maximum velocity @30000ft	500 ft/s
Maximum velocity @20000ft	440 ft/s
Rate of Climb @30000ft	21.78 ft/s
Rate of Climb @20000ft	26.91 ft/s

6.1. Comments on Hybrid Propulsion and Future Works

The size of the wingspan (208 ft) is a drawback for TUYGUN, wingspan may need larger hangars. Therefore retractable wing design may be the solution for housing the aircraft.

After real time simulink, it is concluded that 20000 ft altitude is ideal service ceiling for TUYGUN. However 40% efficient solar cells is a must for achieving 24 hour endurance.

Under current design requirements, especially for 550 lb payload, it is impossible to fly only by solar energy because of the limitations of solar power gained from sunlight. Another limitation is the current batteries which have inadequate energy density. Therefore when performing calculations, batteries which have higher energy density are taken into account.

New hybrid aircraft can be designed using different payload weight or range. Reduction in gross weight may make aircraft have longer endurance. Flying wing configuration may also be designed in order to achieve longer endurance.

REFERENCES

- [1] Raymer, D. P., *Aircraft Design: A Conceptual Approach*, 4th edition, AIAA Education Series, 2006.
- [2] Nicolai L. M., Grant. E. Carichner. *Fundamentals of Aircraft and Airship Design Volume I — Aircraft Design*, AIAA Series, 2010
- [3] Gudmundsson, S., *General Aviation Aircraft Design Applied Methods and Procedures*, BH Series, 2014
- [4] Noth, A., *Design of Solar Powered Airplanes for Continuous Flight*, Ph. D. Dissertation, Autonomous Systems Lab, ETH Zürich, Switzerland, 2008.
- [5] “Solar Impulse.” [Online]. Available: <http://www.solarimpulse.com>, last visited on March 2016.
- [6] “Airfoil profile database.” [Online]. Available: <http://aerospace.illinois.edu/m-selig/ads.html>, last visited on March 2016.
- [7] “Northrop Grumman Corp. Global Hawk.” [Online]. Available: <http://www.northopgrumman.com/Capabilities/GlobalHawk/pages/default.aspx>, last visited on March 2016.
- [8] “Battery University.” [Online]. Available: <http://batteryuniversity.com/>, last visited on March 2016.

- [9] Boucher, R. J., “Sunrise the World's First Solar-Powered Airplane.” *Journal of Aircraft* Vol 22, No 10, 1985.
- [10] Romeo, G., Frulla, G., Cestino, E, and Corsino, G., “Design, Aerodynamic, Structural Analysis of Long-Endurance Solar-Powered Stratospheric Platform”, *Journal of Aircraft*, pp:1505-1520, 2004.
- [11] Boucher, R. J. , “History of Solar Flight.” SAE, and ASME, *20th Joint Propulsion Conference*, Cincinnati, OH, June 11-13, AIAA-1984-1429, 1984.
- [12] “Solar One.”, [Online]. Available: <https://i.ytimg.com/vi/LDZRVLH6QI/maxresdefault.jpg>., last visited on March 2016.
- [13] “Academy of Achievement Photo Credit.” [Online]. Available: <http://www.achievement.org/autodoc/photocredit/achievers/mac0-049>, last visited on March 2016.
- [14] “Solar Challenger Solar Powered Airplane.” [Online]. Available: <http://www.sailingtexas.com/SPEV/Planes/SolarChallenger/solarchallenger.html>, last visited on March 2016.
- [15] Schoeberl, E., “From Sunrise to Solar-Impulse 34 Years of Solar Powered Flight.” *XXIX OSTIV Congress Lüsse*, Germany, 6-13 August 2008.
- [16] “NASA Dryden Flight Research Center Photo Collection.”, [Online]. Available: <http://www.dfrc.nasa.gov/gallery/photo/index.html>.
- [17] “AC Propulsion's Solar Electric Powered SoLong UAV”, [Online]. Available: http://www.tu.no/migraiton_catalog/2005/07/24/solonginfo/binary/SoLong%20info, last visited on March 2016.

- [18] “Autonomus Solar Airplane for Mars Exploration”, [Online]. Available: <http://www.sky-sailor.ethz.ch>, last visited on March 2016.
- [19] “Navair Orders 7 Zephyr Ultra-long Endurance UAV's”, [Online]. Available: <http://www.defenseindustrydaily.com/NAVAIR-Orders-7-Zephyr-Ultra-Long-Endurance-UAVs-05426/>, last visited on March 2016.
- [20] “Solar Impulse Nagoya to Hawaii.” [Online]. Available: <http://www.solarimpulse.com/multimedia-leg-8>, last visited on March 2016.
- [21] “Solar HALE Drones Turn into Atmospheric Satellites”, [Online]. Available: http://defense-update.com/20130813_solar_hale_atmospheric_satellites.html, last visited on March 2016.
- [22] “Martin RB-57F Canberra”, [Online]. Available: <http://www.spyflight.co.uk/rb57.htm>, last visited on March 2016.
- [23] “Nasa Armstrong Fact Sheet: Proteus High-Altitude Aircraft.”, [Online]. Available: <http://www.nasa.gov/centers/armstrong/news/FactSheets/FS-069-DFRC.html>, last visited on March 2016.
- [24] “Apres Harfang: France's Next High -End UAV's.”: [Online]. Available: <http://www.defenseindustrydaily.com/apres-harfang-frances-next-high-end-UAV-06451/>, last visited on March 2016.
- [25] “An Air Force U-2 Dragon Lady flies a training mission. (U.S. Air Force photo by Master Sgt. Rose Reynolds.” [Online]. Available: <http://www.af.mil/AboutUs/FactSheets/Display/tabid/224/Article/104560/u-2stu-2s.aspx>, last visited on March 2016.

- [26] “Boeing's Phantom Eye ISR Technology Demonstrator”, [Online]. Available: http://www.nasa.gov/centers/dryden/multimedia/imagegallery/Phantom_Eye/MC_F13-0015-297.html, last visited on March 2016.
- [27] “Stratospheric Persistent UAS:Global Observer”, [Online]. Available: http://www.avinc.com/uas/stratospheric/global_observer/, last visited on March 2016.
- [28] “Global Hawk High-altitude, long-endurance scienceaircraft”, [Online]. Available: <http://www.militaryaerospace.com/articles/2014/07/northrop-software-radar.html>, last visited on March 2016.
- [29] “Historical Snapshot”, [Online]. Available: <http://www.boeing.com/history/products/condor-unmanned-aerial-vehicle.page>, last visited on March 2016.
- [30] Hoerner, S. F., *Fluid Dynamic Drag*, Brick Town, N. J. USA, 1965.
- [31] Altman, A., Ph.D. thesis, A Conceptual Design Methodology for Low Speed High Altitude Long Endurance Unmanned Aerial Vehicles, 2000.
- [32] Duffie, J.A., Beckman, W. A., *Solar energy thermal proceseses*, 4th edition, John Wiley and Sons, Inc, 2013.
- [33] Deperrois, A., XFLR5 Program, [Online]. Available:<http://www.xflr5.com/xflr5.htm>, 2012, last visited on March 2016.
- [34] Gundlach, J., *Designing Unmanned Aircraft Systems*, AIAA Education Series, 2012.

- [35] Mermer, E., Köker, A., Kurtuluş, D.F., Yılmaz, E., "Design and Performance of Wing Configurations for High Altitude Solar Powered Unmanned Systems," AIAC- 2013-141 2013.
- [36] Anderson, J. D. Jr., *Aircraft Performance and Design*, McGraw Hill, 1999.
- [37] Office of the Secretary of Defense. "Unmanned Aerial Vehicle Reliability Study." February 2003.
- [38] Keidel, B., "Design of a solar-powered high altitude aircraft for year-round operation at intermediate latitudes." Proceeding of the RTO symposium on "UV for aerial, ground and naval military operations", Ankara, Turkey, 2000.
- [39] Nickol, Craig, L., *High altitude long endurance uav analysis of alternatives and technology requirements development*. NASA/TP-2007-214861, National Aeronautics and Space Administration, Langley Research Center, Hampton, VA, 2007.
- [40] Montagnier, O., Laurent, B., "Optimization of A Solar-Powered High Altitude Long Endurance UAV." 27th International Congress of Aeronautical Science, Nice France. September 2010.
- [41] Cestino, E. "Design of solar high altitude long endurance aircraft for multi payload & operations." *Aerospace science and technology* 10.6 (2006): 541-550 2006.
- [42] Roberto, C., Marino, L., "Preliminary Design of a Hybrid Propulsion System For High-Endurance UAV." In: Proceedings of the ASME 2010 International Mechanical Engineering Congress & Exposition IMECE2010, Vancouver, British Columbia, Canada, November 12-18, 2010.
- [43] Roskam, J., *Airplane Design Parts I through VIII*, Darcorporation, 2003

- [44] Gundlach, J., *Designing Unmanned Aircraft Systems: A Comprehensive Approach*, American Institute of Aeronautics & Astronautics Series.2013.
- [45] Harvey, J. R., "Development of a hybrid-electric power-system model for a small surveillance aircraft." 28th International Congress of the Aeronautical Sciences. 2012.
- [46] Flittie, K, Curtin, B., "Pathfinder solar-powered aircraft flight performance", AIAA Atmospheric Flight Mechanics Conference & Exhibit, Boston, 1998.
- [47] Havameydanları Planlama ve Tasarım Teknik Esasları, [Online]. Available: http://www.ubak.gov.tr/BLSM_WIYS/DLH/tr/DOKUMANLAR/20100416_100647_10288_1_10315.pdf, 2007, last visited on March 2016.
- [48] "Williams Engines." [Online]. Available: <https://www.flickr.com/photos/nostri-imagio/2906647142/in/photostream/>, last visited on March 2016.
- [49] "U2-S Aircraft." [Online]. Available: <https://www.af.mil/shaded/media/photodb/photos/030411-F-0000J-102.jpgr> , last visited on March 2016.
- [50] "Phantom Eye." [Online]. Available: <https://www.boeing.com/defense/phantom-eye/>, last visited on March 2016
- [51] "Joby Motors.." [Online]. Available: <https://www.jobymotors.com.>, last visited on March 2016
- [52] Bernard, E., *Dynamics of Atmospheric Flight*, 1th edition, John Wiley and Sons, Inc, 1972.

- [53] “2008 Solar Technologies Market Report.” [Online]. Available: <https://www.nrel.gov/docs/fy10osti/46025.pdf>, last visited on March 2016
- [54] “Gochermann.” [Online]. Available: [https:// http://www.gochermann.com/](https://http://www.gochermann.com/), last visited on March 2016
- [55] “Tuygun Kuşu.” [Online]. Available: https://www.naturephoto-cz.com/gokce-tuygun-picture_tr-22181.html, last visited on March 2016
- [56] “Icare 2.” [Online]. Available: [https:// www.wikiwand.com/de/Icar%C3%A9_II](https://www.wikiwand.com/de/Icar%C3%A9_II), last visited on March 2016
- [57] Özcan, S. G., *Design and Manufacturing of a Solar Powered Unmanned Air Vehicle*, M.Sc. thesis, METU, Turkey, 2015.